MUSA

ON THE INTERACTION BETWEEN MUD AND SAND

Synthesis of MUSA experiments, measurements and modelling

January, 2024; Synthesis of MUSA experiments, measurements and modelling

TKI MUSA project

Author(s)

Leo van Rijn (LVRS-Consultancy)

Bas van Maren (Deltares)

Roy van Weerdenburg (Deltares)

Anne Ton (Deltares)

Márcio Boechat Albernaz (WaterProof)

Synthesis of MUSA experiments, measurements and modelling

TKI MUSA project

Client	MUSA consortium
Contact	Leo van Rijn and Ymkje Huismans
Reference	
Keywords	Sand, mud, laboratory experiments, field measurements, tools, numerical modelling

Document control	
Version	Version 1
Date	31-01-2024
Project nr.	11204950
Document ID	11204950_TKI-MUSA_05
Pages	87
Status	Final

Doc. version	Author	Reviewers
CONCEPT1	dr. ir. L.C. (Leo) van Rijn dr. ir. D.S. (Bas) van Maren ir R.J.A. (Roy) van Weerdenburg dr. ir. A.M. (Anne) Ton (Deltares) M. (Márcio) Boechat Albernaz, MSc	dr. ir. T. (Thijs) van Kessel dr. ir. B. (Bart) Grasmeijer

Summary

This report synthesizes the various research components executed as part of the MUSA project in the period 2020 – 2023. The overall aim of MUSA was to improve our quantitative understanding of erosion rates of sand-mud mixtures under currents and waves. The work included determination of sediment properties, measuring erosion rates in the laboratory and in the field, development and application of numerical models, and improvement of engineering tools.

Sediment samples (for laboratory flume experiments and determination of properties) were collected in the Western Scheldt (the Netherlands), in the Dutch Wadden Sea (the Netherlands), in the Plymouth Estuary (the United Kingdom) and Bengal Bay (Bangladesh). These samples cover a range of sand-mud ratios (from sand-dominated to mud-dominated). The Bengal Bay samples substantially differed from all other samples because of the exceptionally high silt content (relative to clay and sand). Determination of sediment properties included mineral composition, yield stress, Atterberg Limits, dry density, grain size distribution and settling velocity. Both the settling velocity and the particle size distribution were measured with various instruments. Field observations revealed that the settling velocity measured with a flocculation camera (Labsfloc-2) was much larger than with a settling tube device (PIRANHA), resulting from floc destruction in the settling tube, underestimation of small particles by the flocculation camera, or a combination of both. The particle size distribution (PSD) was measured with sieving for the sand fraction, while the finer fraction was measured with Laser Diffraction (LD; using optical scattering), a Sedigraph and a hydrometer (both sedimentation methods, relating the settling speed of particles to a PSD using a Stokes settling velocity). The grain size measured with LD is significantly coarser than the grain size resulting from the hydrometer and the Sedigraph. The LD method also shows much more scattering for similar samples, suggesting a random sensitivity requiring repetition of observations.

Erosion tests were executed with a short flume (currents only, length < 0.5 meter) and a long flume (flow and waves, > 3 meter long). Erosion rates strongly depended on the preparation of the samples. The short flume experiments were carried out with remoulded natural sediments, with diluted (and consolidated over-night) natural samples, and with undisturbed field samples (including biota with stabilizing and destabilizing effects). The critical shear stress for all experiments was established through visual observations, distinguishing between particle erosion (first erosion mode at low bed shear stress) and floc erosion (erosion of larger particles at higher bed shear stress, often accompanied by formation of ripples). For a smaller set of observations, the critical bed shear stress (and the erosion parameter) was additionally determined by fitting erosion formulations to continuous Suspended Sediment Concentration (SSC) observations.

The observed values of the critical bed shear stress were related to both the density and the mud (or sand) content of the sediment bed. The highest critical bed shear stress was typically observed for samples with intermediate density and intermediate sand-mud ratios. High-density mixtures were mostly sand-dominated whereas low-density mixtures were typically mud-dominated; both end members were more easily erodible compared to the intermediate density/mud content samples. The bed shear stress was more coherently related to the density of the sediment bed than to the mud (or sand) content of the bed. Therefore, a formulation was derived to empirically relate the bed shear stress to density. The silt-dominated samples from Bengal Bay were notably different from the samples from Western Europe. The long flume experiments revealed that the erodibility of both sand and of mud decreased with increasing mud content. Earlier experiments predating MUSA related such erosion rate dependence on the critical bed shear stress for erosion. But in contrast to these earlier experiments, the MUSA observations suggest that the erosion rate dependency results from a modification of the erosion parameter (lower at high mud contents).

Field experiments on mud and sand transport were executed near Holwerd, in the Dutch Wadden Sea. This site is characterised by very high SSC (up to several g/l) consisting of both sand and mud. Existing engineering tools computing the transport of sand and of mud were able to predict observed sediment concentrations using local hydrodynamics to remarkable accuracy. These tools therefore appear to be very useful for predicting the sediment dynamics also for such turbid environments. Reproducing the

observed mud concentration required the use of a flocculation model – predicted SSC values using constant settling velocities strongly deviated from observations.

Three types of numerical modelling experiments were executed. First, a new sediment transport formulations was implemented in MIKE3 and tested in a numerical flume resembling the long flume. These experiments revealed that the new formulations resolve observation within a factor 2-5. Secondly, existing sand-mud interaction formulations recently implemented in Delft3D were tested using a similar long digital flume. Numerical experiments revealed some inconsistencies in the implementation of Van Rijn formulations in Delft3D, and that the erosion rates determined with the OBS were probably flawed by the background concentration. And finally, the relationship between density and erodibility which resulted from the MUSA observations was implemented in Delft3D and tested in an idealized tidal basin. These new formulations provide a means to model the development of muddy intertidal areas during tide-dominated conditions which are preserved during subsequent wave-dominated conditions (which is difficult to realize with a model assuming constant critical erosion shear stresses).

Finally, a number of engineering tools were tested (TMUD, Van Rijn (2007) sand transport) or developed (SEDCON, SEDPAR) as part of MUSA. The various laboratory experiments and field observations strengthened confidence in Van Rijn (2007) and TMUD. The new tool SEDCON is a modification of the TMUD model, whereas SEDPAR can be used to determine a range of parameters for input of numerical sediment transport models.

Contents

1 Introduction and approach

1.1 About the MUSA project

Estuaries and tidal basins form the transition zones between land and sea. They contain important habitats for flora and fauna and are extensively used by people, for example for navigation. For ecological and navigational purposes, it is important to understand and predict the evolution of channels and shoals, including sedimentation rates and the composition of the bed sediments. The bed material of large estuaries and tidal basins largely consists of mixtures of mud and sand, with predominantly sandy channels and mainly muddy intertidal areas. The interaction between sand and mud, in combination with currents and waves, leads to complex dynamics in these areas, with migrating channels and shoals.

Much is known about the behaviour of the individual sediment fractions, but the knowledge and understanding of sand-mud interaction remains limited, as do the available tools and models to accurately predict the bed evolution and sediment transport rates in sand-mud areas. Existing models, like the ones by Van Ledden (2003), Soulsby & Clarke (2005) or Van Rijn (2007), have only limitedly been verified with observations due to a lack of high quality observational data. Also, none of the available approaches covers the complete spectrum of sand-mud interaction, which includes settling, erosion processes induced by the combination of waves and currents, and the bed shear stress. Therefore, in practice sand and mud fractions are often treated separately. This decoupled approach limits the predictive capacity of numerical models, and therefore the impact of human intervention such as deepening of channels and port construction on maintenance dredging volumes and other morphological changes.

In the MUSA-research project, an international consortium of contractors, consultants and research organizations (see Table 1.1) joined forces to increase the understanding of sand-mud dynamics by means of fieldwork campaigns and laboratory experiments, and to implement this knowledge in engineering tools and advanced models for the prediction of mud and sand transport and associated morphology in tidal conditions with both currents and waves. The results of the different stages of the project are captured in the project deliverables, which include reports, databases and tools (Table 1.2). All these deliverables are publicly available via this Deltares Public Wiki Page.

This report presents the synthesis of all the results obtained during the MUSA research project in order to assess the progress of knowledge and the availability of tools in relation to the research questions defined at the beginning of the research project.

Table 1.1 Contractors, consultants and research organization in the MUSA consortium.

Consortium partner	Country
Deltares	Netherlands
Leo van Rijn Sediment Consultancy	Netherlands
WaterProof	Netherlands
Boskalis	Netherlands
DEME Group	Belgium
Jan de Nul Group	Belgium
Arcadis	Netherlands
Royal Haskoning DHV	Netherlands
HR Wallingford	United Kingdom
DHI	Denmark

Table 1.2 Deliverables of the MUSA-research project

MUSA reports	
Literature study	Literature review on sand and mud Authors: Van Rijn, L.C., Colina Alonso, A. & Manning, A.J., 2021
	Literature review – Measuring and interpretation of settling velocity and particle size Authors: Van Rijn, L.C. & Koudstaal, K.R., 2021
Laboratory experiments	Results of laboratory experiments Phase 1A & 1B Authors: Boechat Albernaz, M., Van Rijn, L.C., Schoonhoven, D.C. & Perk, L.M., 2022A
	Results of laboratory experiments Phase 1C & 1D Authors: Boechat Albernaz, M., Van Rijn, L.C., Schoonhoven, D.C. & Perk, L.M., 2022B
Field measurements	Results of MUSA field measurement campaigns at Holwerd, the Netherlands Authors: Boechat Albernaz, M., Van Rijn, L.C., Schoonhoven, D.C. & Perk, L.M., 2022C
	Field measurements of settling velocities and floc sizes in the ferry channel near Holwerd Authors: Van Rijn, L.C., Boechat Albernaz, M. & Manning, A.J., 2023
Numerical modelling	Modelling sand-mud dynamics in a digital flume in Delft3d Authors: Van Weerdenburg, R.J.A., Colina Alonso, A. & Van Maren, D.S., 2023
	Multi-fraction Sediment Transport Modelling in MIKE 3 FM Authors: Maycon Machado Fontana, Athanasios Petridis, Kasper Kaergard, 2023
Synthesis (this report)	Synthesis of MUSA experiments, measurements and modelling Authors: Van Rijn, L.C., Van Maren, D.S., Van Weerdenburg, R.J.A., Ton, A.M. & Boechat Albernaz, M., 2023
MUSA Database	
	MUSA Database with results of laboratory experiments. The database contains a characterization of sediment samples and the results of different (flume) experiments.
MUSA Tools	
SEDHAR	SEDHAR is an engineering tool to determine the sedimentation of sand, silt and mud in harbour basins.
SEDPIT	SEDPIT is an engineering tool to determine the sedimentation in channels/pits/traps etc. using two different trap efficiency formulas.
SEDPAR	SEDPAR provides estimates for sediment characteristics and transport parameters.
SEDCON	SEDCON computes the sediment concentration and transport of clay, silt and sand due to combined currents and waves at a local observation point.
TMUD	TMUD computes mud transport as a function of tidal velocities.

1.2 Objectives and research questions

The main objective of the MUSA project is to improve and develop the engineering tools and numerical models that are needed to deal with sand-mud mixtures in estuarine and coastal systems. This requires a fundamental understanding of the behaviour of sand-mud mixtures. After an extensive literature review at the start of the MUSA-research project (Van Rijn et al., 2020), multiple research questions were defined. These were grouped in three categories: 1. Erosion of mud-sand beds, 2. Settling velocity and deposition fluxes, and 3. Bed density. The research questions that were defined for each of the three categories are listed below.

Erosion of mud-sand beds

1. What is the critical bed shear stress and erosion rate of soft mud-sand beds in laboratory and field conditions with currents?
2. What is the role of oscillatory wave motion on the erosion of mud-sand mixtures?
3. What is the effect of varying percentages of clay, silt and sand and consolidation on the erodibility of mud-sand mixtures?
4. What is the role of bed irregularities (gravel, shells) on the erodibility of mud-sand mixtures?
5. How are the critical stresses and erosion rates of the sand and mud fractions related to bulk sediment properties and basic hydrodynamic parameters?

Settling velocity and deposition fluxes

1. What is the influence of settling velocity and sediment concentration distribution on the deposition flux close to the bed, and how can this be related to hydrodynamic forcing and sediment properties?
2. What is the role of sand on mud flocs size, shape, and density and the resulting settling rates?
3. How to obtain an accurate settling velocity distribution from settling tube and video-camera results?

Bulk density

1. What is the best method to measure the density of the upper 50 cm of the bed, with a focus on the transition layer between water and seabed?
2. What is the dry bed density of the upper 50 cm of mud-sand beds in tidal conditions and how does this relate to sediment properties (e.g. composition, compaction)?
3. What is a simple method for extraction and analysis of samples in shallow and in deep water?

1.3 Approach and report outline

Different stages in the MUSA-research project focus on data collection by means of laboratory experiments and field measurements, data analysis, and tool and model development. The approach in these stages is discussed below. How these stages depend on the results of other stages is illustrated schematically in Figure 1.1. Highlights of the results from different stages are discussed in Chapters 2-4 of this report. Answers to the research questions and general conclusions are included in Chapter 6.

Laboratory experiments

First, sediment samples were collected from different field sites. The characteristics of the sediment samples were determined in the laboratory. In flume experiments, the erosion of sand and mud from the bed due to hydrodynamic forcing by currents and waves is addressed. The highlights of these experiments are discussed in Chapter 2 of this report. A more detailed description of these experiments is included in MUSA-report on laboratory experiments by Boechat Albernaz et al. (2022A (MUSA); 2022B (MUSA)).

Field measurements

Field measurements were carried out in the Wadden Sea near Holwerd. These measurements are used to obtain more data and to validate several formulations and engineering tools (MUSA-report on Field measurements by Boechat Albernaz et al., 2022C (MUSA)). Field measurements of settling velocities

and floc sizes are performed with different types of instruments, such that their performance is evaluated (MUSA-report on settling velocities and floc sizes by Van Rijn et al., 2023). The highlights of these field measurements are discussed in Chapter 2 of this report.

Numerical modelling

Delft3D and MIKE models were set up to reproduce some of the flume experiments that were carried out in the laboratory. In this way, the numerical modelling was used to (1) support the analyses of flume experiments and (2) to test sediment transport formulations that are implemented in the numerical modelling software. Highlights of these modelling efforts are discussed in Chapter 3 of this report. More details are included in MUSA-report on numerical modelling by Van Weerdenburg et al. (2023 (MUSA)).

Development and application of engineering tools

A number of engineering tools were tested (TMUD, Van Rijn (2007) sand transport) or developed (SEDCON, SEDPAR) as part of MUSA. The Van Rijn (2007) and TMUD models were tested against various laboratory experiments and field observations SEDCON is a new model developed as part of MUSA, and is a modification of the TMUD model. SEDPAR can be used to determine a range of input parameters for numerical sediment transport models.

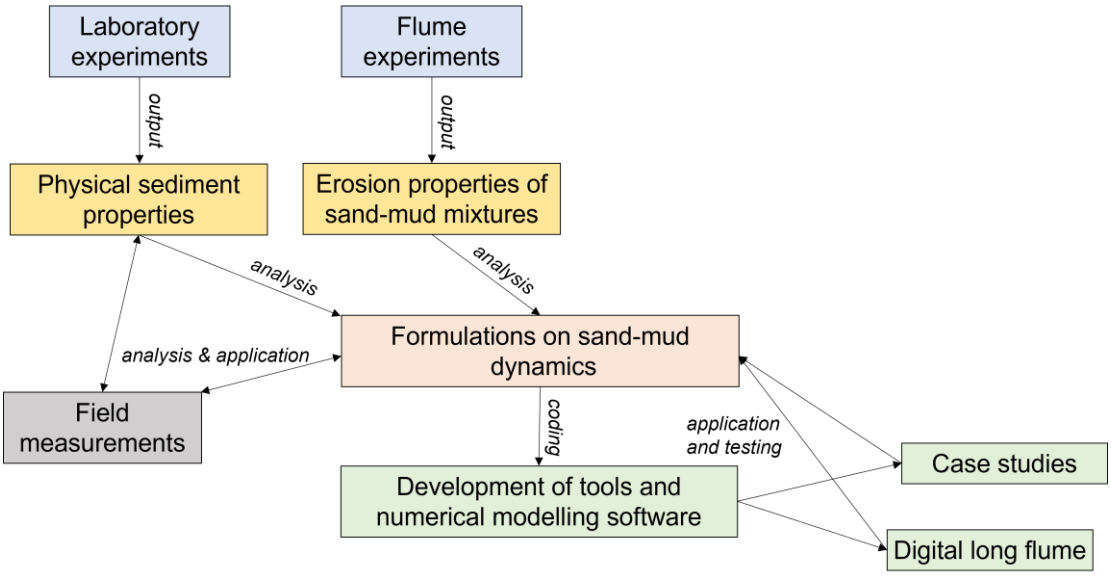

Figure 1.1 Schematic diagram of different stages in the MUSA-research project.

2 Sediment sampling and properties

2.1 Introduction

The analysis of data that was obtained during many of the MUSA laboratory experiments and field measurements is discussed in this chapter. A more detailed description of the data and the data collection is discussed in MUSA reports by Boechat Albernaz et al. (2022A (MUSA); 2022B (MUSA); 2022C (MUSA)) and Van Rijn et al. (2023 (MUSA)).

This chapter starts with a discussion of the locations where sediment samples were taken (Section 2.2). Afterwards, the results of different experiments and measurements are discussed per topic: sediment classification (Section 2.3), particle size distribution (Section 2.4), bulk densities (2.5) and settling velocities (2.6).

2.2 MUSA sediment sampling at intertidal banks and tidal channel beds

Most of the mud-sand samples studied in the MUSA-Project are taken from the intertidal banks (top layer <0.1 m) of the Western Scheldt (WS; Netherlands), Wadden Sea (NPZ (Noordpolderzijl); Netherlands), Plymouth Estuary (PLUK; United Kingdom) and Scheldt River (Belgium). In addition, several samples are taken from the bed of the tidal ferry channel near Holwerd (Netherlands; depth of about 4 m) and from a deeper navigation channel in Bengal Bay (BB; Bangladesh; depth of about 7 m). These sedimentary environments mostly consist of fine-grained sediment beds (mud-sand beds) with small-scale ripples as a manifestation of dynamic sediment transport processes in conditions with combined current and waves and muddy sand beds, see Figure 2.2.1. Ripple-type bed forms are generally absent in very muddy conditions, but bed irregularities due to small drainage channels are often visible.

The MUSA-samples from the different sites show a wide range of clay, silt and sand content. The sand content in the samples varies in the range of 3% to 97% (see in Boechat Albernaz et al. (2022A (MUSA))).

Very clayey, very silty and very sandy samples are distinguished, as follows:

- 6 very muddy samples with $p_{clay\text{-}silt<8\mu m}$ > 25%: NPZ-2016/2017 (25%); PLUK4 (26%); BB3 (30%); NPZ-B5 (35%); NPZ-H2 (38%); WS-PA1 (56%);
- 4 very silty samples with $p_{silt\ 8\text{-}63\mu m}$> 50%: WS-WAW1 (52%); WS-GR1 (77%); WS-ZW2 (64%); PLUK1 (64%); BB3 (64%);
- 5 very sandy samples with $p_{sand>63\ \mu m}$ >50%: WS-BA4 (97%); WS-BH1 (52%); WS-SO3 (56%); WS-APP (77%); WS-HU1 (83%).

The samples show dry bulk density variations in the range of 435 to 1500 kg/m^3.

It is noted that the bulk density of the top layer (< 0.1 m) generally is somewhat lower than that of the upper layer with a thickness of around 0.4 m. Based on the values of Table 3-4 in Boechat Albernaz et al. (2022A (MUSA)), it is found that the dry bulk density of the top layer < 0.1 m is, on average, 10% to 30% lower than that of the upper layer < 0.4 m.

The very muddy samples with a relatively low sand content < 25% have the lowest dry bulk density in the range of 400 to 650 kg/m^3. The very silty and very sandy samples have the highest dry bulk density values in the range of 800 to 1500 kg/m^3. Exceptions are the 2 samples from Plymouth Estuary (PLUK1, PLUK4) with relatively low dry densities in the range of 600 to 650 kg/m^3 for $p_{silt} \cong$ 50% to 60% and $p_{sand} \cong$ 10% to 20%. The very silty samples with almost no organic materials from Bengal Bay have a relatively high dry density and therefore deviate from the other samples (as is discussed in Section 2.5).

Figure 2.2.1 Examples of typical mud-sand beds along the tidal banks and channels at which sediment samples were taken for the MUSA project.

2.3 Sediment classification in terms of mineral composition, plasticity and yield stresses

2.3.1 Mineral composition

The properties of clays are related (to some extent) to the physio-chemical characteristics of the clay minerals and the relative proportions of the minerals in the soil. Clay can be defined as a naturally occurring material, composed mainly of fine-grained minerals (< 8 μm). It becomes plastic in the presence of water. It becomes hard (non-plastic) when dried. Clay can be distinguished from other fine-grained soils on the basis of size difference and mineralogy. Clay mixtures may contain organic materials (peat, muck) and calcareous materials (aragonites). The plasticity of clays is due to the size and geometry of the particles as well as the water content. Plasticity and hardness are greatly affected by the chemical composition of the particles that are present in the clay.

Clay consists primarily of clay minerals, although other minerals like quartz and feldspar may also be present. Clay minerals are essentially hydrated aluminium phyllosilicates with a layered (phyllo) structure in which aluminium can be replaced by magnesium, iron or other alkali metals (kalium, lithium, cesium), resulting in varying chemical compositions. Clay minerals have the capacity to hold water and can be identified by using the method of Röntgen-diffraction, in which each mineral has its own set of specific diffraction peaks. Common clay minerals belonging to the group of layered silicate minerals are Kaolinite (≅0.7nm) and Illite (≅1nm) and a group of 1.4nm-clay minerals consisting of Montmorillonite, Vermiculite and Chlorite. These latter minerals can be identified by heating, which has a different effect on each mineral, or by using glycerol leading to swelling (from 1.4 to 1.8nm) of only Montmorillonite.

Kaolinite, Illite and Montmorillonite often occur in nature as intermixed minerals in the soil. Kaolinite is a soft, white mineral produced by chemical weathering of silicate minerals like feldspar. It has a low shrink-swell capacity in contact with water. Similarly, Illite is a non-expanding (non-swelling) layered silicate mineral. It occurs as aggregates of small to grey crystals produced by chemical weathering of other

silicate minerals like feldspar. Illite is the most common clay mineral. Montmorillonite is a subclass of the Smectite minerals consisting of plate-shaped particles. The individual crystals of Montmorillonite and water can easily intervene, causing this clay to swell. Chemically, it is a sodium (Na)-Calcium (Ca) based clay. A typical example of Montmorillonite clay is bentonite, which is commonly used as a viscous slurry in geo-engineering for the cooling of drilling equipment and to stabilize shafts.

Quartz is a pure silicon dioxide, which is an oxide of silicon that is also known as silica. Silica is non-reactive. It is commonly found in nature as sand, gravel, boulders and granite. Silica flowers with spherical type of particles with sizes between 5 and 50 μm are produced by the grinding of Quartz particles.

Feldspar, Mica (glimmer) and Muscovite are Quartz-type minerals consisting of aluminum silicates including calcium, sodium and potassium. Feldspar is the most abundant mineral group. Micas are a group of minerals that can be easily split into extremely thin elastic plates, of which Muscovite is the most common form.

In the MUSA samples, it was found that the composition of the clay-silt fraction < 10 μm is nicely grouped by geographic location. This implies that the samples from Noordpolderzijl (B5), Western Scheldt (PA1, BAPU and WS-BATH-APP) and Scheldt River (SO3) are very similar, samples from Plymouth (PLUK1 and PLUK4) are very similar and samples from Bengal Bay (BB2 and BB3) are very similar.

- The clay-silt fraction < 10 μm in samples from the Western Scheldt and Noordpolderzijl (NL, BE) is dominated by Illite (55%). The fraction of Smectite is very low < 10% and the fractions Koalinite and Chlorite are of the same order (about 20%).
- The clay-silt fraction < 10 μm in samples from Plymouth are dominated by Kaolinite (50-55%) which originates from Cornish granites and Illite (45-50%). Smectite and Chlorite do not occur in these samples.
- The clay-silt fraction < 10 μm in samples from Bengal Bay are dominated by Illite (80%). The fraction of Chlorite originates from the Himalaya and is much lower (20%). Smectite and Kaolinite do not occur in these samples.

2.3.2 Plasticity (Atterberg limits)

The cohesivity of samples can be expressed in terms of the Plasticity Index based on the Atterberg limits (Atterberg tests). The Atterberg tests consists of a roll test and a cone-penetration test to determine the plastic limit and the liquid limit, respectively:

- The plastic limit is defined as the moisture content at which a thin thread-type roll can be made without crumbling;
- The liquid limit is defined as the moisture content at which the penetration of a standard cone into a sediment sample is 20 mm.

The plasticity index of a soil is the difference between the liquid limit and the plastic limit (expressed as moisture contents in %). These limits define ranges in moisture content at which a soil will behave as solid, plastic or liquid materials. Typical PI-ranges are:

- PI < 30: low plasticity (sandy soils);
- 30 < PI < 50: intermediate plasticity (silty/loamy soils);
- PI > 50: high plasticity (clayey soils).

Clays with relatively large fractions of Montmorillonite minerals, which have a significant swelling capacity, generally have relatively high PI-values. This is particularly the case for the sodium-based Montmorillonite clays (see Figure 2.3.1). A very high PI-value (>70) m is therefore an indication for the presence of a relatively high proportion of Montmorillonite minerals. Clays with high proportions of Kaolinite minerals, which have a relatively low swelling capacity, generally have low PI-values (see Figure 2.3.1).

The measured PI values of the MUSA-samples are given in Figure 2.3.1. For comparison, the PI-values of Kaolinite, Illite and Montmorillonite-dominated clays and three geological clays that are found in the UK are also shown. The sandy MUSA-samples have relatively low PI-values between 12 and 22. The silty MUSA-samples have PI-values between 15 and 30. The clayey MUSA-samples have relatively high PI-values between 45 and 60, which is in the range of the Montmorillonite (Ca) clays.

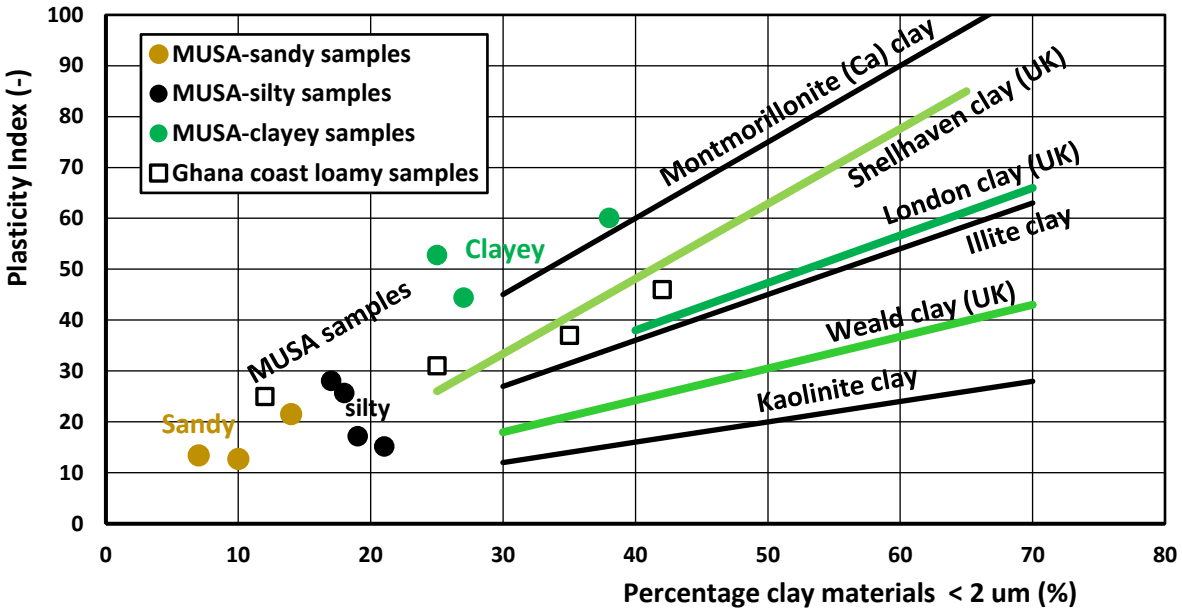

Figure 2.3.1 Plasticity Index as function of percentage clay (< 2 μm), see Appendix A for more details on MUSA samples.

2.3.3 Yield stresses

The yield stress (undrained shear strength) is a parameter that quantifies the internal resistance of mud-sand samples. The yield stress can be determined by a vane test in-situ, which can be carried out in the laboratory using a small soil sample. The vane is pushed into the soil and rotated at slow speed (5 to 10 degrees per minute). The torque is measured at regular time intervals, as is illustrated graphically in Figure 2.3.2. If the soil fails, the rotation rate will suddenly increase and the torque will decrease to a lower constant value. This value is used as an estimate of the undrained remolded shear strength. The yield stress is the stress just before initiation of viscous deformation (creep). The yield stress is generally somewhat smaller (factor 1.5 to 2) than the remolded shear strength.

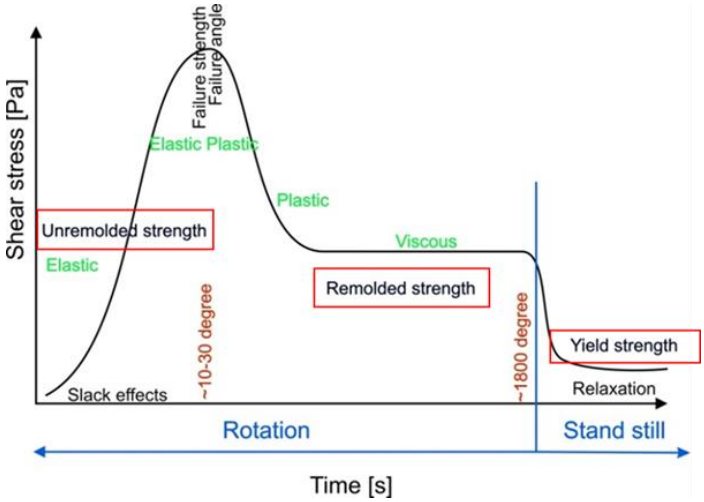

Figure 2.3.2 Procedure of vane experiments to determine the yield strength of sediment samples.

The flow stress is the stress that is required to initiate flow (i.e. plastic deformation) of sediment mixtures. It can be determined from a graph of the shear stress against the shear rate at the intersect of the higher shear stresses (values for shear rates > 10) with the stress axis. If the shear stress exceeds the flow

stress, the sediment sample behaves as a fluid. The flow stress is somewhat larger than the undrained remolded shear strength.

The yield stress of the MUSA-samples was determined using the Brookfield Rheometer DV3T with a vane-type spindle at the Soil Mechanics Laboratory of Wiertsema. Figure 2.3.3 shows three typical examples of the measured shear stress versus the measured strain of the sample.

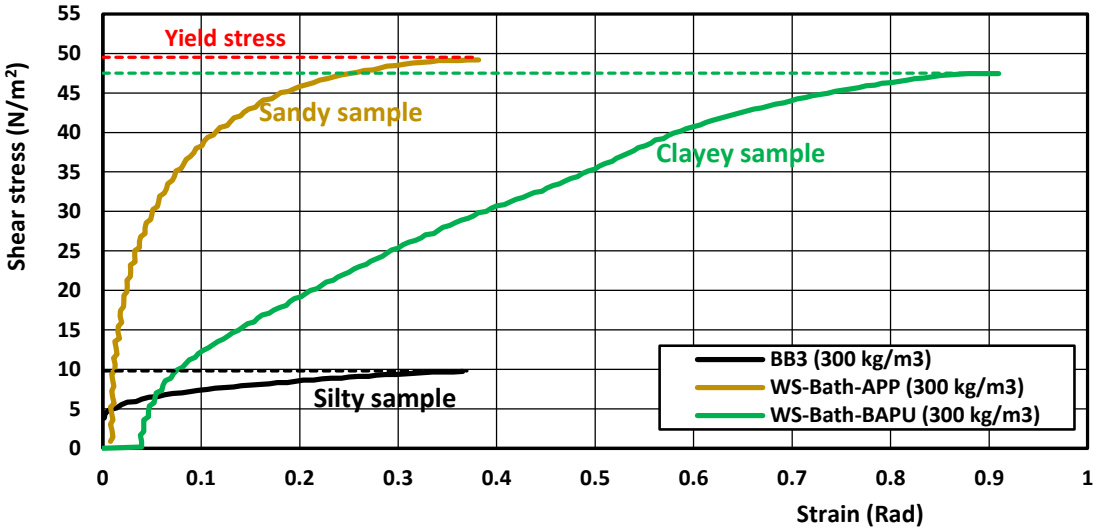

Figure 2.3.3 Shear stress against Strain for three mud samples (MUSA samples) at dry density of 300 kg/m^3.

2.4 Particle size distribution

Determining the particle size distribution generally starts by taking sediment samples (Van Rijn & Koudstaal, 2021 (MUSA); Veld et al., 2016). Different sampling devices are available for different sampling depths:

- Grabs such as the Van Veen Grab are commonly used for samples of the upper 0.1 m of the bed;
- Box-corers are commonly used for undisturbed samples of the upper 0.5 m of the bed; and
- Piston- and vibro-corers are commonly used for undisturbed samples with lengths up to 6 m.

The classification of sediment samples into fractions of sand, silt and clay is generally defined by the grain size distribution of the primary particles, using the Wentworth (1922) scale (Table 2.4.1). Sediment fractions may be expressed either as mass percentages or volume percentages.

Various methods are available to determine the particle size distribution (PSD) of the primary particles:

- Coarser particles such as the sand fraction > 63 μm can be classified into a mass-based PSD by sieving. The size of spherical and ellipsoid sand particles is usually measured by using the sieve method with a rectangular mesh size (between 63 μm and 2000 μm). The PSD size of fine particles < 63 μm and especially of the very fine silt fraction < 32 μm cannot easily be determined by sieving.
- The shape and size of clay-type particles can be studied by scanning electron microscopy (SEM-method). Quantitative results are obtained by scanning many samples, such that the results are representative for the variations in grain size within the sediment sample.
- Sedimentation methods to determine settling velocities are used in combination with the relation for the Stokes-diameter to determine the mass-based PSD for the fine fraction < 63 μm. Several sedimentation methods exist, such as the Pipet/TAP-method, the Hydrometer-method and the Sedigraph-method.
- Laser-light diffraction methods such as the Malvern particle sizer and the LD-method are most appropriate to determine the volume-based PSD for spherical particles of silt and sand. The methods are less suitable for flaky clay particles and mixtures with a wide range of sediment sizes, as smaller particles are shaded by larger particles.
- Particle count methods such as the Coulter counter determine the PSD based on changes of electrical resistance of particles with different sizes.

Table 2.4.1 Wentworth (1922) scale for the classification of sediment fractions.

Size [mm]	Wentworth Grade	Phi-Scale	Sediment	Sedimentary rock
> 256	Boulder	-8	Gravel	Conglomerate
256 – 64	Cobble	-6		
64 – 4	Pebble	-2		
4 – 2	Granule	-1		
2 – 1	Very coarse sand	0	Sand	Sandstone
1 – 1/2	Coarse sand	1		
1/2 – 1/4	Medium sand	2		
1/4 – 1/8	Fine sand	3		
1/8 – 1/16	Very fine sand	4		
1/16 – 1/32	Coarse silt	5	Mud	Mudstone
1/32 – 1/64	Medium silt	6		
1/64 – 1/128	Fine silt	7		
1/128 – 1/256	Very fine silt	8		
< 1/256	Clay	> 8		

In mud-sand samples, the shape of most sand and silt particles is nearly spherical, but the shape of clay-type particles is more platy/flake. The shape of most silt particles is nearly spherical, but the shape of clay-type particles is more platy or flaky. The size of clay particles can only be measured accurately by using scanning electron microscopy (SEM-method). However, this method is very laborious and requires many subsamples for representative analysis results.

The particle size that is determined in sedimentation methods based on Stokes' settling equation is an equivalent spherical diameter and it therefore does not represent the effect of the non-spherical shape of clay particles. The spherical Stokes diameter is generally much smaller (factor 2 to 5) than the plate diameter of clay particles, which are found to be as large as 4 to 5 μm for clayey samples in China.

The particle size that is measured by the Laser-Diffraction method is an equivalent spherical diameter derived from the side view of particles. It represents the major diameter of the particles, which is close to the actual size of disc-type (platy/flaky) clay particles. The LD-method may produce less accurate results for mixtures of sand and mud, as the fine mud particles in the test sample are partly shaded by the larger sand particles. This may result in a bias in the particle size distribution. Separating the sand and mud fractions and performing the LD-measurements for both fractions separately may increase the accuracy of results. At the same time, separating the fractions may in practice lead to a loss of fines and reduces the advantage of the LD-method of being able to measure the full sample at once.

Determining the clay fraction < 2 μm is laborious and prone to errors. This may be overcome by defining a clay-dominated fraction < 8 μm as an indication of the presence of cohesive clay-type particles in a sediment sample. The clay-dominated fraction < 8 μm can be determined more accurately by both the sedimentation methods and the LD-method. For example, the percentage of clay-type particles < 8 μm for a sample from Noordpolderzijl (NPZ) is about 50% and the percentage < 2 μm is about 35%. The first value (50%) is more reliable than the latter value (35%), because the (systematic) inaccuracy of the sedimentation methods increases for particles smaller than 8 μm.

Important results from the literature study and the sediment classification by different instruments on determining settling velocities of fine-grained sediments are (Van Rijn et al., 2021 (MUSA); Boechat Albernaz et al., 2022C (MUSA)):

- The disc-type diameter of clayey particles (< 8 μm) is up to 5 times larger than the equivalent Stokes diameter ($d_{plate,clay} \cong 5\ d_{sphere;Stokes}$) and up to 1.5 times larger for silty particles in the practical range of 8 to 32 μm;

- The equivalent diameter (d_{LD}) of the LD-method is much larger than the equivalent Stokes' diameter for platy clay particles ($d_{LD} \cong 5\ d_{sphere;Stokes}$). The LD-diameter ($d_{LD}$) is slightly smaller than the plate diameter of clay-type particles ($d_{LD} \cong 0.7$ to $0.8\ d_{plate}$). The LD-diameter may be somewhat larger than the sieve diameter for non-spherical (ellipsoid) sand particles ($d_{LD} \cong 1.2$ to $1.3\ d_{sieve}$), because ellipsoid sand particles may pass through a sieve mesh with their smallest diameter;
- The percentage of clayey sediments (< 8 μm) as measured by the Pipet/TAP-method on the one hand and as measured by the Hydrometer-method on the other hand lead to a maximum difference in results of 20% for muddy samples. For silty samples with a small amount of clay, the differences in the measured percentage of clayey sediments goes up to 50% to 100%;
- The sedimentation methods overestimate the percentage of clay < 2 μm, as many clay-type particles have plate diameters in the range of 2 to 4 μm, which are seen as spherical diameters < 2 μm by the sedimentation methods.

The most important results from the comparison between the LD-method, the Sedigraph-method and the Hydrometer-method for analysis of the PSD of mud-sand samples are (see Figure 2.4.1 and Figure 2.4.2):

- The Sedigraph and the Hydrometer-methods produce significantly smaller d_{10}, d_{50} and d_{90}-values than the LD-method. The Sedigraph-method produces somewhat smaller values than the Hydrometer-method;
- The LD-method provides a particle size distribution which is shifted to the right (i.e. towards coarser sediment) compared to that of the Sedigraph-method and the Hydrometer-method. This corresponds to earlier findings that are discussed in scientific literature;
- Organic and calcareous particles are relatively large. Removing them results in smaller values for the characteristic sediment diameters (d_{50}) and a higher percentage of fines (< 63 μm);
- The LD-method shows a relatively large variability between similar samples, which implies that multiple measurements are required to obtain accurate and representative results;
- The median particle size (d_{50}) decreases exponentially for increasing percentage of fines < 63 μm.

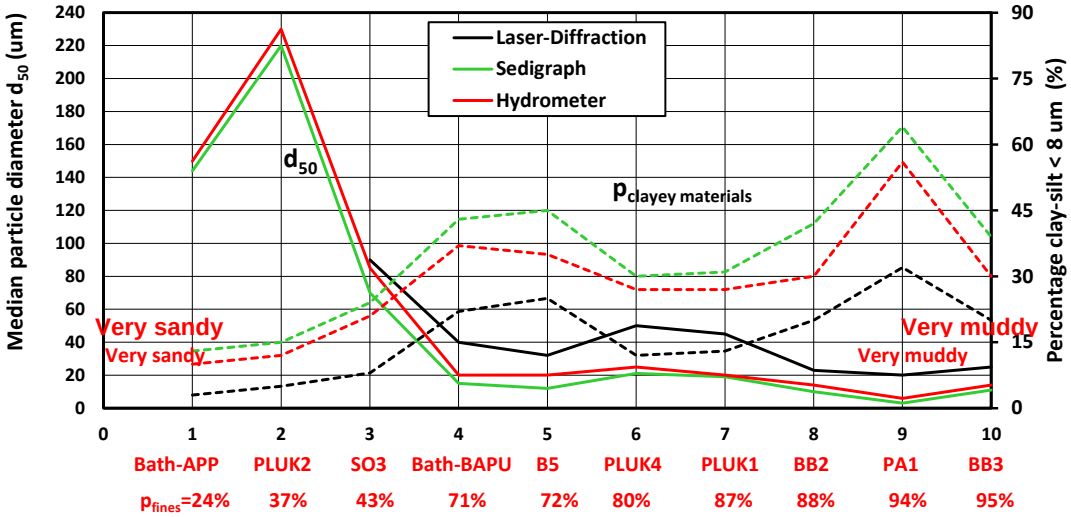

Figure 2.4.1 Median particle (d_{50}; left axis, solid line) and percentage of clayey materials ($p_{clay\text{-}silt< 8\ \mu m}$; right axis, dashed line) of samples based on three methods ($p_{fines<63\ \mu m}$ = percentage of fines < 63 μm based on average values of SE and HY-methods).

An additional data set of 20 samples from Bengal Bay (Bangladesh) provided by Jan de Nul Group (JDN) shows very similar results:

- the hydrometer-method including wet sieving to separate the sand fraction produces smaller particle sizes of the fine fraction and lower percentage of sand values than the LD-method;
- the LD-method was used with and without pretreatment of anti-flocculant; the test results with anti-flocculant show substantially lower d_{50}-values (shift of psd-curve to the left) indicating the necessity of pretreatment.

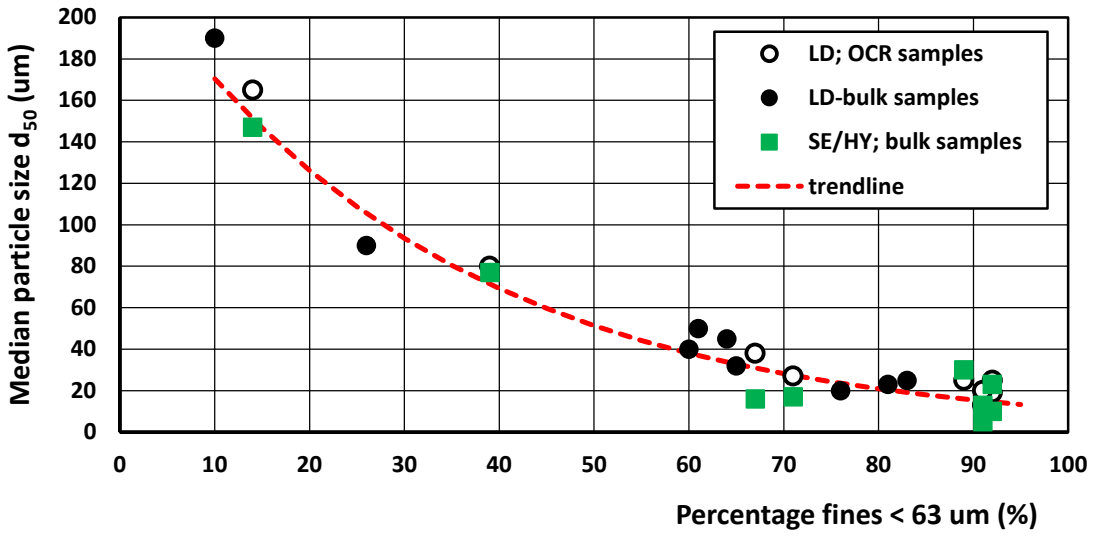

Figure 2.4.2 Median particle size as function of percentage fines < 63 um (LD=Laser-Diffraction method; SE/HY=sedimentation methods; OCR=organic materials removed)

The actual size of individual clay particles is best represented by the Laser-Diffraction method. The Sedigraph and the Hydrometer sedimentation methods produce an effective settling diameter and are therefore preferred in case the results are used to determine settling velocities, for example in siltation studies. The Hydrometer method is more laborious, but the variability in the results is low due to the relatively large sample that is measured. The LD-method offers an attractive solution for a rapid indication of particle sizes, but many (small) samples are required to obtain representative results.

2.5 Bulk density of mud-sand mixtures

Earlier experimental work on the consolidation of mud-sand mixtures (Van Rijn and Barth, 2018) shows that the consolidation process of soft mud-sand mixtures under water consists of three distinct phases:

1. flocculation and hindered settling with a duration of a few hours;
2. primary (short-term) consolidation with a duration of 2 to 3 weeks; and
3. secular (long-term) consolidation with a duration of months to years, depending on the percentage of sand (Terzaghi-type consolidation).

The consolidation process of mud mixtures strongly depends on three parameters, which are the percentage of clay/lutum< 2 to 8 μm, the percentage of sand particles > 63 μm and the layer thickness. Other parameters like the type of mud (i.e. mineral composition) and the percentage of organic materials in the range of 0 to 10% are of minor importance. Mud suspensions of 1 to 2 m thick with initial concentrations of 50 to 100 kg/m^3, as present in near-bed layers of a natural muddy tidal channels, can consolidate to a dry density of about 150 to 200 kg/m^3 during a period of 3 hours (Van Rijn and Barth, 2018), which is a typical value for the tidal slack period when deposition takes place. The transition from the hindered settling phase to the primary consolidation phase is characterized by the formation of a network structure. The gelling concentrations with some degree of matrix (skeleton) structure are in the range of 100 to 150 kg/m^3.

Natural muds with initial concentrations of 150 to 300 kg/m^3 and a low sand content (< 20%) can reach a dry density of about 350 kg/m^3 after 1 day. Natural muds with high sand content (40%-50%) can reach a dry density of about 450 kg/m^3 after 1 day. Dry density values in this range are the onset of the primary consolidation phase with the gradual build-up of grain stresses in a matrix-type network structure.

The primary (short-term) consolidation process proceeds quickly (10 to 40 days) if the percentage of sand (> 62 μm) is larger than about 30%, see Figure 2.4.3. Natural muds with low sand content (≅ 20%) and thickness of 1 to 2 m can consolidate to 400 to 450 kg/m^3 after 20 to 50 days. Natural muds with a high sand content of 40% to 50% and thickness of 1 to 3 m can consolidate to dry density values of 600 to 700 kg/m^3 after 10 to 30 days. The time scale is relatively small up to 60 days for a small thickness of 1 m and increasing to 180 days for a mud thickness of about 3 m and low sand content.

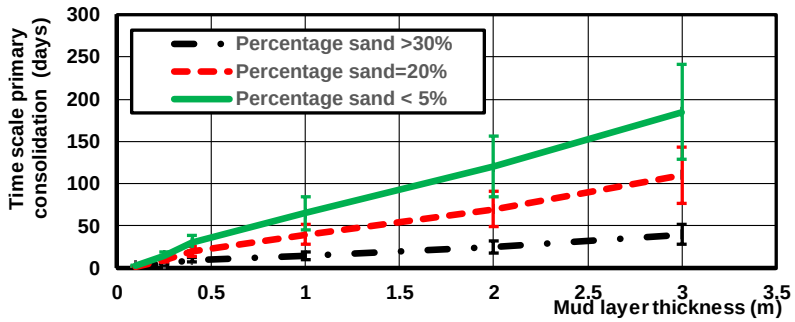

Figure 2.5.1 Time scale of primary consolidation process (Van Rijn and Barth, 2018)

Based on Van Rijn and Barth (2018), the dry bulk density of the top layer (with thickness of the order of 0.5 to 1 m) of the bed at the end of the primary consolidation phase can be related to the percentages of organic matter (p_{org}), clay+very fine silt ($p_{clay\text{-}silt<8\ \mu m}$), silt ($p_{silt\ 8\text{-}63\ \mu m}$) and sand ($p_{sand>63\ \mu m}$), as follows:

$$\rho_{dry} = f_c\,(1 - p_{org}/100)\,[400\,p_{clay\text{-}silt<8\mu m}/100 + 800\,p_{silt\ 8\text{-}63\mu m}/100 + 1600\,p_{sand>63\ \mu m}/100] \qquad (2.5.1a)$$

with:

f_c = consolidation factor; f_c = 0.7 for low consolidation stage of fresh deposits of top layer of bed; f_c=0.9 to 1 for more consolidated deposits of lower subsoil layers at end of primary consolidation phase;
$p_{clay\text{-}silt<8\mu m} + p_{silt8\text{-}63\mu m} + p_{sand>63\ \mu m}$=100%, which implies that the percentage of organic materials and the percentages of clay, silt and sand are determined from two separate subsamples;
p_{org} = percentage organic materials; the percentage organic materials is used in Equation (2.5.1a) to slightly correct the dry bulk density.

Figure 2.5.2 shows the relationship between p_{fines} and the dry bulk density based on Equation 2.5.1a; p_{fines} is assumed to consist of clay and silt fractions with ratio of 1 to 2. The dry bulk density varies from 670 kg/m^3 for p_{fines}=100% to 1600 kg/m^3 for p_{fines}=0. The consolidation factor is set to f_c = 1.

The curve in Figure 2.5.2 is approximated by:

$$p_{fines<63\ um} = 160 - 0.1\rho_{dry} \quad \text{for } \rho_{dry} > 600\ \text{kg/m}^3 \quad \text{or} \quad \rho_{dry} = 1600 - 10\,p_{fines<63\ um}$$

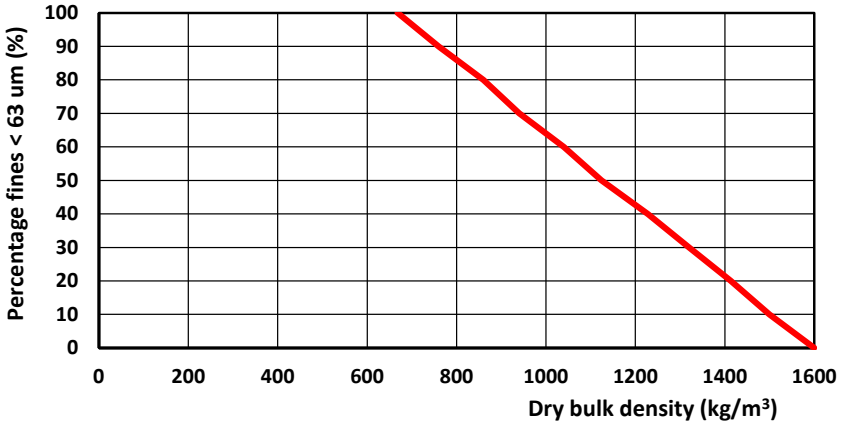

Figure 2.5.2 Dry bulk density as function of the percentage of fines based on Equation 2.5.1a and f_c = 1, $p_{fines} = p_{clay} + p_{silt}$ and $p_{silt} = 2\,p_{clay}$.

An alternative equation to estimate the dry bulk density also valid for very silty samples ($p_{silt} > 50\%$) is:

$$\rho_{dry} = f_c\,(1 - p_{org} / 100)\,[(400\,p_{clay\text{-}silt<8\mu m} / 100 + \{1000 + 200\tanh(0.5\,(p_{silt8\text{-}63\mu m} - 50))\}\,p_{silt8\text{-}63um} / 100 + (1600\,p_{sand>63\mu m} / 100)] \quad (2.5.1b)$$

The term 1000 + 200 tanh (0.5 (p_{silt} - 50)) gives a silt density of 800 kg/m^3 for $p_{silt} < 45\%$ and 1200 kg/m^3 for $p_{silt} > 55\%$ and a gradual transition for p_{silt} between 45% and 55%. Equations 2.5.1a and 2.5.1b provide the same results for $p_{silt} < 45\%$.

Generally, the dry bulk density of the freshly deposited top layer (0.01 to 0.1 m) of the bed surface is somewhat smaller (up to 30%, see Table 3-4 in Boechat Albernaz et al. (2022A (MUSA)). The thin upper part of the layer in direct contact with the water column may have a much lower (fluffy) density of the order of 50% of the overall density of the top layer. The f_c-factor can be used to account for the consolidation stage of the different layers.

Figure 2.5.3 shows the measured and predicted dry bulk densities of the MUSA-samples (see Table 3-13 in Boechat Albernaz et al. 2022A (MUSA)). The predicted results are based on Equation 2.5.1b, using the measured values of $p_{clay\text{-}silt}$, p_{silt} and p_{sand} and a consolidation factor f_c=1. The predicted values overestimate the measured dry bulk densities slightly (10% to 15%) for p_{sand} > 20%. The difference between measured and predicted values is larger for the muddy/silty data of p_{sand} <15%. Somewhat better results can be obtained by using a consolidation factor of $f_c \cong 0.8$ to 0.9 for muddy samples. An outlier in Figure 2.5.2 is the silty sample BB3 from Bengal Bay, with $p_{clay\text{-}silt<8\mu m}$ = 30%, p_{silt} = 64% and p_{sand} = 6% and a dry bulk density of 1260 kg/m^3. Most likely, the clay fraction of particles from 2 to 8 µm is also very silty, resulting in a relatively high density. Equation 2.5.1b yields a value of 925 kg/m^3 for this sample, thereby underestimating the measured dry bulk density with about 25%.

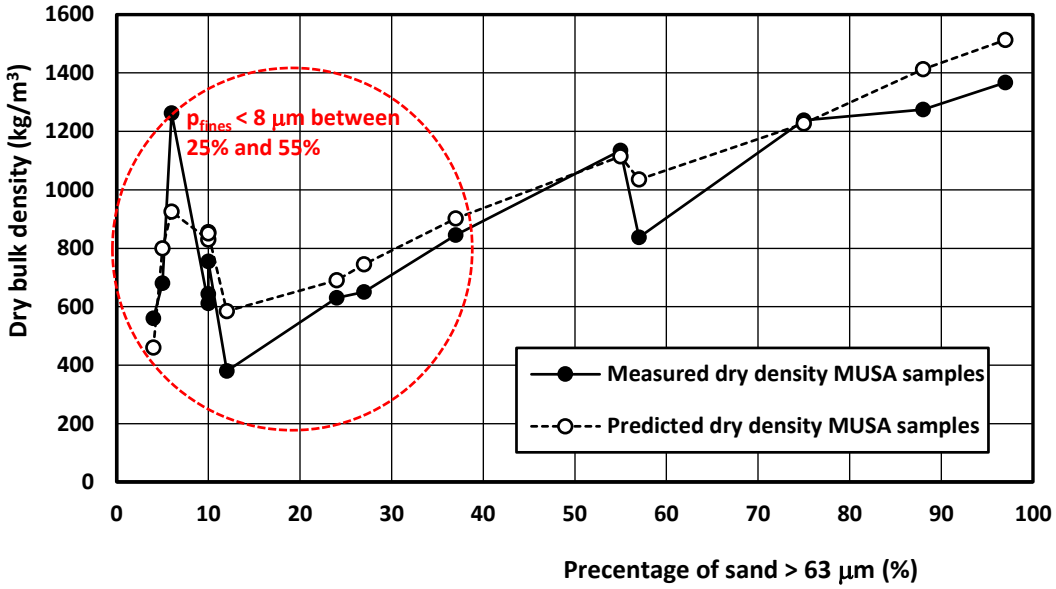

Figure 2.5.3 Measured and predicted dry bulk density (top layer <0.1 m) as a function of sand percentage (Equation 2.5.1b; f_c=1) for MUSA samples.

Figure 2.5.4 shows a comparison of measured and predicted dry bulk densities for the MUSA samples that were collected along the ferry channel near Holwerd. The consolidation factor f_c is set to 1. The measured values represent the dry bulk density of the top layer of the bed <0.1 m. Because the percentage of clay is not determined for these samples, it is assumed that the ratio of $p_{clay\text{-}silt}/p_{silt} \cong 0.5$. The percentage organic materials is estimated to vary between 0% for very sandy samples to 5% for muddy samples, which is based on practical experience with other sediment samples. The predicted values of Equation 2.5.1b overestimate the measured dry bulk densities with about 10% to 15% for p_{sand} > 50%. This may be partly caused by the inclusion of small air bubbles during the transfer of samples

from the Van Veen grab to small sample pots, but also to the consolidation period. Equation 2.5.1b is most valid for the dry bulk density of the subsoil (0.1 to 0.4 m), which generally is somewhat higher (10% to 30%) than that of the top layer <0.1 m. The predicted values are much too high (up to 40%) for the 2 muddy samples with p_{sand} < 25% that were taken close to the ferry pier.

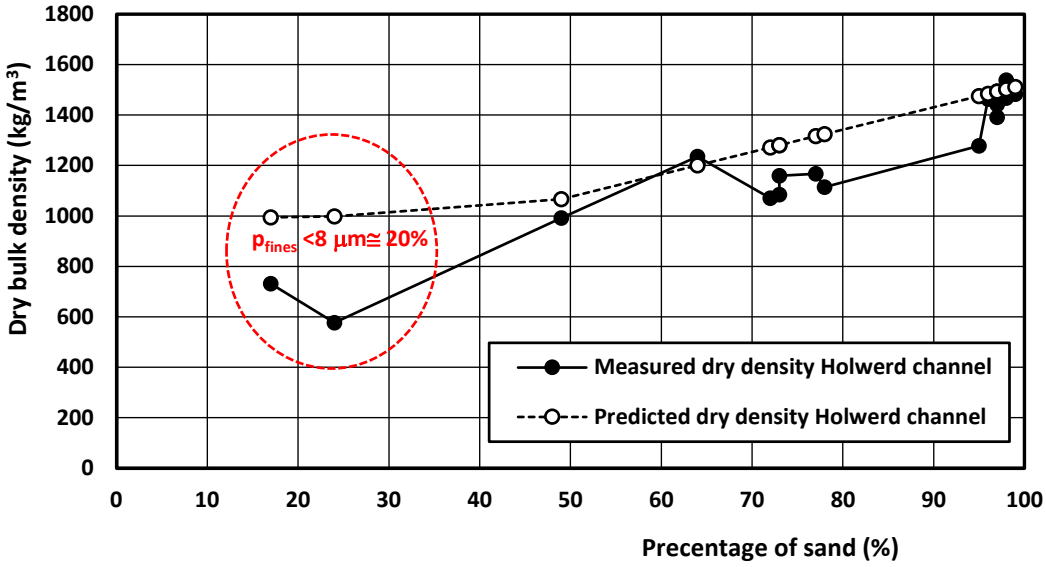

Figure 2.5.4 Measured and predicted dry bulk density (top layer <0.1 m) as a function of sand percentage (Equation 2.5.1b; f_c=1) for samples taken along the Holwerd ferry channel.

An extra set of field samples from sites all over the world was provided by Jan de Nul Group (JDN). The measured sediment characteristics are listed in Table 2.5.1. The predicted dry density values based on Equation 2.5.1a and Equation 2.5.1b with f_c=1 are listed in Table 2.5.2. Two different methods were used to determine the particle size compositions, which are the Laser-Diffraction method and the Settling Hydrometer-Sieving method. The SHS-method yields much higher values (twice as high!) for the clay-silt fraction < 8 µm for samples AA02, AB01 and AC01 (table 2.5.1), which emphasizes the importance of the methodology for determining the particle size composition.

The predicted dry density values based on the sediment composition as determined by the LD-method are much too high (factor 2), except for sample AC01 (Bengal Bay sample). The predicted dry density values based on the sediment composition as determined by the SHS-method are substantially lower and in better agreement with the measured values, except for sample AC01. Better prediction results can be obtained by using a lower f_c-factor (≅0.7) for the muddy samples.

Table 2.5.1 Sediment composition of 6 samples that were provided by JDN Group.

	Fraction organic materials (%)	Laser Diffraction method (LD)				Settling Hydrometer Sieving method (SHS)			
		$p_{clay<}$ 2 µm (%)	$p_{cl-silt}$ <8µm (%)	$p_{silt\ 8-}$ 63 µm (%)	p_{sand} >63 µm (%)	$p_{clay<}$ 2 µm (%)	$p_{cl-silt}$ <8µm (%)	p_{silt} 8-63 µm (%)	$p_{sand>}$ 63 µm (%)
AA02 Belgium	4	2	33	54	13	40	65	30	5
AB01 Belgium	3	2	32	51	17	40	65	20	15
AC01 Bengal Bay	1	1	13	52	35	20	30	55	15
AD01 Guyana	-	7	45	39	16	-	-	-	-
AE01 Equador	-	2	32	47	21	-	-	-	-
AE02 Equador	-	2	30	43	27	-	-	-	-

Table 2.5.2 Measured and predicted dry bulk density of 6 samples that were provided by JDN Group.

Sample	Measured dry density	Predicted dry density (kg/m³) based on Equation 2.5.1a		Predicted dry density (kg/m³) based on Equation 2.5.1b	
		based on LD-values	based on SHS-values	based on LD-values	based on SHS-values
AA02	340	748	551	954	551
AB01	450	784	627	928	627
AC01	1110	998	760	1175	967
AD01	380	725	-	725	-
AE01	380	815	-	823	-
AE02	420	870	-	870	-

2.6 Settling velocities

Various MUSA experiments provide settling velocity data. Laboratory experiments with the LABSFLOC-2 are carried out to determine the settling velocities of individual particles and flocs for sediment samples from different estuaries and tidal basins. Hindered settling velocities are determined for these samples based on consolidation experiments in settling tubes. Field measurements with multiple different instruments have been caried out to compare the result from different instruments.

2.6.1 Settling velocities of particles and flocs in MUSA samples; laboratory tests

The settling velocities of individual particles and flocs in prepared sediment suspensions are determined for some of the MUSA sediment samples by using the LABSFLOC-2 video camera system in laboratory setup. This system utilizes a low-intrusive, high resolution video camera to observe flocs as they settle in a settling column. MUSA-samples from Noordpolderzijl (NL), the Western Scheldt (NL), the Scheldt river (BE), the Plymouth estuary (UK) and Bengal Bay (Bangladesh) are analyzed. Figure 2.6.1 and Figure 2.6.2 show the resulting settling velocity distributions for low (< 500 mg/L) and high (> 1500 mg/L) initial concentrations in laboratory conditions. The settling velocities are in the range of 0.5 to 30 mm/s, although settling velocities in the range from 1 to 10 mm/s are much more common. The median settling velocity of all samples is about 8 ± 4 mm/s. The percentage of fines < 35 μm with a settling velocity < 1 mm/s is relatively small (< 15%).

The floc sizes d_{10}, d_{50}, d_{90} are estimated from similar curves for the floc size (not shown; see Van Rijn et al., 2022). The floc sizes are in the range of 50 to 350 μm. The median floc size of all samples is about 150 ±50 μm.

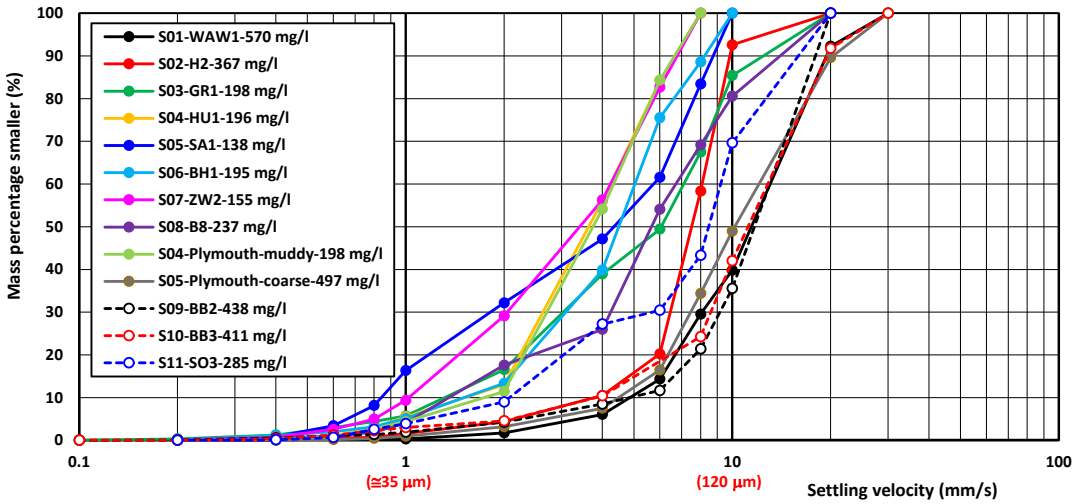

Figure 2.6.1 Settling velocity distributions for MUSA-samples as determined by the LABSFLOC-2 video camera system with low initial concentrations (<500 mg/L).

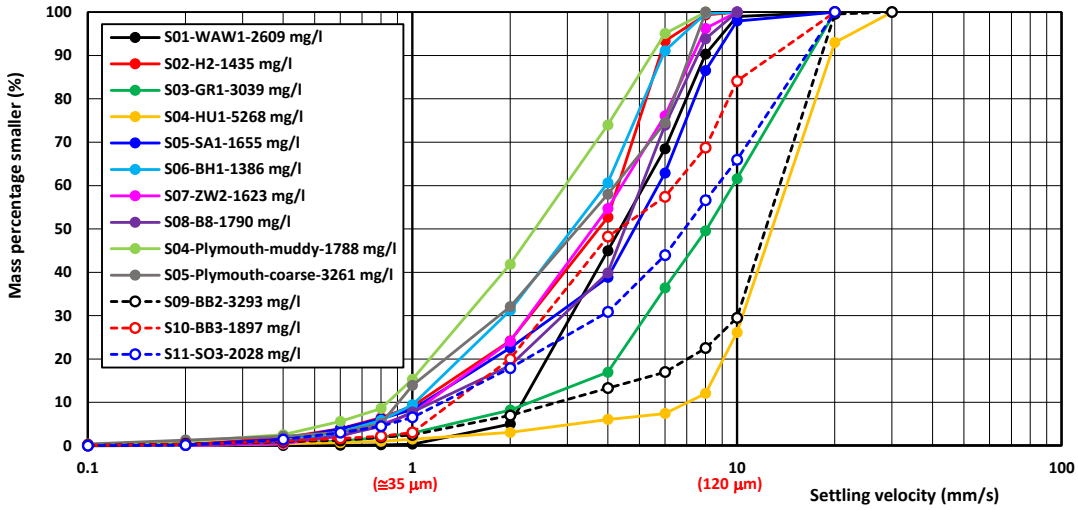

Figure 2.6.2 Settling velocity distributions for MUSA-samples as determined by the LABSFLOC-2 video camera system with high initial concentrations (>1500 mg/L).

The effect of the initial concentration on the median settling velocity is shown in Figure 2.6.3. The settling velocity increases strongly for increasing concentrations in the low concentration range (< 500 mg/l), most likely because of flocculation. The median settling velocities are relatively low for initial concentrations >1500 mg/l, with exception of the two values of very sandy samples. The reduction of the settling velocity for higher concentrations may be caused by hindered settling processes affecting the macro-flocs. However, the onset of the hindered settling processes is generally believed to occur for concentrations higher than about 5 000 to 10 000 mg/L (Van Rijn 1993).

Figure 2.6.4 shows the measured median settling velocity ($w_{s,50}$) as function of the percentage sand in the sample. The settling velocity is, on average, higher in a suspension with low initial concentrations (< 500 mg/l) than in a suspension with high initial concentrations (> 1000 mg/l), which is most likely related to flocculation and hindered settling effects. The variability may also be related to the sampling and test procedure.

Three samples (WesternScheldt-HU1; Plymouth-coarse and Bengal Bay-BB2) are very sandy with percentage of sand >70%. The median settling velocity of these samples is most likely in the order of 10 mm/s given the high sand content (median diameter of the order of 100 µm). Each of these very sandy samples is tested at a low and a high initial concentration, resulting in 6 test results. Four test results show median settling velocities > 10 mm/s, but two test results show relatively low values in the range of 3 to 3.5 mm/s. Sample HU1 has a relatively low settling velocity of 3.5 mm/s at a low initial concentration and sample Plymouth-coarse shows the opposite behaviour with a low settling velocity of 3.3 mm/s at a high initial concentration. Thus, these very sandy samples show a rather high variability range of 3 to 14 mm/s, which is difficult to explain for sandy samples. This high variability may be partly related to imperfections of the sample preparation procedure, which involves the preparation of a base suspension with very small amounts of sand and mud. Having below-average amount of coarse material in the subsample leads to an underestimation of the median settling velocity.

Although there is considerable scatter (variability), the trendlines in Figure 2.6.4 show a weak increase of the median settling velocity for increasing percentage of sand; the settling velocity increases from about 2 to 8 mm/s for very muddy samples to about 4 to 14 mm/s for very sandy samples. The settling range of 2 to 8 mm/s for muddy samples is rather high in comparison to the settling results of the traditional sedimentation methods (e.g. hydrometer), which typically give $w_{s,50}$-values in the range of 0.1 to 2 mm/s for muddy samples.

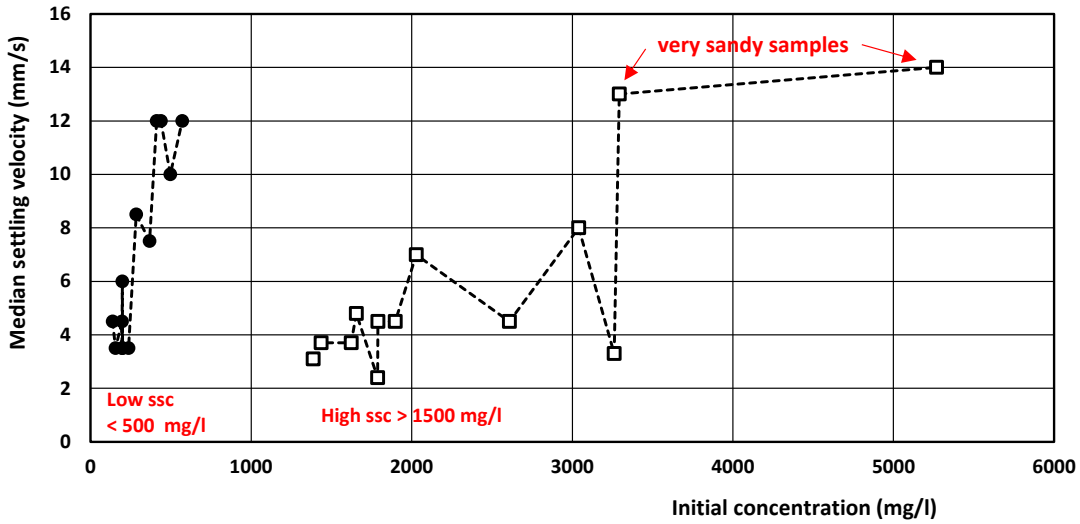

Figure 2.6.3 Median settling velocity of MUSA-samples as function of the initial concentration.

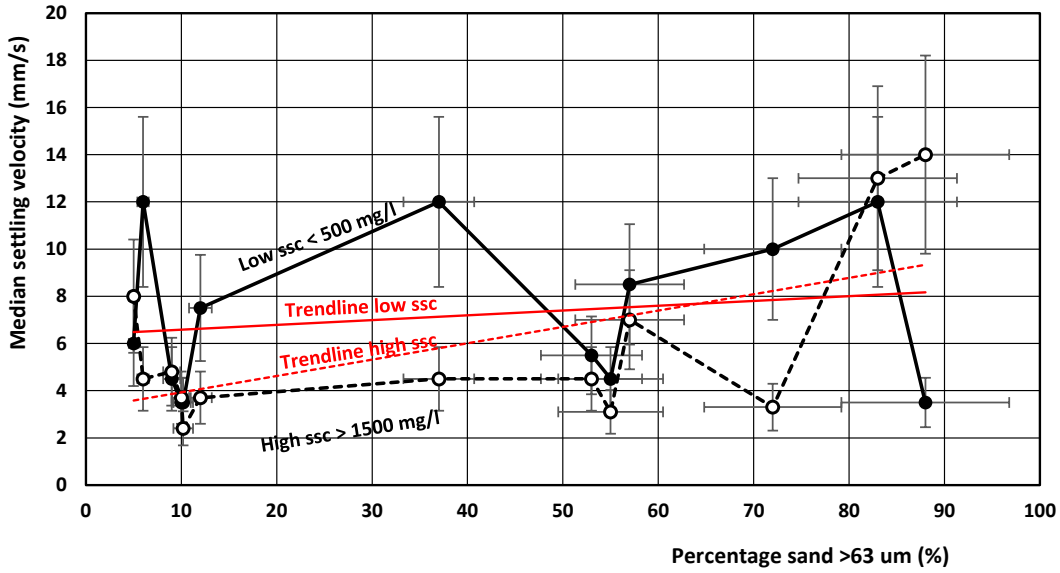

Figure 2.6.4 Median settling velocity of MUSA-samples as function of percentage of sand for low (<500 mg/L) and high (>1500 mg/L) initial concentrations.

The present results with relatively high floc sizes and settling velocities raise the question whether the video-camera results (LABSFLOC-2-instrument) have a bias towards the better visible macro-flocs with higher settling velocities. Analysis of the basic data shows that the amount of data in each population with floc sizes < 30 μm is extremely small: often zero and up to 4% in some cases. Based on this, two conclusions are possible: particles/flocs < 30 um are not present in the MUSA-samples or the LABSFLOC-2-system (camera and software) is not capable to observe particles/flocs smaller than 30 μm. This will be discussed further based on field measurements with multiple instruments in Section 2.6.3.

2.6.2 Hindered settling velocities; laboratory tests

The effect of high sediment concentrations on the settling velocity (i.e. hindered settling) was studied by performing sedimentation tests in settling columns with initial concentrations in the range of 10 to 300 kg/m^3. The initial concentrations are made by diluting the original samples using native (sea)water. Such

a test involves the generation of a uniform suspension by mechanical stirring after which the settling process starts. The hindered settling velocity can be derived from the settling of the sediment interface with respect to the initial position over the measured time period. The results are presented as function of the initial sediment concentration > 10 kg/m^3 in Figure 2.6.5. The maximum settling velocities are in the range of 0.05 to 2 mm/s at initial concentration of about 10 kg/m^3. For concentrations > 10 kg/m^3, there is a clear decrease in settling velocity. The settling velocity decreases by a factor of 20 for concentrations in the range of 10 to 100 kg/m^3. The settling velocity is in the range of 0.01 to 0.1 mm/s for concentrations of 200 kg/m^3. Gel concentrations are of the order of 150 kg/m^3.

The very muddy samples (NPZ-B5/H2; WS-PA1) yield the lowest settling velocities. The sandy and silty samples (WS-HU1; WS-APP; PLUK4; WS-BH1) yield the highest settling velocities. The results of the MUSA samples are in reasonable agreement with earlier data (Van Rijn, 1993), indicated by the dashed green curves in Figure 2.6.5. Assuming a gel concentration $c_{gel} \cong 150$ kg/m^3, the decrease in settling velocity in the concentration range of 10 to 100 kg/m^3 can be represented by a factor $(1\text{-}c/c_{gel})^n$ with $n \cong 3$.

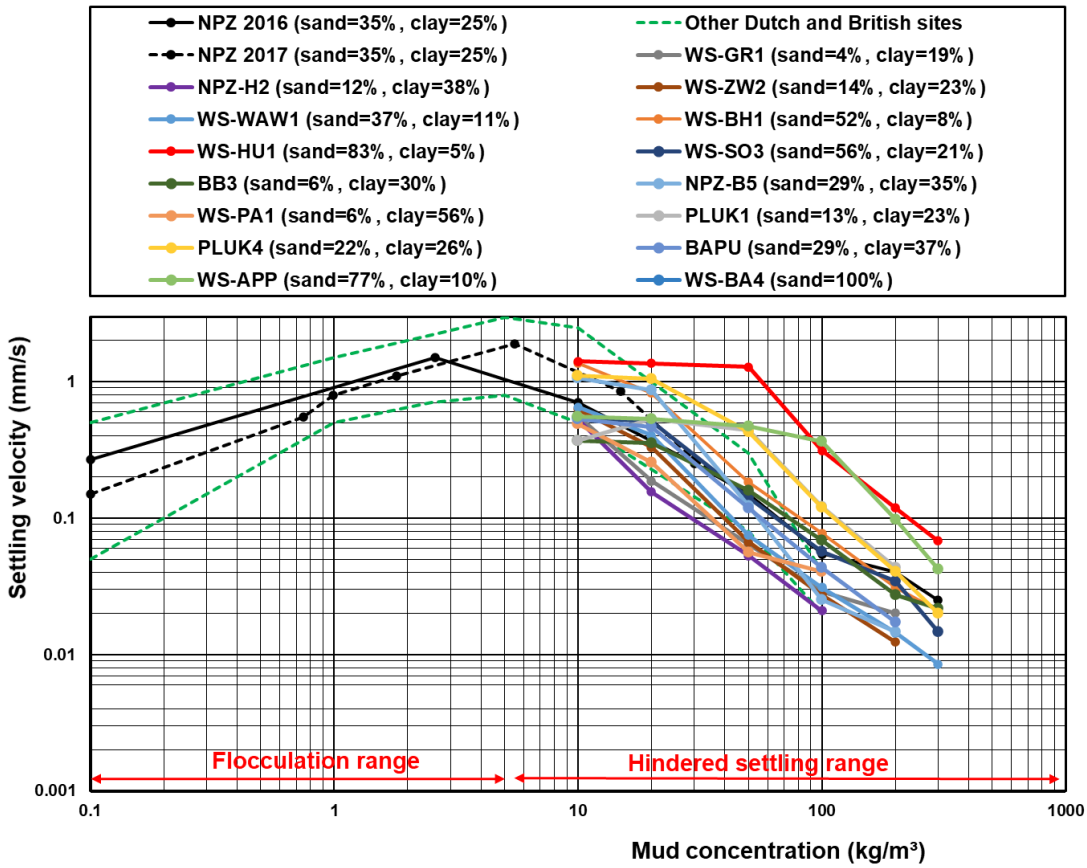

Figure 2.6.5 Settling velocity of mud-sand samples for different initial concentrations.

Te Slaa et al. (2013) performed a detailed study of hindered settling velocities of very silty samples from the Yangtze Estuary and the Yellow River delta. The silt percentages of their samples are in the range of 50% to 85%. The results show that a transition in settling/consolidation behaviour occurs around clay contents of about 10%. Above this threshold, sediment mixtures consolidate in a cohesive way, whereas for smaller clay percentages only weak cohesive behaviour occurs. The settling behaviour of silt-rich sediment is found to be in analogy with granular material at concentration below 150 g/l. Above 150-200 g/l, the material settles in a hindered settling regime and segregation is limited or even prevented. The gelling concentrations is in the range of 100 to 150 kg/m^3.

Table 2.6.1 lists results for hindered settling velocities of silty samples measured in the MUSA-project and those of the Yangtze Estuary and Yellow River delta (Te Slaa et al., 2013). The settling velocities of the silty samples from Bengal Bay are in good agreement with those of the samples from China. The silty sample from the Western Scheldt has somewhat smaller settling velocities. This may be caused by the relatively high clay content of 19% in this sample, whereas the samples from China have clay contents in the order of 10%.

Sediment concentration range (kg/m^3)	Hindered settling velocity (mm/s)			
	BB3 (Bengal Bay; MUSA) p_{silt}=64%	GR1 (Western Scheldt; MUSA) p_{silt}=77%	Clay-fine silt fraction in overlying suspension (Yangtze Estuary) p_{silt}=60-85%	Granular fraction of coarse silt and fine sand (Yangtze Estuary and Yellow river delta) p_{silt}=50-80%
10-25	0.6-0.3	0.5-0.15	0.5-0.3	<1
25-50	0.3-015	0.15-0.07	0.3-0.1	1-5
50-100	0.15-0.07	0.07-0.03	0.2-0.1	1-6
100-150	0.07-0.04	0.03-0.025	0.1-0.03	2-6
150-200	0.04-0.025	0.025-0.015	0.03-0.01	0.5-5
200-300	0.025-0.02	-	0.01-0.003	0.5-3

Table 2.6.1 Measurement data of hindered settling velocities in silt-rich MUSA samples and in samples from China of Te Slaa et al. (2013).

2.6.3 Field measurements with multiple instruments

In the MUSA project, settling velocity measurements were carried out with multiple instruments at the ferry pier in Holwerd in the Dutch Wadden Sea (MUSA-report on settling velocities and floc sizes by Van Rijn et al., 2023, see Table 1.2). Samples were taken near the ferry pier, where the water depth varies between 1.5 and 4 m over the tidal cycle and where the local sediment bed consists of soft, muddy sediments with a wet density of about 1400 kg/m^3 and a dry density of about 650 kg/m^3. The settling velocities were determined by using the LABSFLOC-2 video camera system and the mechanical PIRANHA settling tube (Figure 2.6.6). The PIRANHA-instrument was used to take water-sediment samples for the LABSFLOC-2 instrument (operated in a van close to the site) and to do in-situ settling tests.

2.6.3.1 Results from the in-situ settling tube (PIRANHA)

The PIRANHA-instrument (P-instrument) is a combination of a water-sediment sampler and – after placing it in upright position standing on its tail vin – a settling tube (Figure 2.6.6). The P-instrument has valves on both ends and is lowered in horizontal position with open valves to the sampling point in the water column. The valves are closed by pulling a rope, after which the instrument is raised in horizontal position and transferred to the on-site laboratory (Figure 2.6.7). There, it is gently turned over a few times to create a homogeneous suspension and then placed in vertical position to start the settling process (t=0). Small subsamples are taken by opening a small tap on the side of the tube at preset times over a period of 3 hours. After determining the sediment concentration for each subsample, the settling velocity curve can be derived from the decrease of the sediment concentration over time.

Comparative laboratory measurements have shown that the settling results of the P-instrument are in good agreement with the settling results of the hydrometer tests (Van Rijn & Koudstaal, 2021). This implies that the side-tap does not introduce significant errors. It is noted that the P-instrument is designed for measurements of the settling velocity of mud particles and microflocs. It cannot very accurately measure high settling velocities of sand and macroflocs (range of 5 to 10 mm/s), as the first subsample is taken only after 1 minute when the initial eddies have died out. It is assumed that 100% of the sediment has a settling velocity < 10 mm/s, which corresponds to the settling velocity of a 120 micron sand particle. An additional cause of errors in results of the P-instrument may be the breakup of flocs into smaller flocs

due to the vibrations that are generated during closure of the valves on both ends of the tube or due to homogenisation of the sample, resulting in more smaller flocs with a lower settling velocity.

Figure 2.6.6 Pictures of the PIRANHA-instrument, which is used to take samples and to perform settling experiments.

Figure 2.6.7 Test procedure with the PIRANHA-instrument: (A) instrument is lowered with open valves and (B) raised with closed valves and (C) samples are transferred to the settling. Alternatively (D), samples are pumped into the settling tube.

A detailed description of in-situ settling tests (IST) and laboratory settling tests (LST) is included in MUSA-report on field measurements by Boechat Albernaz et al. (2022C (MUSA)). The samples of the LST tests are taken both by using a pump and using the P-instrument. Figure 2.6.8, Figure 2.6.9 and Table 2.6.2 show the most important results for samples with low and high concentrations. At low concentrations, the pumped samples yields a much higher fraction of fines than the samples taken the P-instrument. This may be caused by the destruction of the flocs in the pump. At high concentrations, the results are fairly similar for the different samples, although results of the IST tests show more variations. The median settling velocity increases for high concentrations, which is probably due to effects of flocculation.

Another method to determine the average mass-weighted settling velocity of the whole population of particles in the suspension is to assume that the decrease of the sediment concentration is represented by an exponential distribution:

$$c = c_o \exp(-w_s t / h) \qquad (2.6.1)$$

with c_o = initial concentration, t = time , h = settling depth, w_s = settling velocity.

Using the data of the first measurement after 60 seconds, the average mass-weighted settling velocities of the population as a whole can be determined, resulting in values in the range of 0.15 to 0.77 mm/s

(see values between brackets in Table 2.6.2). These values are mostly smaller than the median settling velocities of the settling tube data.

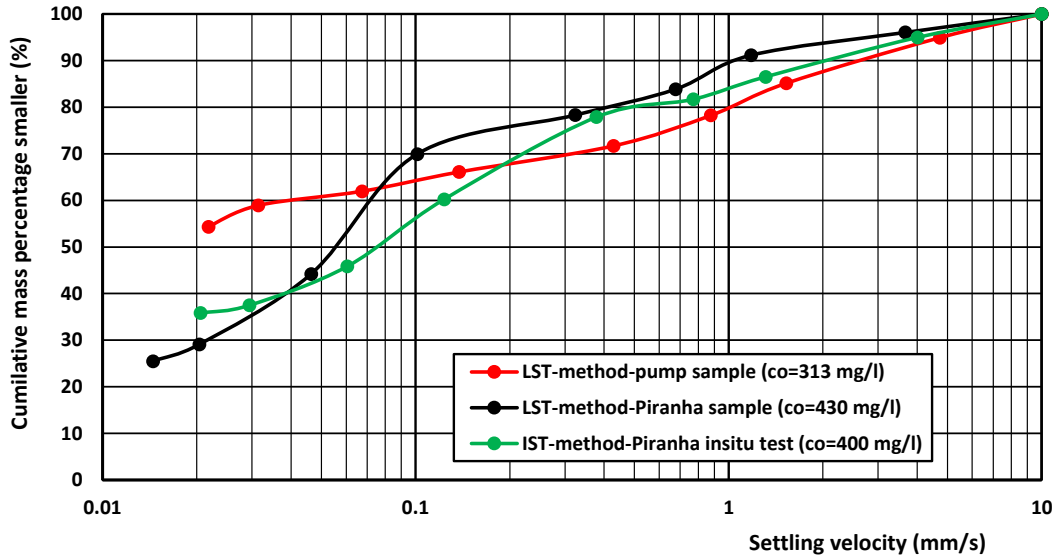

Figure 2.6.8 Settling velocity curves derived from settling tube tests with low concentrations (300 to 400 mg/l).

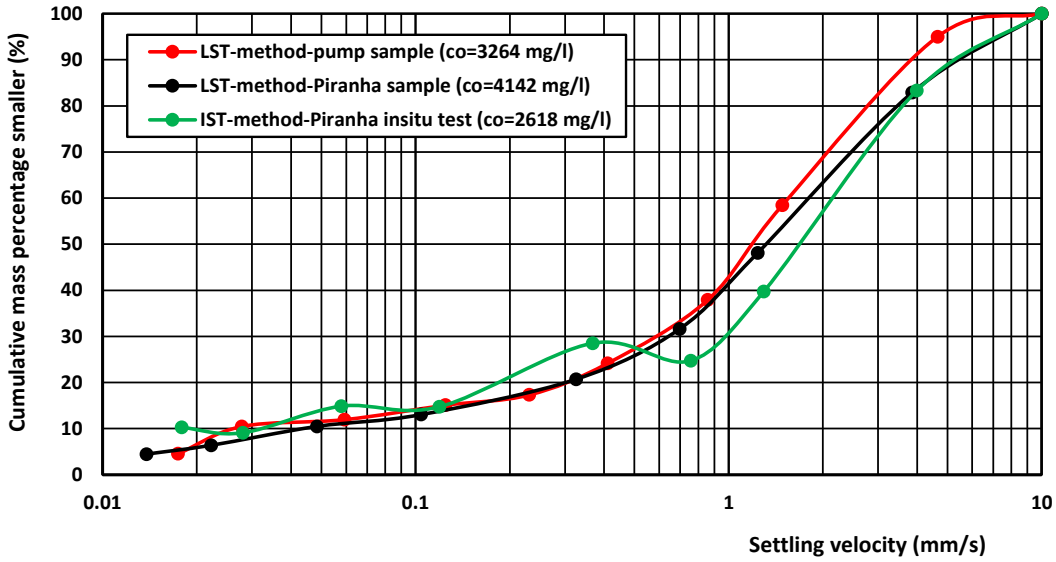

Figure 2.6.9 Settling velocity curves derived from settling tube tests with high concentrations (2500 to 4000 mg/l).

Table 2.6.2 Characteristics of the settling velocity data. The mass-weighted settling velocity is indicated between brackets.

Sampling method	Settling velocity (mm/s) Low concentrations 300-400 mg/l				Settling velocity (mm/s) High concentrations 2500-4000 mg/l			
	$w_{s,10}$	$w_{s,50}$	$w_{s,90}$	$w_{s,max}$	$w_{s,10}$	$w_{s,50}$	$w_{s,90}$	$w_{s,max}$
Laboratory Settling Test (LST) -Pump	<0.01	0.02 (0.02)	2.5	4.7	0.02	1.0 (0.25)	3.8	4.7
Laboratory Settling Test (LST) -PIRANHA	<0.01	0.055 (0.015)	1	3.7	0.05	1.5 (0.76)	5.5	3.9
Insitu Settling Test (IST) -PIRANHA	<0.01	0.075 (0.02)	2	4.0	0.035	1.8 (0.77)	5.5	4.0

2.6.3.2 Results from the LABSFLOC-2 video camera system

The LABSFLOC-2 video camera system, introduced in Section 2.6.1, was set up in a van to be used during the measurement campaign at the field site of Holwerd (NL). The 5 mL samples that are used in the LABSFLOC-2 were taken from the same sample as used in the settling tubes. The results of all field samples based are presented in Figure 2.6.10. The median floc sizes are in the range of 80 to 160 μm (120±40 μm). The median settling velocities are in the range of 2 to 12 mm/s (7±5 mm/s). This variation may be due to variations in the sand content in the samples.

Detailed analysis of the test S06 (Figure 2.6.10) shows that about 65% of the suspended mass is in the three highest velocity classes 10 to 30 mm/s, although only 15% of the measured settling velocity values are > 10 mm/s. As a result, the median settling velocity ($w_{s,50}$) is quite high (12 mm/s) for test S06. The mean settling velocity of all data points (259) is 3.5 mm/s. Thus, the median settling velocity based on mass-related percentages is strongly related to the (largest, heaviest) flocs with the highest settling velocities.

The effect of the initial sediment concentration on the median ($w_{s,50}$) settling velocity is shown in Figure 2.6.11. Except for test S07-385 mg/l, the settling velocity increases for initial concentrations < 800 mg/L and decreases for initial concentrations > 800 mg/l. The results in Figure 2.6.11 are a bit suspicious in the sense that relatively low settling velocities are measured by the LABSFLOC-2 for relatively high mud concentrations. This may partly be related to the extremely small subsample of 5 mL: the mud concentration of one single subsample of 5 mL may not be representative for the mud concentration of the larger water-sediment sample of about 1 liter.

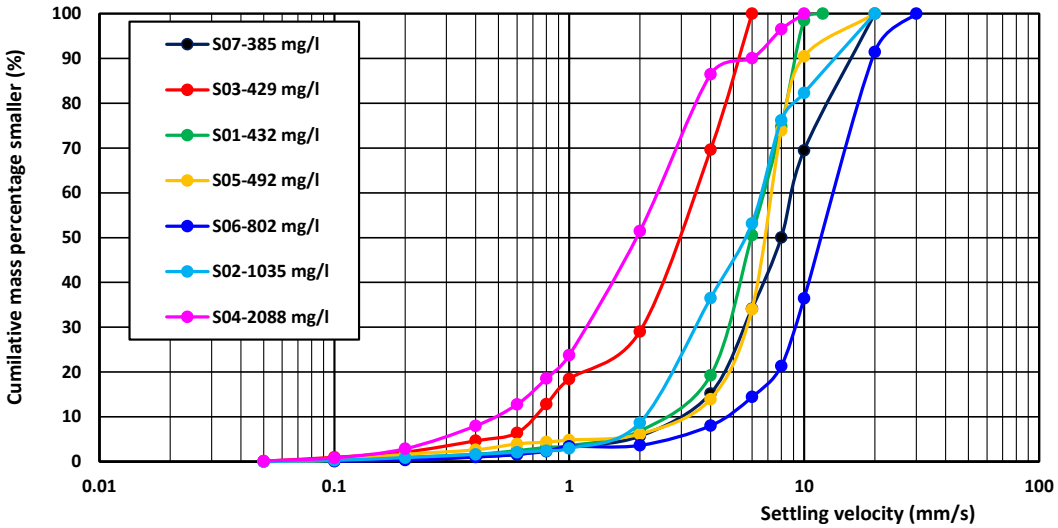

Figure 2.6.10 Settling velocity curves derived from LABSFLOC-2 video camera system.

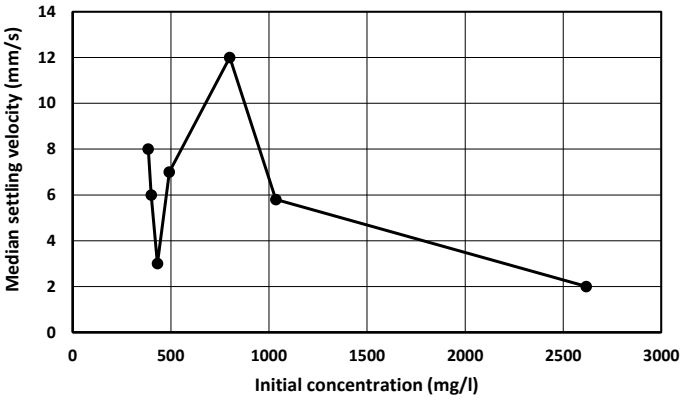

Figure 2.6.11 Relation between the initial concentration in samples and the median settling velocity.

2.6.3.3 Comparison of results from different instruments

The settling velocity distributions of samples with low and high initial concentrations as measured by the P-instrument and the LABSFLOC-2 are compared in Figure 2.6.12. For high initial concentrations > 200 mg/L, the median settling velocities are reasonably similar for both methods. The median settling velocities are in the range of 1.5 to 2 mm/s. The P-instrument measures a much larger fraction with low settling velocities than the LABSFLOC-2: settling velocities are below 0.1 mm/s for 20% of the total sediment mass for the P-instrument and for only 2% of the total sediment mass for the LABSFLOC-2.

The results of both methods deviate significantly for low initial concentrations. The P-instrument yields a median settling velocity in the order of 0.1 mm/s for an initial concentration of about 400 mg/l, whereas the LABSFLOC-2 gives a median settling velocity in the order of 2 to 12 mm/s. Based on the results of the P-instrument, 80% of the particles have a settling velocity < 0.5 mm/s, whereas based on the LABSFLOC-2 maximum 10% of the particles have a settling velocity < 0.5 mm/s.

The deviations between the results of different instruments at low initial concentrations may be because the amount of the larger macro-flocs is underestimated by the P-instrument, as the fragile flocs may have been broken during sampling (i.e. bias towards smaller sizes). Another option is that the amount of individual particles and mini-flocs (< 30 μm) is severely underestimated by the LABSFLOC-2 (i.e. bias

towards larger sizes), as sizes smaller than about 30 μm are less frequently measured. This fraction < 30 μm is generally relatively high in conditions with relatively low concentrations < 500 mg/L when flocculation processes are not so strong. Consequently, the median settling velocity of the LABSFLOC-2-instrument for low concentration conditions may be systematically on the high side (values >1 mm/s).

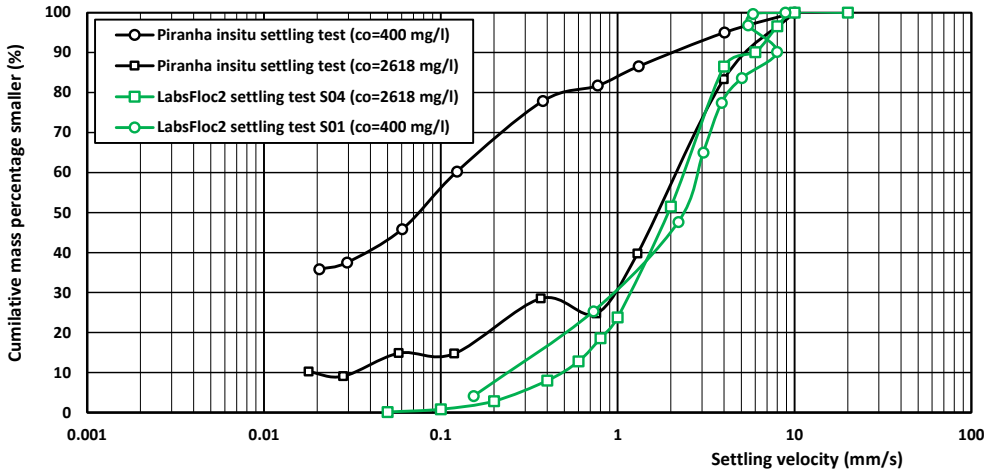

Figure 2.6.12 Settling velocity distributions of samples measured by the PIRANHA-instrument and the LABSFLOC-2 video camera system.

Good estimates of the settling velocity are of prime importance for engineering projects regarding the siltation in channels and harbour basins. However, the in-situ settling tube and the video-camera system provide very different estimates for the median settling velocity, as results for the PIRANHA instrument are in the range of 0.1 to 2 mm/s and results for the LABSFLOC-2 are in the range of 2 to 10 mm/s. In engineering projects, the total mass (and volume) of sediment that deposits in channels or harbour basins is most relevant. Larger flocs with a relatively high settling velocity have a larger mass (and volume) and are therefore most relevant for the total deposition. If a small percentage of the smaller flocs are not represented in the median settling velocity, the total deposition rate may be only slightly affected.

In sediment transport models, generally two or three sediment fractions are required for accurate modelling of the fines with a wide settling velocity range of 0.1 to 10 mm/s. Settling velocity curves can be used to estimate the most relevant settling velocity ranges. In mixed-sediment environments, flocs may consist of both mud and sand, resulting in relatively high settling velocities as derived from video registrations of settling velocities. The standard models that separate the settling of sand and mud may then over-simplify the involved physics.

In many (fine) sediment transport models, the fraction 0.5-2 mm/s is the dominant fraction. These models are capable of providing reasonable estimates of deposition rated in comparison to dredged volumes. For example, the mud sedimentation model of Deltares that is used to provide estimates of dredging volumes in the navigation channel from Holwerd to Ameland (Grasmeijer et al., 2021) uses two sediment fractions with settling velocities of 0.4 and 1.5 mm/s. If the LABSFLOC-2 results with settling velocities in the range of 2 to 10 mm/s would be adopted in this model, the deposition would be largely overestimated.

Conclusive proof on the correctness of settling velocities of the PIRANHA-instrument and the LABSFLOC-2 video camera system is not yet available. More laboratory experiment and field monitoring is required, with focus on:

1. Whether the LABSFLOC-2 is correctly identifying the settling velocities of both micro- and macroflocs and whether the settling velocities in very small subsamples are representative for field conditions;
2. Why the particles with relatively high settling velocities are so dominant in the results of the LABSFLOC-2 system;
3. What the effect of sand particles is on the measured settling velocities in the PIRANHA-instrument and in the LABSFLOC-2 video camera system.

3 Description flume and field experiments

Erosion experiments have been carried out with four types of sediment beds: three short beds and one long bed (section 3.1). The flume experiments have been executed to determine critical bed shear stresses (section 3.2), erosion rates (section 3.3) and mud and sand transport (section 3.4). More detailed descriptions of the experiments can be found in Boechat Albernaz (2022A (MUSA), 2022B (MUSA)).

3.1 Critical bed shear stress

3.1.1 Short bed tests with remolded natural mixtures

Important characteristics of the short bed tests with remolded mixtures of mud-sand are the following:

- Initially, the bed surface is very smooth, often with a grey film on top of the surface after overnight consolidation. The bed surface is scraped off to have the sample levelled with the bottom of the flume;
- Forms of scour (craters and grooves) are often generated around small initial disturbances and at the edges of the sediment sample (i.e. surface erosion);
- Sudden failure of the bed surface occurs locally, with lumps of sediment breaking loose from the surface (i.e. mass erosion).

3.1.2 Short bed tests with diluted natural mixtures

To determine the critical bed-shear stress for samples with lower dry density values than the ones that were discussed in the previous section, some of the samples (H2, GR1, ZW2, WAW1 and BH1) have been diluted by using native (saline) water. The dilution percentages are in the range of 10% to 40% of the original sample volume. The experiments and the results are discussed in detail in the MUSA-report on laboratory experiments by Boechat Albernaz et al. (2022A (MUSA)).

The diluted samples were thoroughly mixed and tested in the flume after overnight consolidation. The characteristics of the erosion of the diluted samples is very similar as for the remolded samples: Initially, the bed surface is relatively smooth. Scour marks start to form (i.e. surface erosion) and suddenly the bed surface fails locally (i.e. mass erosion).

3.1.3 Short bed tests with undisturbed field samples

The most important characteristics of the erosion of undisturbed field samples during short bed tests with currents and waves are listed below. The undisturbed field samples were collected along the banks of the Western Scheldt Estuary near Bath (samples BA-4, BA-APP and BA-PU).

- On top of the sediment sample a film with fluffy mud, benthic fauna, structures, tubes, holes and bulges is present. This layer creates bonding effects, but also additional roughness and turbulence;
- The start of erosion is being limited by the presence of a cohesive top layer;
- Bed forms do not develop during the experiments with these samples.

The flume experiments with undisturbed field samples showed the presence of many tube worms that are partly sticking out of the sediment bed. These tube worms are a variety of marine worms with diameters in the order of 0.5-1 mm, living in tiny tubes. The tubeworms anchor their tail to an underwater surface and secrete a mineral tube around their body, into which they can withdraw their entire body. The tubes are made of a tough but flexible material, coated with a layer of detritus, mud and sand.

The biofilm and secretions showed to have a stabilizing effect on the sediment sample during the flume experiments by holding the sediment particles together. On the other hand, tubes and structures increased the roughness and therefore the turbulence after parts of the top layer started to erode. Therefore, the benthic biota was both stabilizing and destabilizing the bed. Most parts of the sample

remained stable during the flume experiments. The tubes were moving forward and backward in the oscillating water motion. Mud erosion occurred gradually.

In addition, the effect of shells, gravels and pebbles on the critical bed-shear stress was investigated by placing these on a short mud-sand bed in a flume with unidirectional flow. This is discussed in section 2.8.7.

3.1.4 Long bed tests with remolded artificial mixtures with currents and waves.

Several long-bed experiments were carried out with remolded artificial mixtures of sand and mud. In addition, one experiment was carried out with a remolded natural mixture of silty mud from Bengal Bay (MUSA report on laboratory experiments by Boechat Albernaz et al., 2022B (MUSA)). The most important characteristics of the long bed experiments with artificial mixtures of sand and mud and with waves and currents are listed below.

- Relatively low, symmetrical isolated ripple-type sand spots are developing during the experiment, with muddy spots between the ripple crests (see Figure 3.1.1). Sand particles are re-organizing into low ripples, migrating as bed load transport. Mud is being transported as suspended load;
- For more energetic hydrodynamic conditions, sandy ripples are more asymmetrical and start to migrate over the muddy spots. Mud is being entrained from the muddy spots between the sandy ripple crests;

The silty mud from Bengal Bay was quite stable for most of the wave conditions during the long bed experiment. Very flat ripples < 1 mm high developed when waves were almost breaking.

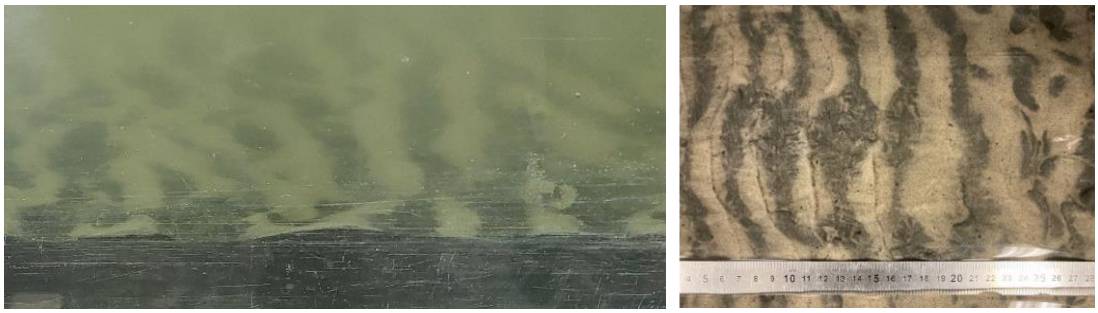

Figure 3.1.1 Artificial mixture developing into sandy ripples (lighter-coloured) and muddy (darker) troughs between sandy crests.

3.2 Critical bed shear stresses for erosion of sand-mud mixtures

All flume experiments described in section 3.1 are used to determine critical bed shear stresses.

3.2.1 Methods for determining the critical bed shear stress

The critical bed-shear stresses (cbs) for erosion of sand-mud mixtures are determined in different types of flume experiments with short (<0.5 m) and long sediment beds (approximately 3 m). Herein, two types of critical bed-shear stresses are distinguished, which are the critical bed-shear stress for particle erosion and surface erosion. Particle erosion is defined as the (lowest) flow stage at which individual sand particles and/or fine mud particles/flocs are eroded from the sediment surface. The critical shear stress for particle erosion of individual mud and sand particles is assumed to be almost the same. Usually, mud particles are washed away first, before sand particles start sliding or rolling over the bed. Surface erosion is defined as the flow stage at which the formation of ripples, grooves or small craters at the sediment surface occurs. Often, these small-scale bed features are generated at initial disturbances in the sediment sample that are introduced during the sample preparation.

The critical bed-shear stress has been studied for a range of conditions in different flume experiments. These experiments vary in the length of the bed (short <0.5 m and long = 3 m beds) and the way in which the sediment sample is prepared. Many of the experiments were carried out with natural remoulded

sediment mixtures. In several experiments, diluted mixtures or artificial mixtures with an additional amount of sand were used. In addition, undisturbed field samples were used in some of the experiments (Boechat Albernaz et al., 2022B (MUSA)).

3.2.1.1 Observations

For all the flume experiments, the critical bed shear stress was determined by two methods: i) by visual observations and ii) based on timeseries of the observed suspended sediment concentrations (SSC) in the flume for a selected set of experiments. This is done by deriving the erosion rate from the increase in SSC over time. The critical bed shear stress that results from this analysis represents the erosion threshold for surface erosion. The results of this analysis are more reliable for a larger increase in SSC during the flume experiments, such as for the experiments with diluted sediment samples.

The critical bed shear stresses that follow from visual observations of eight flume experiments are compared to the critical bed shear stresses that follow from the SSC analysis in Figure 3.2.1 and Table 3.2.1. In general, the different methods lead to similar results, which increases our confidence in the accuracy of visual observations to determine the critical bed shear stresses, also for other flume experiments for which no SSC data is available. Only for experiment H2-325 the critical bed shear stress ($\tau_{crit,e}$ = 0.59 N/m^2) is significantly different from visual observations ($\tau_{crit,e,surface}$ = 1.0 N/m^2). Most likely, this is because both the reported value for the visual observation is too high and the fit to the SSC data poorly captures the erosion during the experiment.

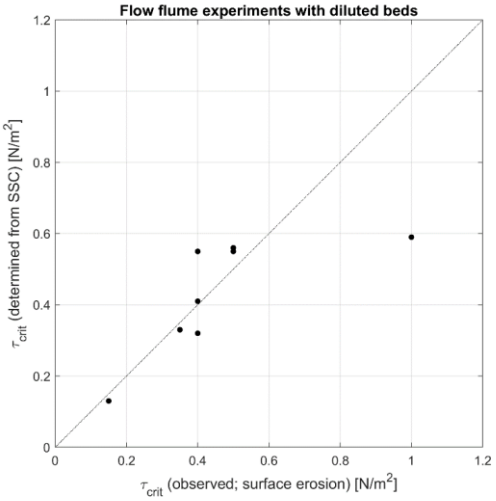

Figure 3.2.1 Validation of the critical bed shear stresses for surface erosion for flume experiments with diluted beds from visual observations (horizontal axis) by SSC analysis (vertical axis).

Table 3.2.1 Erosion thresholds for flume experiments with diluted beds as determined by SSC analysis and by visual observations.

Remolded diluted short beds	SSC analysis	Visual observations	
	$\tau_{crit,e,surface}$ [N/m^2]	$\tau_{crit,e,surface}$ [N/m^2]	$\tau_{crit,e,mass}$ [N/m^2]
BH1-600	0.56	0.5	0.8
GR1-250	0.33	0.35	0.65
H2-325	0.59	1	1.4
HU1-400	0.32	0.4	0.8
HU1-600	0.55	0.4	0.8
ZW2-250	0.13	0.15	0.3
ZW2-400	0.55	0.5	0.8
WAW1-400	0.41	0.4	0.89

3.2.1.2 Predictions

Standard formulations based on the depth-averaged velocity and friction factor are used to determine the bed-shear stress due to currents. Two different methods are used to determine the additional bed shear stress due to waves. The first method (VR-method) by Van Rijn (1993) yields the time-averaged bed shear stress over the wave cycle (τ_w). The second method by Soulsby (1997) yields the maximum bed-shear stress over the wave cycle ($\tau_{w,max}$). Generally, the combined bed shear stress ($\tau_{c;w}$) of the Van Rijn-method is somewhat higher than the current-related bed shear stress (τ_c). The $\tau_{c;w,max}$-value of the Soulsby method is always much higher (up to factor 2) than the current-related critical bed shear stress (τ_c).

Three methods to predict the critical bed-shear stress for erosion are herein presented.

Method 1: Van Rijn (2020) has proposed a method to predict the critical bed-shear stress for particle and surface erosion of the mud and sand fraction, which depends on the fraction of fines and reads as follows:

Fine fraction < 63 μm: $\tau_{cr,pef} = \phi_{cohesive}\ \tau_{cr,fines,o} = (1+p_{fines})^{\beta}\ \tau_{cr,fines,o}$ (3.2.1a)

Sand fraction > 63 μm: $\tau_{cr,ses} = \phi_{cohesive}\ \tau_{cr,sand,o} = (1+p_{fines})^{\beta}\ \tau_{cr,sand,o}$ (3.2.1b)

with:

$\tau_{cr,fines,o}$=critical bed-shear stress for particle erosion of fine fraction without cohesive effects using the separation diameter of 63 μm ($\tau_{crp,fine,o} \cong$ 0.1 to 0.2 N/m^2 for a diameter of 63 μm);

$\tau_{cr,sand,o}$ = similar for sand fraction ($\tau_{cr,sand,o} \cong$ 0.15 to 0.25 N/m^2 for diameters in the range of 100 to 200 μm).

In earlier work (Van Rijn 1993; 2007), the β-coefficient was used as a constant in the range of 1.5 to 3. Later research has shown that this coefficient is dependent on the percentage of clay < 8 μm, the percentage of fines < 63 μm and the dry bulk density. According to Van Rijn and Barth (2018), the β-coefficient is assumed to be related to the percentage of clay and the dry bulk density of the bed, as follows:

$$\beta = [1 + (p_{clay}/p_{fines})^{\alpha 1} + (\rho_{dry,mixture}/\rho_{dry,max})^{\alpha 1}]^{\alpha 2} \quad (3.2.1c)$$

with :

$\rho_{dry,mixture} = (1-p_{fines})\ \rho_{dry,sand} + p_{fines}\ \rho_{dry,fines}$;

$\rho_{dry,max}$ = maximum dry bulk density of mud-sand mixture ($\cong$ 1600 kg/m^3);

p_{clay}= percentage of clay-dominated particles < 8 μm;

p_{fines}= percentage of fines < 63 μm of the bed layer;

$\rho_{dry,sand}$ = dry bulk density of sand ($\cong$ 1600 kg/m^3);

$\rho_{dry,fines}$= dry bulk density of mud ($\cong$ 200 kg/m^3 for soft mud up to 1200 kg/m^3 for firm mud bed);

$\alpha 1$, $\alpha 2$= empirical coefficient ($\cong$ 1.5 for sand fractions and $\cong$2 for fine fractions).

The dry density follows from: $\rho_{dry,mix} = [\rho_{dry,wet} - \rho_w]\ [\rho_s / (\rho_s - \rho_w)]$ with ρ_s = sediment density ($\cong$ 2650 kg/m^3) and ρ_w = sea water density ($\cong$ 1020 kg/m^3). The wet density ($\rho_{wet,mix}$) can be determined most easily by measuring the wet mass and volume of the sample. If $\rho_{dry,mix}$ and p_{fines} (by wet sieving using mesh of 63 μm) are known, the $\rho_{dry,fines}$ can be computed from: $\rho_{dry,mix} = p_{fines}\ \rho_{dry,fines} + p_{sand}\ \rho_{dry,sand}$.

Equation 3.2.1 provides an estimated value for the critical bed-shear stress depending on the mud and clay content and the density values involved. However, the equation provides limited flexibility to calibrate the bed-shear stress to the observed density-dependence. The MUSA observations also reveal a greater dependence of the critical bed-shear stress on the density than based on Equation 3.2.1.

Method 2: An alternative method is proposed to represent the critical bed-shear for erosion of the fines:

$$\tau_{cr,fines} = \tau_{cr,min1} + [(\rho_{dry} - \rho_{dry,min})/(\rho_{dry,*} - \rho_{dry,min})]^{\alpha 1}(\tau_{cr,max} - \tau_{cr,min1}) \quad \text{for } \rho_{dry} < \rho_{dry,*} \qquad (3.2.2a)$$

$$\tau_{cr,fines} = \tau_{cr,min2} + (\rho_{dry,max} - \rho_{dry})/(\rho_{dry,max} - \rho_{dry,*})^{\alpha 2}\ (\tau_{cr,max} - \tau_{cr,min2}) \quad \text{for } \rho_{dry} > \rho_{dry,*} \qquad (3.2.2b)$$

with:

$\tau_{cr,fines}$ = critical bed-shear stress of fines at dry bulk density ρ_b;

$\tau_{cr,min1}$ = critical bed-shear stress of fines (about 0.1 to 0.2 N/m^2) at dry bulk density $\rho_{dry,min}$;

$\tau_{cr,min2}$ = critical bed-shear stress of fines (about 0.2 to 0.3 N/m^2) at dry bulk density $\rho_{dry,max}$;

$\tau_{cr,max}$ = maximum critical bed-shear stress of fines (about 1 to 2 N/m^2) at dry bulk density $\rho_{dry,*}$;

ρ_{dry} = dry bulk density depending on p_{fines}, p_{silt} and p_{sand};

$\rho_{dry,min}$ = minimum dry bulk density (about 200 kg/m^3) ;

$\rho_{dry,max}$ = maximum dry bulk density (of about 1600 kg/m^3);

$\rho_{dry,*}$ = dry bulk density (range of 1000 to 1200 kg/m3) for which the critical bed-shear stress is maximum;

$\alpha 1$, $\alpha 2$ = coefficients (0.5 to 1.5).

Some example values from Equation 3.2.2 are (using $\alpha 1=1$, $\alpha 2=1$, $\tau_{cr,min1}$=0.2 N/m^2 at $\rho_{dry,min}$= 200 kg/m^3; $\tau_{cr,min2}$=0.3 N/m^{2}at $\rho_{dry,max}$= 1600 kg/m^3; $\tau_{cr,max}$= 1.5 N/m^2 at $\rho_{dry,*}$=1200 kg/m^3) :

ρ_{dry}= 400 kg/m^3: $\tau_{cr,fines} = 0.2 + [(400-200)/1000]^1\ (1.5-0.2) = 0.2+0.2x1.3 = 0.46$ N/m^2;

ρ_{dry}= 1000 kg/m^3: $\tau_{cr,fines} = 0.2 + [(1000-200)/1000]^1\ (1.5-0.2) = 0.2+0.8x1.3 = 1.24$ N/m^2;

ρ_{dry}= 1200 kg/m^3: $\tau_{cr,fines} = 0.2 + [(1200-200)/1000]^1\ (1.5-0.2) = 0.2+1x1.3 = 1.5$ N/m^2;

ρ_{dry}= 1400 kg/m^3: $\tau_{cr,fines} = 0.2 + [(1600-1400)/(1600-1200]^1\ (1.5-0.3) = 0.3+0.5x1.2 = 0.9$ N/m^2;

ρ_{dry}= 1600 kg/m^3: $\tau_{cr,fines} = 0.2 + [(1600-1600)/(1600-1200]^1\ (1.5-0.3) = 0.3+0.x1.2 = 0.3$ N/m^2.

The results from Equation 3.2.2 are also shown in Figure 3.2.2 for $\rho_{dry,*}$= 700, 1200 and 1400 kg/m^3 and various combinations of input values.

Low bed-shear stress conditions at low densities (on left end of Figure 3.2.2) represent mud-dominated, poorly consolidated sediments. These kind of sediment samples occur in nature because there is too little time for consolidation. The high density conditions (on right end of Figure 3.2.2) are pure sand beds which have a fairly low critical bed shear stress. The intermediate density conditions represent mixtures of sand and mud with higher critical bed shear stresses resulting from the cohesive effects of mud. Such mixtures consolidate more rapidly than pure mud beds and therefore have a higher critical bed shear stress in field conditions.

Method 3: This method to predict the critical bed-shear stress of the fine fraction is based on the d_{50} of the mud-sand mixture:

$$\tau_{cr,fines} = 1+2[(d_{sand}-d_{50})/d_{sand}]^{\gamma}\ \tau_{cr,fines,o} \qquad (3.2.3)$$

$$d_{50} = d_{sand}\ e^{-0.03 p_{fines}}$$

with:

d_{50} = median diameter of mud-sand mixture;

d_{sand} = 250 μm = sand diameter at which percentage of fines is close to zero;

$\tau_{cr,fines,o}$ = critical bed-shear stress for particle erosion of fine fraction without cohesive effects using the separation diameter of 63 μm ($\tau_{cr,fine,o} \cong$ 0.1 to 0.2 N/m^2 for a diameter of 63 μm);

γ = exponent ($\cong$2).

The d_{50} of mud-sand mixtures strongly depends on the percentage of fines, see Figure 2.4.2. The data of this latter plot can be represented by $d_{50} = d_{sand}\ e^{-0.03p_{fines}}$ with p_{fines}= percentage of sand (%) and d_{sand} = 250 μm = sand diameter at which the percentage of fines is close to nil. More data are required to improve Figure 2.4.2.

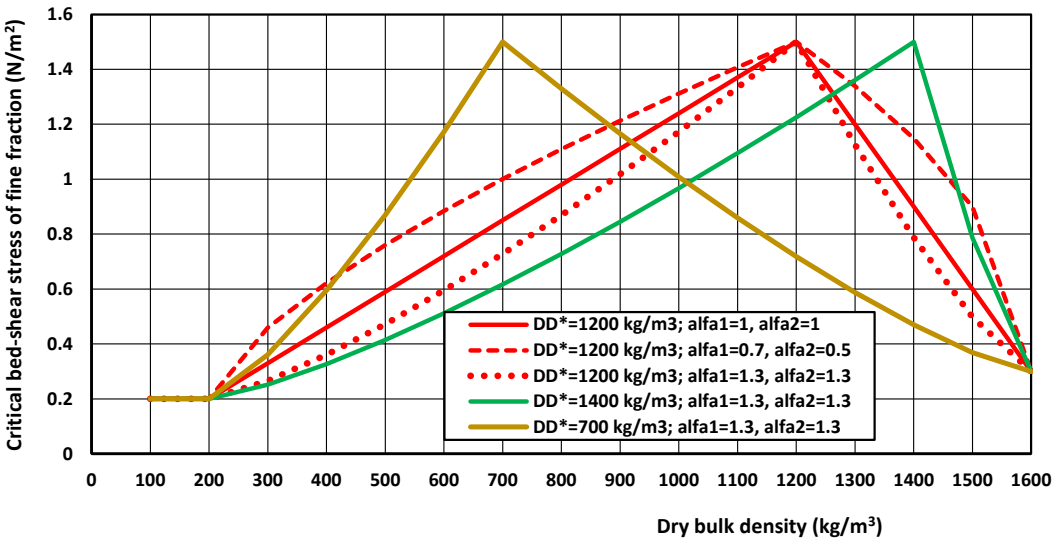

Figure 3.2.2 Critical bed-shear stress of fine fraction based on Equation 3.2.2; DD=dry bulk density.

3.2.2 Short bed tests with remolded natural mixtures in current alone

Figure 3.2.3 shows the observed critical bed-shear stresses (cbs) for surface erosion of all short-bed samples in the flume with only a current, illustrated as function of the dry density (ρ_{dry}) and the percentage of fines (p_{fines}). The measured cbs-values represent the deeper layers below the fluffy top layer (1 to 3 mm thick) because the mud surface was scraped off. Although substantial variation can be observed in the MUSA-results, the critical shear stress shows an increasing tendency for increasing dry bulk density up to a certain density value in the range of 700 to 1200 kg/m^3 or p_{fines} >50%. For very high-density values >1200 kg/m^3, the trend decreases. These high-density samples are mostly sandy with a critical shear stress approaching the value of pure fine sand of about 0.2 N/m^2 at a dry density of about 1600 kg/m^3.

For very low density values < 300 kg/m^3, the $\tau_{cr,se}$-value for surface erosion decreases to about 0.2 N/m^2, as was found in earlier studies (Van Rijn, 2018, 2019). Similarly, the $\tau_{cr,se}$-value decreases to that of pure sand (0.2 N/m^2 for sand of 0.2 mm) for a high dry density of 1600 kg/m^3 and p_{fines} approaching 0. For p_{fines} <45%, the $\tau_{cr,se}$-values gradually decreases, except for very silty samples.

Earlier results of samples from Noordpolderzijl (Van Rijn, 2018; 2019) and Holwerd (WaterProof, 2019ab) are also included in Figure 3.2.3. Most samples from the tidal channel at Noordpolderzijl (taken at the intertidal banks) are sandy muds with a percentage of fines < 63 μm in the range of 10% to 70%. The samples from Holwerd are taken from the bed of the channel and contain both sandy and muddy samples with percentages of fines in the range of 5% to 85%. The cbs-data of Winterwerp et al. (1992) are shown in the red box in Figure 3.2.3. These data were derived from long bed carousel-flume experiments with deposited sediment beds with low density values in the range of 100 to 250 kg/m^3.

It follows from the MUSA and earlier measurements on short beds, synthesized in Figure 3.2.3, that:

- The measured critical bed-shear stress for surface erosion shows an increasing trend from approx. 0.3 N/m^2 to approx. 0.7 N/m^2 for a dry density <400 kg/m^3 (low-density range);
- The observed critical bed-shear stresses for surface erosion are increasing in the range of 0.7 N/m^2 to 2 N/m^2 for a dry density between 400 to 1200 kg/m^3;

- The measured critical bed-shear stress gradually decreases from its maximum at medium density to approximately 0.2 N/m^2 (Shields's curve) for fine to medium fine sand with density >1300 kg/m^3 and almost no fines <5%.

Two outliers in Figure 3.2.3 are the MUSA samples from Bengal Bay (p_{fines} = 94%) and from the sandy banks along the Western Scheldt near Hulst (p_{fines} = 12%). Although the amount of fines in the sample from Bengal Bay is very high, it has a relatively high density and a significant critical shear stress for erosion of around 1.5 N/m^2. The sandy sample from Hulst was found to have a fairly high critical bed-shear stress of 1.3 N/m^2. However, photographs of the local bed show sandy ripple marks indicating substantial sediment dynamics and thus a lower critical stress.

The results of the prediction method for the critical bed-shear stress for surface erosion in Equation 3.2.1 (Method 1) are also shown in Figure 3.2.3, using the input data that is listed below.

ρ_{dry} [kg/m^3]	300	400	500	600	700	800	900	1000	1100	1200	1300	1400
p_{fines}	0.8	0.8	0.8	0.8	0.8	0.7	0.6	0.5	0.4	0.3	0.2	0.1

$\tau_{cr,silt}$=0.2 N/m^2; p_{clay}/p_{fines}=0.3, α1=1 and α2=2

The percentages of fines in this example are set to 80% for dry densities between 300 and 700 kg/m^3 to account for variations in mud characteristics (e.g. water content and mineralogy). Between 800 and 1400 kg/m^3, the percentage of fines is linearly reduced towards 10%, representing the transition of mud-sand to pure sand as in natural samples. The prediction method yields very reasonable results for mud-sand mixtures with dry density values in the range of 400 to 1000 kg/m^3, but underestimates the critical bed-shear stress up to a factor of 2 for high-density mixtures. Apparently, the parameters p_{fines}, p_{clay} and ρ_{dry} are not sufficient to characterize all effects that are involved across the range of mud-sand mixtures.

The results of Equation 3.2.2 (Method 2) are also shown in Figure 3.2.3 based on the following input:

$\tau_{cr,min1}$=0.2 N/m^2 at $\rho_{dry,min}$ = 200 kg/m^3;

$\tau_{cr,min2}$=0.3 N/m^2 at $\rho_{dry,max}$ = 1600 kg/m^3;

$\tau_{cr,max}$= 1.5 N/m^2 at $\rho_{dry,*}$ = 1150 kg/m3;

α1=0.7 and α2=1.5.

The agreement of the results from Equation 3.2.2 with the measured data of MUSA is quite good. The maximum critical bed shear stress is 1.5 N/m^2 for a dry bulk density of about 1150 kg/m^3. A dry bulk density of 1150 kg/m^3 is obtained for p_{fines} of about 40% to 50% (see Figure 2.5.2). Hence, the critical stress is maximum for $p_{fines} \cong$ 40% to 50%. This reasonably corresponds to the critical value brought forward by Van Ledden et al. (2003). They argue that the critical shear stress for erosion is dominated by cohesion at a clay content exceeding 10% (which typically corresponds to a mud content of 30%). At lower clay content the sand skeleton dominates erosion processes. A mud content of 30% corresponds to a density of typically 1260 kg/m^3 (see Figure 2.5.1).

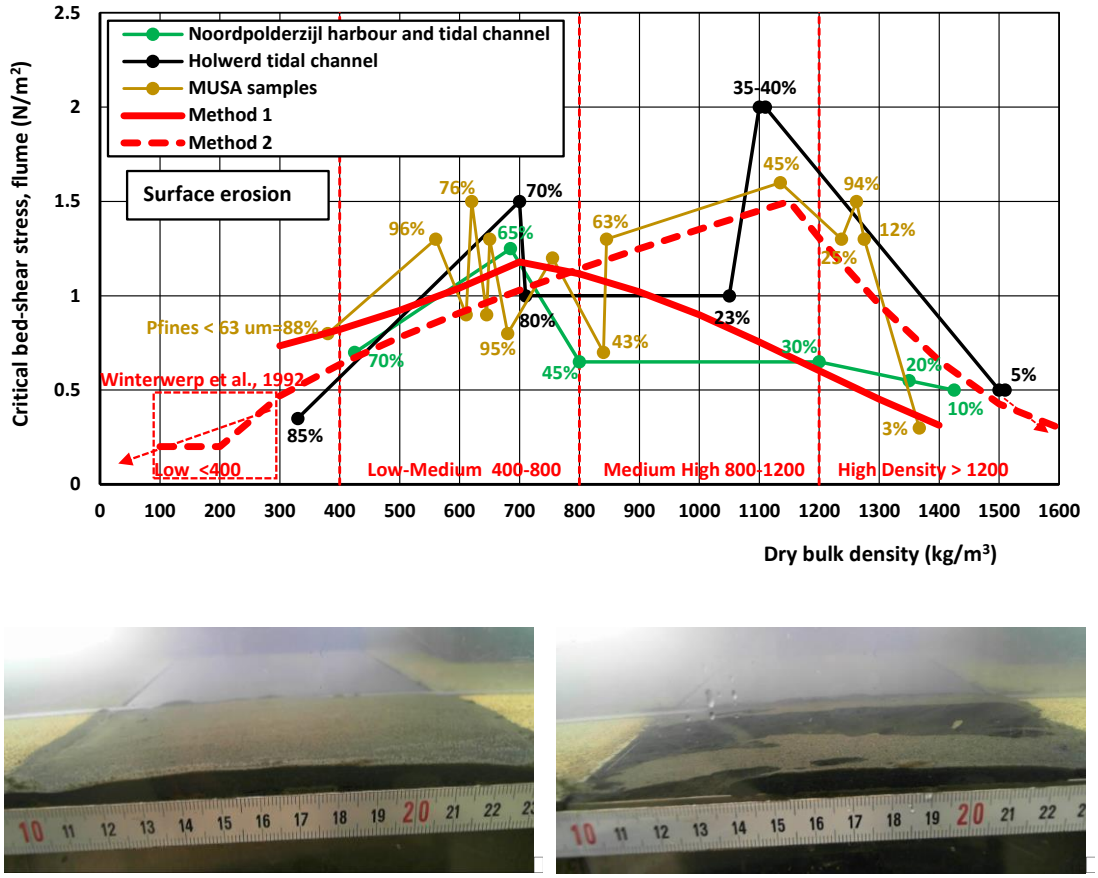

Figure 3.2.3 Critical bed-shear stress for surface erosion due to current as function of the dry bulk density and the percentage of fines < 63 μm for short bed tests (photos of WS-HU1 sample before and after test; $p_{fines<63\mu m}$ = 12%; dry density = 1280 kg/m^3; cbs = 1.3 N/m^2).

Figure 3.2.4 shows the same data as in Figure 3.2.3, but as function of the percentage of fines < 63 μm. Trendlines are also indicated. The data in the high-density range shows that the cbs-values are relatively low for very sandy muds with p_{fines} < 30% and maximum for p_{fines} around 50%. The cbs-values decrease again for very muddy beds with p_{fines} > 70%. The cbs-data in the low-density range < 400 kg/m^3 are only available for very muddy beds with high percentage of fines > 80%. Most likely, the critical bed-shear stresses of low-density samples with a low percentage of fines < 30% are smaller than about 0.3 N/m^2 (Shields's range) in most natural cases.

The critical bed shear stress for erosion was for two samples (BAPU and PLUK1) also determined from timeseries of the SSC in the flume. For other experiments, no SSC data is available or the SSC data does not show a clear increase in SSC over the duration of the flume experiment. The results are listed in Table 3.2.2 and provide a form of validation of the visual observations. The results from SSC analysis are in between the observed values for surface erosion and mass erosion. As we consider the critical bed shear stress from the SSC analysis for remolded beds to be representative for the start of mass erosion, values are slightly lower than those from visual observations.

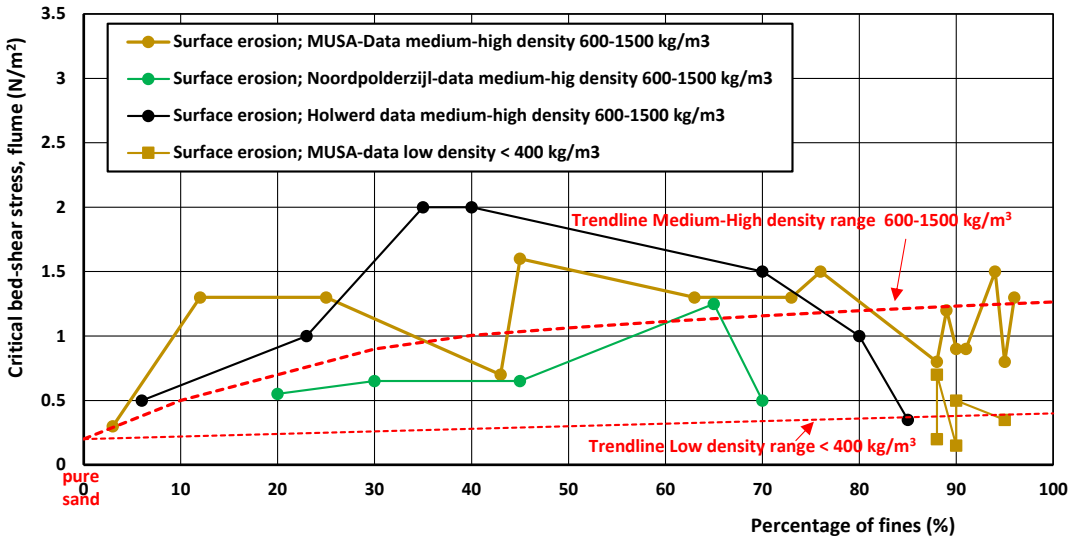

Figure 3.2.4 Critical bed-shear stress for surface erosion due to currents as function of the percentage of fines < 63 μm for short bed tests.

Remolded beds	SSC analysis	Visual observations	
	$\tau_{crit,e,mass}$ [N/m²]	$\tau_{crit,e,surface}$ [N/m²]	$\tau_{crit,e,mass}$ [N/m²]
BAPU	1.76	1.3	2
PLUK1	1	0.9	1.5

Table 3.2.2 Critical bed-shear stresses for erosion as determined by SSC analysis and by visual observations for experiments with remolded beds.

3.2.3 Short bed tests with diluted natural mixtures in current alone

Figure 3.2.5 presents the cbs-values of the diluted samples in comparison to the cbs-values of the undiluted (remolded) samples. The cbs-values of the diluted samples are much smaller than those of the remolded samples. This may be caused by the dilution process disturbing the internal structure of the samples, resulting in lower cbs-values of the order of 0.2 to 0.3 N/m^2 for the lowest dry density. These latter values may be representative for the thin (≅ 10 mm) fluffy top layer of a natural channel bed.

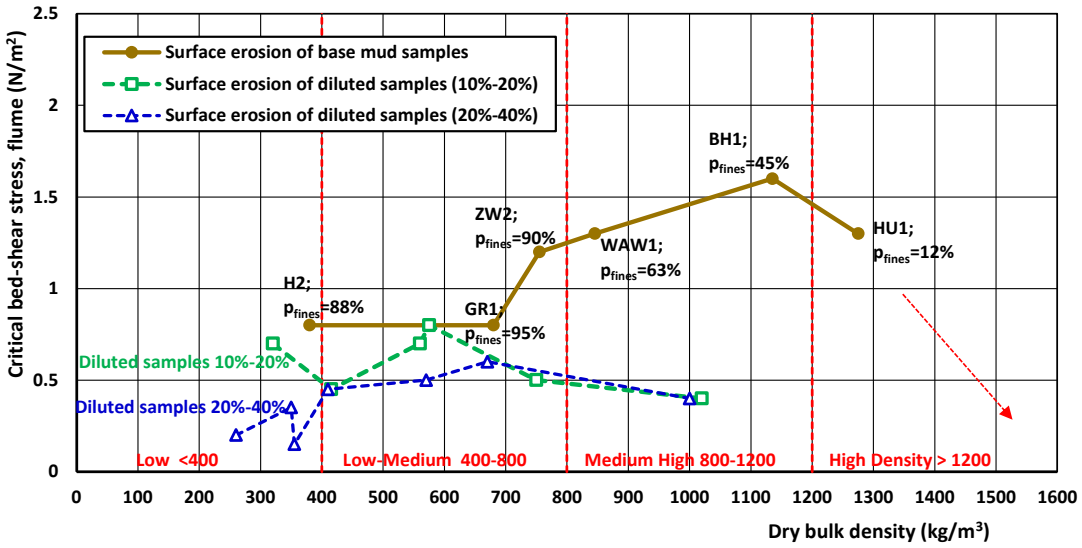

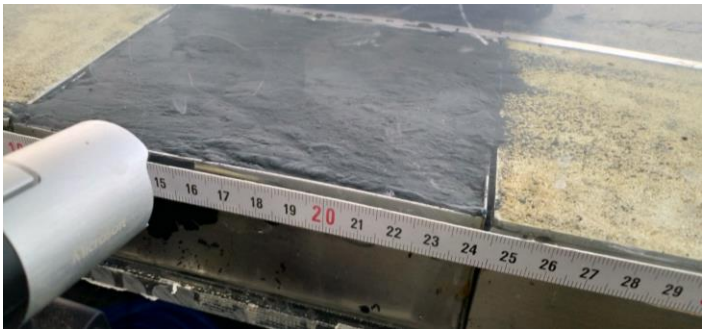

Figure 3.2.5 Critical bed-shear stress for surface erosion due to currents as function of the dry bulk density and percentage of fines < 63 μm for short bed tests (photo of sample NPZ-H2 during the test; $p_{fines<63\mu m}$=88%; dry density=260 kg/m^3; cbs=0.2-0.3 N/m^2).

3.2.4 Short bed tests with undisturbed bed samples in combined currents and waves

The observed critical bed-shear stress values of the fairly stable beds are 0.35 to 0.5 N/m^2 for particle erosion and 0.7 to 0.8 N/m^2 for surface erosion. Both values were increasing slightly for increasing percentages of fines. The results of these experiments with undisturbed beds are also presented in Figure 3.2.9.

3.2.5 Long bed tests with remolded artificial and natural mixtures in combined currents and waves

3.2.5.1 MUSA experiments

Figure 3.2.6 shows the observed critical bed shear stress (cbs) values for particle erosion (dashed line) and for surface erosion (solid line) for the long bed experiments that were carried out in the MUSA project.

Particle erosion: The cbs-values of fines are slightly lower than that of sand particles. The bed shear stress values that are determined by the VR-method (Van Rijn 1993) for tests with only waves are roughly 20% to 40% higher than those in tests with only currents.

Surface erosion: The cbs-vales in tests with waves alone are almost the same as in tests with currents alone (i.e. in case the bed shear stresses are determined by the VR-method. The cbs-values of the fines are somewhat higher than the cbs-values at which small sand ripple marks are generated, because the fine particles are lying in the trough of the ripples, requiring higher erosion stresses.

It is noted that the bed-shear stress in conditions with waves is largely dependent on the method that is used to determine the bed shear stress. It is found that the wave-related critical bed-shear stress ($\tau_{w,cr}$ in tests with waves alone) of the VR-method is mostly somewhat higher than the current-related critical bed shear stress ($\tau_{c,cr}$ in tests with current alone). However, it is also noted that the small (0.05 to 0.1 N/m^2) difference may be introduced by other effects, such as small differences in the preparation of the bed and the accuracy by which the start of erosion can be determined. The wave-related critical bed-shear stress of the Soulsby-method is always much higher (up to factor 2) than the current-related critical bed shear stress (see Section 3.2.2). Therefore, the VR-method is preferred.

The results of cbs-values that are presented in Figure 3.2.6 are all based on visual observations. It was not possible to derive the cbs-values from the measured SSC for these long bed experiments because the wave and current conditions were increased in steps, whereas a gradual transition in the energy of the hydrodynamic forcing is required to derive the cbs-values from the SSC.

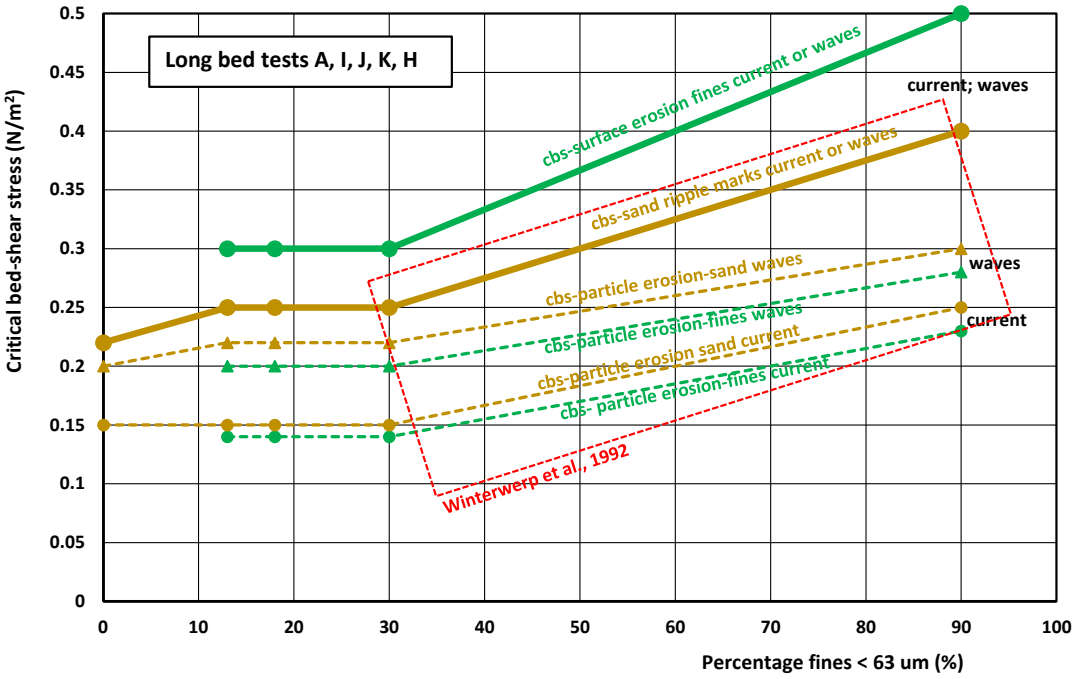

Figure 3.2.6 Critical bed-shear stress (cbs) for particle erosion (dashed) and surface erosion (solid) of sand (yellow) and fines < 63 μm (green) due to currents or waves for long bed tests.

3.2.5.2 Comparisons with earlier work

The generation of ripples along a bed of mud-sand in conditions with combined currents and waves was studied in detail by Wu et al. (2021). The experimental results revealed two distinct types of equilibrium ripples on mixed sand-clay beds: i) large asymmetrical ripples with geometries comparable to clean-sand beds for $p_{clay} \leq 10\%$ and ii) much lower, flat barchan-type ripples for $p_{clay} > 10\%$. For low percentages of clay, the ripples were found to develop to similar ripples as for a clean sand-bed, only the ripple formation takes more time for higher amounts of clay. The ripple height decreases substantially for p_{clay} beyond ~10%, whereas the ripple length is only slightly affected.

Winterwerp et al. (1992) present an interesting and important data set of critical bed-shear stresses (cbs) for surface erosion over long beds of natural sediments, derived from experiments in an annular flume

with samples from both saline and fresh water systems. The results of these experiments are copied in Table 3.2.3. Important observations are:

- The erosion of the top layer was observed to be very gradual and smooth for low shear stresses < 0.3 N/m^2. Deeper scour holes up to 20 mm near the inner wall of flume were generated locally for higher shear stresses in the range of 0.3 to 0.5 N/m^2;
- The critical shear stress (cbs) for surface erosion within the upper 10-20 % of the bed (thickness of about 10 to 15 mm) varies from about 0.1 to 0.5 N/m^2 for a consolidation time of 1 day and from about 0.2 to 0.6 N/m^2 for a consolidation time of 7 days. An increase in consolidation time from 1 to 7 days resulted in an overall increase of the critical shear stress by about 0.1 N/m^2;
- The critical shear stress for surface erosion in the top layer was found to increase for increasing dry density. The variation in the cbs-values for surface erosion of experiments with 8 different mud beds is minor at the same bed density;
- The cbs is somewhat lower (20%) for mud beds with a relatively high sand content (60%-70%);
- The critical shear stress for surface erosion of the top layer (1 cm) is found to be in the range of 0.15 to 0.3 N/m^2 for ρ_{dry} = 100 to 150 kg/m^3 and of 0.3 to 0.5 N/m^2 for ρ_{dry} = 150-250 kg/m^3;
- During and at the end of some tests (some) mass erosion was observed for shear stresses in the range of 0.5 to 0.8 N/m^2.

The data from Winterwerp et al. (1992) are in reasonably good agreement with the long bed test results of the MUSA project. The data range of Winterwerp et al. (1992) is shown in the red boxes in Figure 3.2.3 and in Figure 3.2.6.

Table 3.2.3 *Data of critical bed-shear stress for surface erosion of natural muds (Winterwerp et al., 1992). F = fresh water conditions; S = saline conditions.*

Mud type	Sand (%)	Organic material (%)	Dry density (kg/m^3) at top/bottom of mud layer after 1 and 7 days	Critical shear stress for surface erosion (N/m^2)		
				100-150 kg/m^3	150-200 kg/m^3	200-250 kg/m^3
Hollands Diep Sassenplaat (F)	9	19	1 day: 150-350 7 days: 250-350		0.4±0.05	0.5±0.05
Hollands Diep Moerdijkbrug (F)	23	9	1 day: 175-350 7 days: 215-350		0.4±0.05	0.4±0.05
Lake Ketel (F)	7	12	1 day: 100-450 7 days: 160-450	0.2±0.1 0.2±0.1		
Maas River (F)	36	8	1 day: 140-500 7 days: 160-500	0.2±0.05	0.5±0.05	
Biesbosch Spijkerboor (F)	8	8	1 day: 100-400 7 days: 160-450	0.15±0.05	0.3±0.05	
WesterSchelde Breskens (S)	27	5	1 day: 110-650	0.25±0.05		
Eems Dollard Delfzijl-harbor (S)	60	2	1 day: 160-180	0.15±0.05		
North Sea Loswal-Noord (S)	69	2	1 day: 100-1500 7 days: 100-1500	0.15±0.05 0.3±0.1		

3.2.6 Discussion on observations of the critical bed shear stress

Many of the MUSA-results are combined in Figure 3.2.7, which shows the critical bed-shear stress values (cbs) for particle erosion and surface erosion of fines with long and short beds. Only results from the experiments with remolded beds without dilution are shown. Overall results are:

- The cbs-values for particle erosion of sand increases from 0.15 N/m^2 for a pure fine sand bed (0.13 mm) to a value in the range of 0.2 to 0.6 N/m^2 for a mud-sand-mixture with $p_{fines<63\ um}$=30%, depending on the bed preparation. The cbs-values for particle erosion of fines are slightly smaller than those of sand, as the fines are washed out first. Long bed experiments with larger variability

of mud-sand percentages and bed roughness of the top layer yield much lower cbs-values than short bed experiments;

- The cbs-values for surface erosion of fines from the trough (muddy spots) between the sandy ripple crests increases from low values of 0.2-0.3 N/m^2 for $p_{fines<63\ um}$ = 5% to values in the range of 0.3 to 1.3 N/m^2 for $p_{fines<63\ um}$ in the range of 10% to 30%, depending on the type of bed (i.e. long beds lead to much lower values than short beds).

The critical bed-shear stress for surface erosion derived from the experiments with diluted beds show lower cbs-values in the range of 0.2 to 0.8 N/m^2.

An important difference between different type of flume experiments may be the preparation of the sediment sample. Except from the few undisturbed field samples, the top layer represents relatively freshly deposited sediment material, as can be found at the bed of a tidal channel in dynamic conditions with cyclic erosion and deposition of sand and mud. Scraping off the top of the sediment sample to level the surface of the sample with the bottom of the flume in the short bed test caused the fluffy top layer to be removed. This may be an important reason why the cbs-values of (scraped) short bed tests are significantly larger than those of long bed tests. Another possible reason for different result between the short and the long bed tests is the spatial variation in the strength (i.e. cohesivity) and roughness of the sediment samples. Surface erosion generally starts at a weak or exposed spot of the sediment sample, and the larger the sediment sample the higher the chance that such a weak or exposed spot is present.

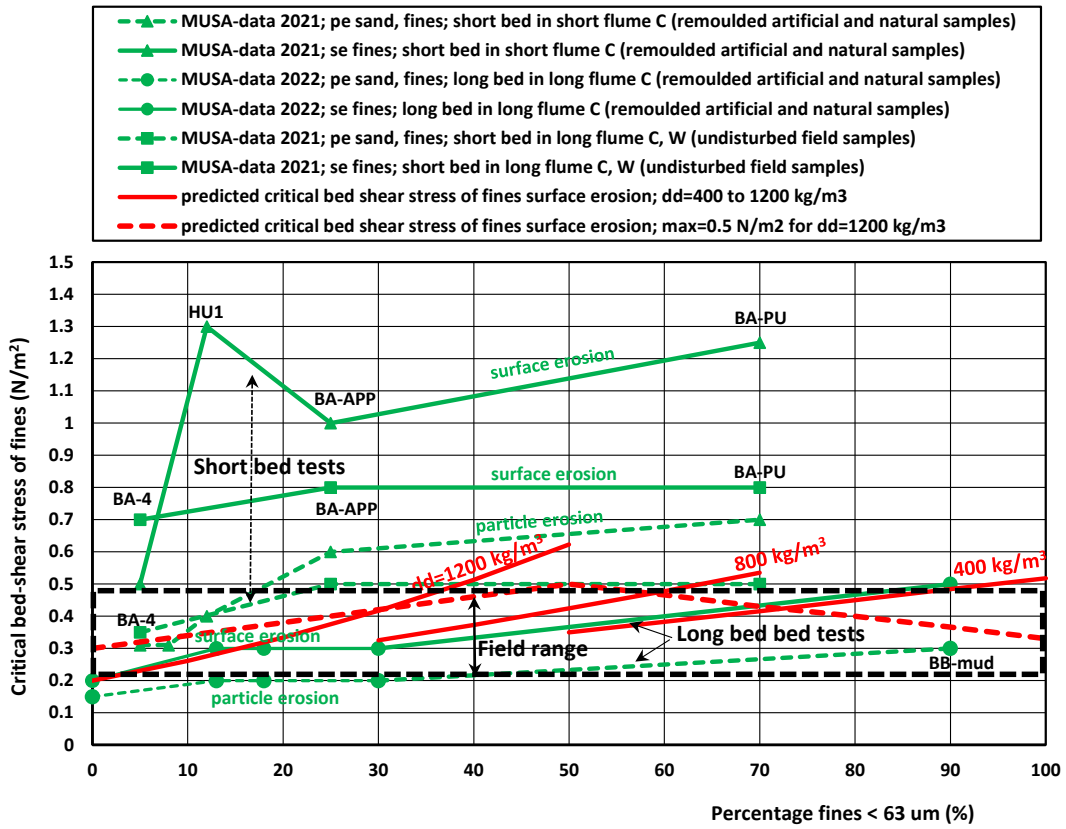

Figure 3.2.7 Critical bed-shear stress for particle erosion and surface erosion of fines for all MUSA experiments (dashed=particle erosion; solid=surface erosion).

The cbs-data of the long bed flume experiments are in good agreement with the cbs-data measured in the long bed carousel-flume of Winterwerp et al. (1992).

The black dashed box in Figure 3.2.7 represents cbs-values in field conditions that are reported in literature. The cbs-values from long bed experiments are in the same range as these field measurements. The field measurements are summarized in Table 3.2.4.

Location	Type of bed	Fines (%)	Dry density (kg/m^3)	Type of flow	Critical bed-shear stress for surface erosion (N/m^2)	
					fines	sand
Holwerd, Dutch Wadden Sea (Boechat Albernaz et al., 2022C (MUSA))	dynamic mud-sand	10-55	700-1200	tidal; depth=3-5 m	0.15-0.2 (c= 0.2-0.3 m/s)	0.2-0.5 (c= 0.3-0.5 m/s)
Nessmersiel, German Wadden Sea (Bauamt, 1987)	dynamic mud-sand	10-25	700-1200	tidal; depth=2-3 m	0.15-0.2 (c= 0.2-0.3 m/s)	0.2-0.4 (c= 0.3-0.4 m/s)
Intertidal flats in Wadden Sea (Houwing, 2000)	dynamic mud-sand	5-25	>1000	tidal; depth=0-2 m	0.1-0.2 (in situ flume measurements)	
	dynamic mud-sand	35	800-1000	tidal; depth=0-2 m	>0.5 (in situ flume measurements)	
Slijkplaat, Haringvliet, the Netherlands (Deltares, 1993)	dynamic mud-sand with many shells	80-90	450-900	tidal; depth=0-2 m	1-2 (scour marks/scour pits)	0.25-0.5 (minor bed load transport)
Haringvliet channel deeper excavated layer (Deltares, 1966)	firm mud-sand bed	60-80	800-1200	tidal	1-1.5 (in situ flume measurements)	
Fraser River, Canada (Amos et al., 1997)	dynamic mud-sand	65-95	<500	tidal depth=0-4 m	0.1-0.5 (in situ flume measurements)	

Table 3.2.4 Critical bed-shear stress values of field data

Results of Equation 3.2.1 (Method 1) are shown in Figure 3.2.7 by red solid curves (using 400 kg/m^3 for p_{fines}>50% , 800 kg/m^3 for p_{fines}=30%-70% and 1200 kg/m^3 for p_{fines}<50% and $\tau_{cr,silt}$=0.2 N/m^2, p_{clay}/p_{fines}=0.3, α1=2 and α2=2). The estimated cbs-values in the range of 0.2 to 0.6 N/m^2 are somewhat larger than the observed values in the range of 0.2 to 0.3 N/m^2 for long-bed experiments with samples with a relatively high density. The very silty BB-mud sample is considered to be an outlier with rather cohesionless properties and a very low cbs-value despite the high percentage of fines (about 90%).

Results of Equation 3.2.2 (Method 2) are shown in Figure 3.2.7 by the red dashed curves (using a maximum bed shear stress of $\tau_{cr,max}$ = 0.5 N/m^2 at a dry bulk density of 1100 kg/m^3, $\tau_{cr,min1}$ = 0.2 N/m^2, $\tau_{cr,min2}$ = 0.3 N/m^2 and α1 = α2 = 1; the percentage of fines is derived from the equation $p_{fines<63um}$ = 160-0.1ρ_{dry}, resulting in p_{fines} = 100% for ρ_{dry} = 600 kg/m^3 to p_{fines} = 50% for 1100 kg/m^3 and p_{fines} = 0% for 1600 kg/m^3. Eventually, this gives $\tau_{cr,max}$ = 0.5 N/m^2 for $p_{fines} \cong$ 50%).

Equation 3.2.3 (Method 3) with γ=2 and $\tau_{cr,fines,o}$=0.2 N/m^2 gives the following values: $\tau_{cr,fines}$ =0.23 to 0.55 N/m^2 for p_{fines}=10% to 90%, which is the correct range for field data shown in Figure 3.2.7.

Effect of high silt content

The sediment samples from Bengal Bay with a relatively high content of silt particles (60% to 70%) and a low percentage of clay and organic material show results which are systematically different from the results for other MUSA-samples. The dry density of these silty samples is relatively high with values of 1200 to 1500 kg/m^3 for $p_{fines<63\ \mu m}$ in the range of 85% to 95%. The plasticity index (PI) is low with values <20. Based on the short bed tests with only a current, the critical bed-shear stress for surface erosion of these samples is rather high at 1.5 N/m^2. However, the long bed test with the mud from Bengal Bay yields a much lower critical stress for surface erosion in the range of 0.2 to 0.5 N/m^2. The latter value is more realistic given the relatively low permeability of silty samples.

The erosion threshold of silty materials was also studied by Yao et al. (2022). Their results suggest that there exists a critical silt content ($p_{silt\ 8\text{-}63um}$) of about 35%, separating two domains:

- For $p_{silt} < 35\%$, the critical bed shear stress follows the values of the Shields' curve with $\tau_{cr} \cong 0.1$ N/m^2, which is in agreement with earlier research (Van Rijn, 1993; Van Ledden, 2003);
- For $p_{silt} > 35\%$, the erosion threshold of a mixed bed is higher and remains constant at about $\tau_{cr} \cong 0.2$ N/m^2 for further increasing silt content.

The critical bed-shear stress values for surface erosion of the Bengal Bay samples (τ_{cr}=0.2 to 0.5 N/m^2) are thus somewhat higher than what is suggested by Yao et al. (2022) for silty samples, which is most likely caused by the small fraction of clay in the samples from Bengal Bay.

Effect of bed roughness

The effect of shells, gravels and pebbles on the critical bed-shear stress was investigated by placing these on a short mud-sand bed in a flume with unidirectional flow. Three ranges of coverage were explored (low < 10%, medium ≅ 10%-20% and high ≅ 20%-40%), as can be seen in Figure 3.2.8. In general, it was found with these experiments that the critical flow velocities for erosion are smaller, but that the critical bed-shear stresses are higher.

The presence of stones and pebbles lead to somewhat lower critical flow velocities due to additional turbulence created around the stones/pebbles. In most cases the erosion is initiated around the individual stones and pebbles or at the craters of stones and pebbles that have already been displaced by the flow. The increased roughness causes the presence of stones or pebbles to increase the critical bed-shear stress for surface erosion. In the case of a high percentage of stones/pebbles, the sediment particles are hiding between the much bigger stones or pebbles requiring a much higher bed-shear stress for erosion.

A mid percentage (10% to 20%) of stones/pebbles has not much effect for sandy mud samples, but a substantial effect (25% increase of critical bed-shear stress) for more muddy samples.

A low percentage (<10%) of stones/pebbles has not much effect on the critical bed-shear stress (within 15% being the experimental error range). The critical bed-shear stress may be somewhat higher or lower than that of a mud bed without stones/pebbles, depending on the orientation and scatter of stones and pebbles.

A low percentage of shells (<10%) has not much effect on the critical bed-shear stress (within 15% being the experimental error range). A mid percentage of shells (10% to 20%) has not much effect on the critical bed-shear stress for a sandy mud sample, but a substantial effect (20%-increase of critical bed-shear stress) for more muddy samples.

Figure 3.2.8 Flume experiments with short beds and low coverage of shells (<10%; left), a medium coverage of stones (10-20%; middle) and a high coverage of stones (20-40%; right).

Effect of benthos

The presence of biological or benthic activity in the sediment bed may have a significant effect on the erosional behaviour of a mud-sand bed. The bed surface may become cemented due to slimes that are produced by diatoms and bacteria. In addition, bioturbation may cause spatial variations in the resistance of the bed surface against erosion. These effects may be different at locations that are always submerged, such as tidal channels, and exposed mudflats.

The experimental results of undisturbed field samples show the presence of biological activity at the bed surface. The tubeworms that were largely present in these samples have opposing effects on the stability of the sample: i) increase in roughness and turbulence resulting in higher shear stress; ii) higher porosity (loosening) of the bed surface layer; and iii) higher cohesivity between the particles due to the presence of biofilms and secretions. Most parts of the samples remained stable during the flume experiments, whereas mud was gradually eroded from around these stable parts. The critical bed-shear stress values are quite high with values in the range of 0.7 to 0.8 N/m^2 (solid green squares in Figure 3.2.7).

De Smit et al. (2021) studied the effect of benthos on critical bed-shear stresses of undisturbed field mud-sand samples using a wave tunnel (OSCAR) with sediment cores directly taken from the field. Their results show low critical bed-shear stress-values of 0.2 N/m^2 for $p_{fines<63\mu m}$ = 7% and higher values for $p_{fines<63\ \mu m}$ in the range of 25% to 55%. Overall, the presence of benthos in these experiments seems to lead to lower cbs-values due loosening of the top layer sediments.

Andersen et al. (2010) used the in-situ EROMES instrument to study the effect of biological activity on the critical bed-shear stress. The erosion thresholds for the sediments generally varied between 0.2 and 0.6 N/m^2 but significantly higher thresholds (up to 1.8 N/m^2) were observed in September and April when higher contents of chlorophyll were observed.

3.3 Erosion rates

The erosion and deposition of sediment particles and flocs occur simultaneously. In general, erosion is dominant in accelerating tidal flow whereas deposition is dominant in decelerating tidal flow. Basically, the bed level change (mass change) in time is equal to difference between the erosion rate (E) and the deposition rate (D). To study the erosion processes under controlled conditions, detailed flume experiments with mud-sand beds are of essential importance. Although the flume experiments with different type of beds in the MUSA project have focused on the relationship between the critical bed-shear stress for surface erosion and governing sediment parameters, some of the flume experiments can be used to determine the erosion rate. These results are discussed after a general discussion of formulations for the erosion of mud and fine sand.

3.3.1 Formulations for the erosion of mud and fine sand

Mud

Generally, the erosion rate of pure mud (E_{mud}) is determined by a Partheniades type of equation:

$$E_{mud}=M\,[\tau/\tau_{cr,e} - 1]^n \qquad (3.3.1)$$

with τ = bed-shear stress; $\tau_{cr,e}$ = critical bed-shear for erosion, n = exponent in the range of 1 to 1.5, M=erosion parameter (range 0.00001-0.0005 kg/m^2/s).

Fine sand

Van Rijn (1984, 1986) derived an empirical pick-up formulation for sand particles from experimental data that is based on the difference between the dimensionless Shields parameter (θ) and a threshold value (θ_{cr}):

$$E_{sand}= \alpha_{sand}\,\rho_s\,[(s-1)\,g\,d_{50}]^{0.5}\,(D_*)^{0.3}\,[(\theta' - \theta_{cr})/\theta_{cr}]^{1.5} \qquad (3.3.2)$$

with:

E = pick-up rate (in $kg/m^2/s$);

$D_* = d_{50}\,[(s-1)g/\nu^2]^{1/3}$ = dimensionless grain size parameter (-);

d_{50} = median grain size (m);

ν = kinematic viscosity coefficient of fluid (m^2/s);

$S = \rho_s/\rho_w$ = relative density (-);

ρ_s = sediment density (kg/m^3);

ρ_w = fluid density (kg/m^3);

θ' = grain-related parameter (-) = $\tau_b'/[s-1)g\,d_{50}]$;

τ_b' = grain-related bed-shear stress (N/m^2) = $\rho\,g\,[U/C']^2$;

U = depth-averaged flow velocity (m/s);

R = hydraulic radius (m; assumed to be equal to the water depth);

$C' = 5.75\,g^{0.5}\log(12R/3d_{90})$ = Chézy-coefficient ($m^{0.5}/s$);

θ_{cr} = Shields value at initiation of motion (-);

G = gravity acceleration (m/s^2);

α_{sand} = erosion coefficient for sand (=0.00033; 30% uncertainty).

Equation 3.3.2 is derived for the erosion of single grains (grain by grain pick-up) and is only valid for relatively low flow velocities (< 1.5 m/s). For higher flow velocities (> 1.5 m/s), the pick-up process is affected by the shearing of multiple layers of sand on top of each other, resulting in a slight increase of the porosity which is known as dilatancy behavior (Van Rhee, 2010). The dilatant behavior yields a hydraulic gradient that pulls sediment particles into the sandy bed and thereby reducing the amount of erosion.

Additional processes that are relevant for high flow velocities are taken into account in Equation 3.3.2 by introducing a damping factor f_D. The most important additional processes are the damping of turbulence (turbulence collapse) in the near bed-area where the sand concentrations are extremely large, the increase in the kinematic viscosity and the dilatant behavior of the top of the sand bed. The adjusted pick-up function reads as:

$$E = \alpha_e\,\rho_s\,[(s-1)\,g\,d_{50}]^{0.5}\,(D_*)^{0.3}\,f_D\,[(\theta' - \theta_{cr})/\theta_{cr}]^{1.5} \qquad (3.3.3)$$

with: $f_D = 1/\theta'$ for $\theta' > 1$.

Based on Equation (3.3.3), it follows that $E \sim [(\tau' - \tau_{cr})/\tau_{cr}]^{1.5}$ for $\theta' < 1$ and $E \sim (\tau')^{0.5}$ for $\theta' > 1$.

Sand-mud mixtures

Following the approach by Van Ledden (2003), the erosional behavior of sand and mud within sand-mud mixtures is mutually coupled. According to this approach, sand-mud mixtures can be either non-cohesive or cohesive, depending on the composition of the sediment mixture. The transition between the non-cohesive and cohesive regime depends on the clay content; it takes place at a critical clay content ($p_{cl,cr}$) of 5-10%. From experimental and theoretical studies, it follows that the erosion fluxes of sand and mud are proportionally coupled. Herein, erosion of both sand and mud depend on the erosion properties of the non-cohesive or cohesive mixture (Mitchener & Torfs, 1996; Winterwerp & Van Kesteren, 2004; Van Ledden, Van Kesteren, & Winterwerp, 2004; Jacobs et al., 2011; Le Hir et al., 2008). In the schematization following Van Ledden (2003), erosion fluxes of sand and mud both depend on the erosion behavior of the sand fraction in case the mixture is non-cohesive, whereas in a cohesive mixture, sand and mud erosion depends on the erosion behavior of the mud fraction, such that the following relations hold when accounting for sand-mud interaction:

Non-cohesive regime:

$$E_{sand} = p_{sand}\, E_{sand;0} \quad (3.3.4)$$
$$E_{mud} = p_{mud}\, E_{sand;0}$$

Cohesive regime:

$$E_{sand} = p_{sand}\, E_{mud;0} \quad (3.3.5)$$
$$E_{mud} = p_{mud}\, E_{mud;0}$$

in which $E_{sand;0}$ is the erosion rate of pure sand, calculated following for example Van Rijn (1993) or Van Rijn (2007), and $E_{mud;0}$ is the erosion rate of pure mud, calculated following the Partheniades formulation (Equation 3.3.1).

3.3.2 Erosion of mud-sand mixtures in flume experiments

The erosion rate in the MUSA experiments was determined by the volume loss of the sediment sample as determined at the end of the experiments and based on the increase in suspended sediment concentration (SSC) during the flume experiment. During the flume experiments, the sediment samples were tested for a series of hydrodynamic forcing conditions. The volume loss of a sediment sample therefore provides an estimate of the total erosion for a range of forcing conditions, whereas most of the erosion took place in the most energetic conditions. Timeseries of the SSC, however, provide an estimate for the erosion rate of each of the forcing conditions. The erosion rate was determined from the change in sediment concentration over time, following:

$$E_{mud} = (V_w\, \Delta C)/(A_s\, \Delta t) \quad (3.3.6)$$

in which ΔC is the increase in suspended sediment (mud) concentration over time interval Δt, V_W is the volume of water in the flume system and A_S is the surface area of the sediment sample in the flume. In here, it is assumed that the SSC signal that is measured by an OBS instrument is representative for the average increase in mud concentration in the flume. Scaling the erosion rate of mud (E_{mud}) with the availability of mud in the bed (p_{mud}) yields:

$$E_{tot} = E_{mud} / p_{mud} \quad (3.3.7)$$

Figure 3.3.2 shows the mud erosion rates that are found based on the SSC data for flume experiments with long mud-sand beds (p_{mud} between range 13% and 30%) in conditions with currents and waves. Figure 3.3.2 shows the modeled erosion rate after scaling with the availability of mud in the bed. Despite the limited number of data points, the observations reveal that the erosion rate of mud decreases for increasing mud content. The highest modeled erosion rate were generally found for experiment J with p_{mud} = 13%. This implies that the erosion rate decreases, whereas the availability of mud increases.

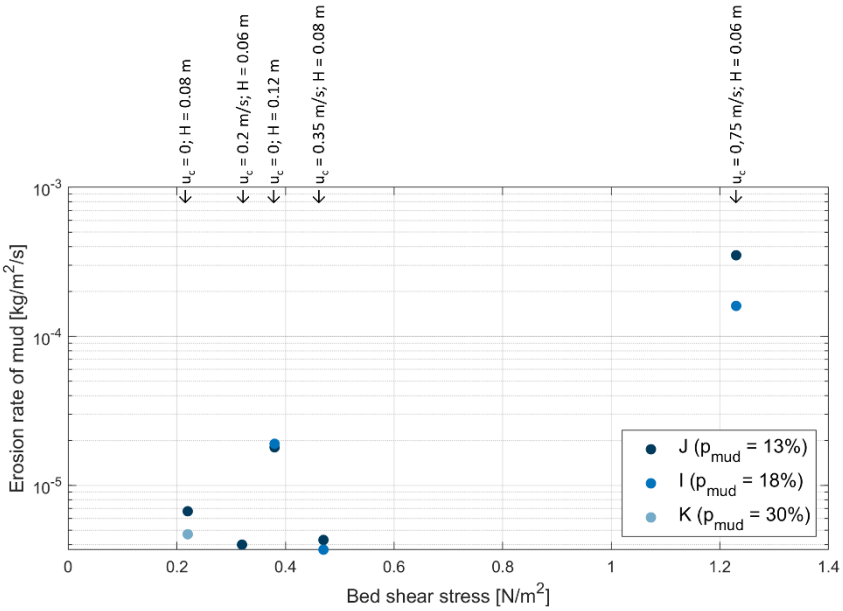

Figure 3.3.1 Estimated erosion rate (vertical axis) of mud for long bed experiments with different sediment samples and different hydrodynamic conditions, which characterized by the total bed shear stress on the horizontal axis.

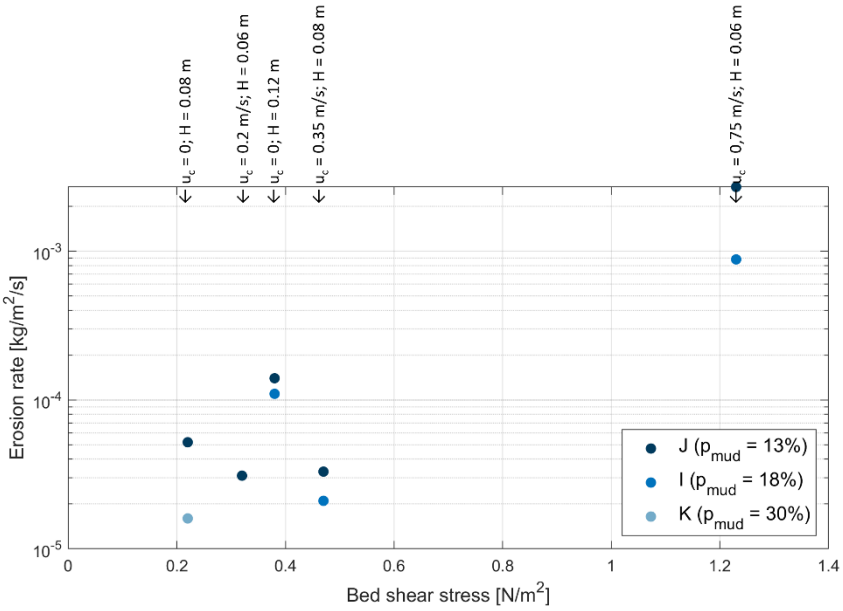

Figure 3.3.2 Estimated total erosion rate (vertical axis) for long bed experiments with different sediment samples and different hydrodynamic conditions, determined by scaling the erosion rate of mud by the availability of mud in the bed.

Van Rijn (2018, 2019) has given a rough indication of the erosion rates of mud-sand mixtures with dry density values in the range of 400 to 1000 kg/m^3. These estimates are included in Figure 3.3.3 by the colored lines. The erosion rate increases for increasing bed-shear stress ($E \sim \tau_b^2$) and decreases strongly for mixtures with increasing dry density and thus higher critical bed-shear stress values. The erosion rate of fine cohesionless sand of 63 μm is shown as the black dashed curve (Van Rijn et al., 2018) based on equation 3.3.2. The erosion rate of mixtures of clay-silt-sand is smaller than that of fine cohesionless sand due to the cohesive effects of the very fine clay fraction.

The range of erosion rates in the MUSA experiments is indicated by dashed red lines in Figure 3.3.3. The upper range reflects the erosion rates for diluted beds (dry bulk density of 300 to 1000 kg/m^3), as determined from the sample volume loss (Boechat Albernaz et al., 2022A (MUSA)). The lower range reflects the erosion rates from SSC analysis of long bed tests (dry bulk density > 1000 kg/m^3). The estimated erosion rates from the sample volume loss of the long bed tests with currents of 0.75 m/s are shown as black dots (Boechat Albernaz et al., 2022B (MUSA)).

Equation 3.3.2 is also shown for fine cohesionless sand (d_{50}=63 μm; $\tau_{cr,se}$=0.1 N/m^2) and for silt (d_{50}=31 μm; $\tau_{cr,se}$ = 0.3, 0.5 N/m^2). The computed erosion rate decreases strongly for finer sediments with higher critical bed-shear stress-values. The computed values are of the right order of magnitude.

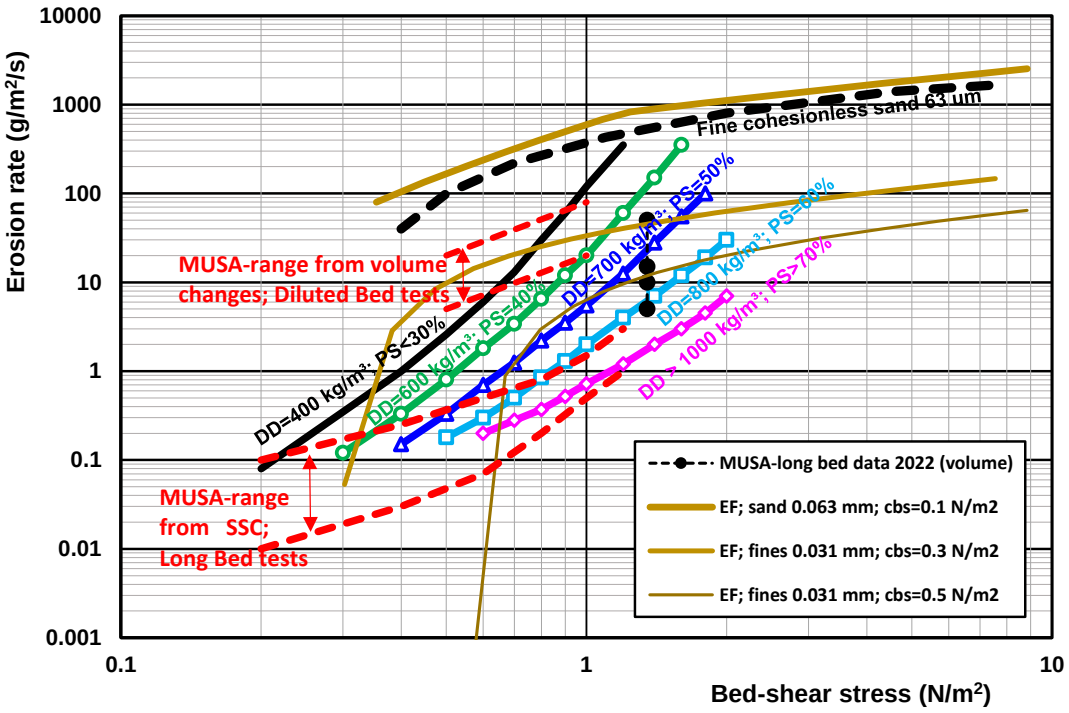

Figure 3.3.3 Erosion rates for mud-sand mixtures (EF = Erosion function; DD = dry density; PS = percentage of sand).

3.4 Mud and sand transport

3.4.1 Flume experiments with long beds

MUSA flume experiments with a long bed of pure fine sand (d_{50}=0.13 mm) and mixtures of mud (fines) and fine sand were performed to measure sand concentration profiles and transport in conditions with waves alone and combined currents and waves. The percentage of fines <63 μm ($p_{fines<63\ \mu m}$) in these experiments is in the range of 0% to 90% (Boechat Albernaz et al. 2022B (MUSA)).

So far, experimental results on the behavior of mud-sand bed mixtures under currents and waves have only been done by Peng Yao et al. (2015), who performed a series of flume experiments with beds of fine sand (≅90 μm) and silt (≅45 μm) collected from tidal flats in China.

The MUSA experiments with mud-sand bed mixtures show that the mud particles at the surface of the bed are washed out from between the sand particles when the bed-shear stress is higher than the critical bed-shear stress (cbs) for erosion. Small-scale isolated barchan-type sand ripples are slowly build up with darker grey/black spots (troughs) between the sandy crests. The sand ripples remain relatively flat (i.e. ripple suppression), as the availability of sand is limited and the sand particles are partly bonded by

cohesive effects. Ripples have a symmetrical shape when waves are dominant but become more asymmetrical for increasing current speeds. The suppression of ripple development already occurs for p_{fines} of about 10% but increases strongly for increasing percentage of fines (10% to 30%), resulting in a strong reduction (up to factor of 10) of the near-bed sand concentrations and transport. When the bed-shear stress is sufficiently high, the mud is eroded from between the sandy crests and almost immediately suspended into the water column.

A typical result of the MUSA-long bed tests with mud-sand mixture is presented in Figure 3.4.1, which shows sediment concentrations and transport over mud-sand bed with a percentage of fines < 63 μm in the range of 0% to 90%. The key findings of these experiments are:

- Sand concentrations near the bed are substantially reduced for increasing percentages of fines in the bed (reduction up to factor of 10 for p_{fines} > 10% and currents <0.35 m/s);
- Mud concentrations are rather uniform over the water column;
- Mud transport rates are higher than sand transport for p_{fines} >30% to 50%, which is partly caused by the increase in suspended sediment concentrations over the duration of flume experiments, such that the mud concentrations build up over time.

It is noted that the present results are valid for the artificial mixtures of mud and fine sand (0.13 mm). Additional experiments with natural mixtures of sand and mud are needed to confirm that the present results are also valid for natural sand-mud mixtures.

Figure 3.4.1 also shows some of the flume results of Peng Yao et al. (2015) with two types of fine sediment beds from the silty tidal flats of the Jiangsu Coast in China. In these experiments, a thin (~20 mm) layer of high concentrations (10 to 50 kg/m^3; mostly fine sand and coarse silt) formed in wave-only cases with H/h=0.3-0.45 and a sediment sample with 70% fines. Silt concentrations were much lower (0.5-1 kg/m^3) below this layer. With a 0.35 m/s current, the silt concentrations increase to values of 1-3 kg/m^3. Sand concentrations increased to 0.3-1 kg/m^3, as illustrated in Figure 3.4.1. In an experiment with a sample with 30% fines, sandy ripples (8 to 15 mm high and 50 to 100 mm long) were generated at the bed. A thin layer of high concentrations with values up to 10 kg/m^3 was generated in wave-only conditions (regular waves). Silt concentrations above the high concentration layer reached up to 0.5 kg/m^3. With a 0.35 m/s current, the silt concentrations increased to values of 0.5-2 kg/m^3. Sand concentrations were in the range of 1 to 10 kg/m^3 (Figure 3.4.2).

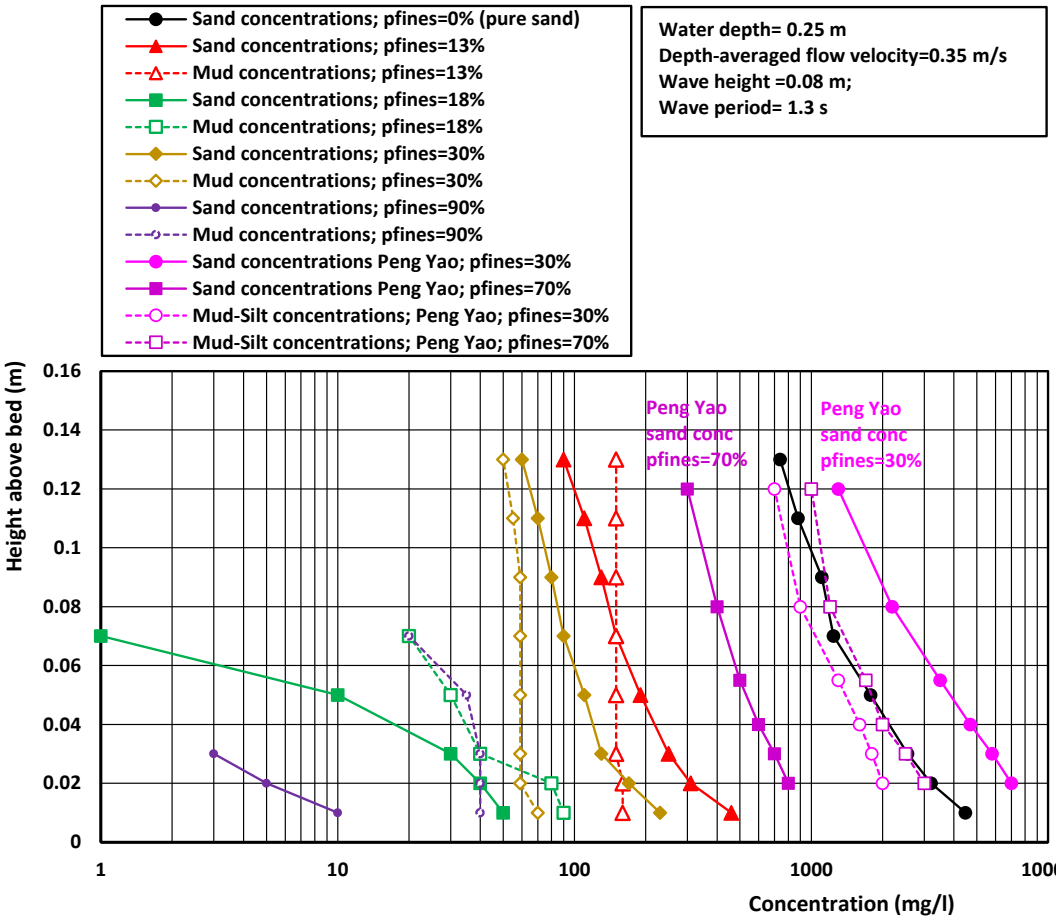

Figure 3.4.1 *Sand and mud concentration profiles of Test K: current=0.35 m/s; wave height=0.08 m; water depth=0.25 m*

Figure 3.4.2 shows the depth-averaged mud and sand concentrations in the long-bed experiments with U = 0.35 m/s and H = 0.08 m for samples with p_{fines} = 0%, 13%, 18%, 30% and 90%. The measured sand concentrations strongly decrease from 1800 mg/L to 200 mg/L when the percentage of fines increases to 13%. This is caused by the strong suppression of the bed ripples. The mud concentration increases to about 200 mg/L but remains fairly constant for a further increase in the mud content in the bed. It is noted however that the instantaneous mud concentrations may be largely determined by the background concentrations in flume system, such that the response to the actual hydrodynamic forcing condition is difficult to assess based on these data.

Figure 3.4.3 shows the depth-integrated transport of mud-silt and sand derived from the measured concentrations that are shown in Figure 3.4.2 and from the data of Peng Yao et al. (2015). The sand transport decrease for increasing percentage of fines, while the mud-silt transport increases for increasing percentage of fines. In the MSUA experiments, the sand transport is reduced by a factor of 10 for $p_{fines} \cong$ 30% and reduced by a factor of 1000 for $p_{fines} \cong$ 90%. In the data of Peng Yao et al. (2015), the maximum reduction of the sand transport rate is a factor of about 10 for $p_{fines} \cong$ 70%. The mud-silt transport in these flume experiments is higher than the sand transport for p_{fines} in the range of 40% to 50%. The mud-silt transport remains fairly constant for p_{fines} > 30%.

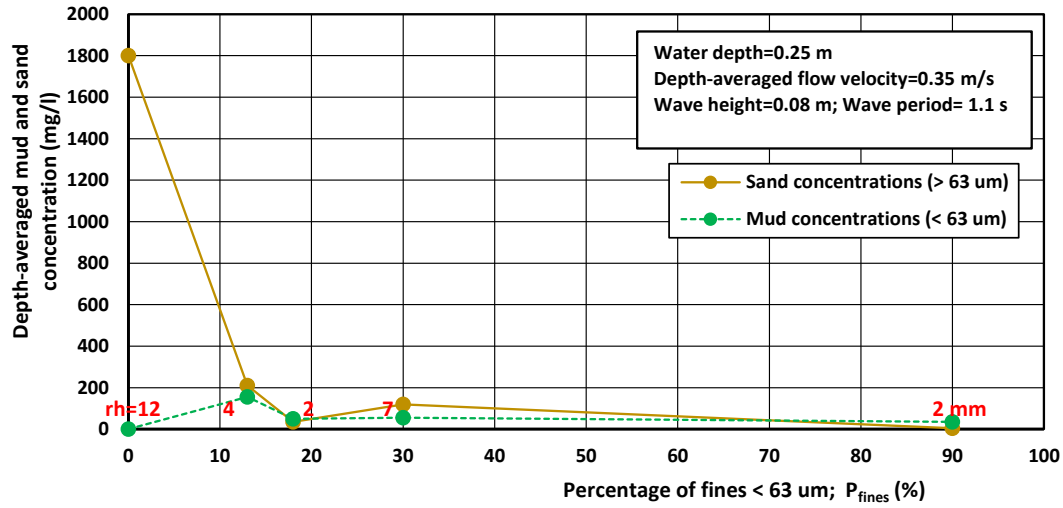

Figure 3.4.2 *Depth-averaged sand and mud concentrations of Test K: current =0.35 m/s; wave height=0.08 m; water depth=0.25 m*

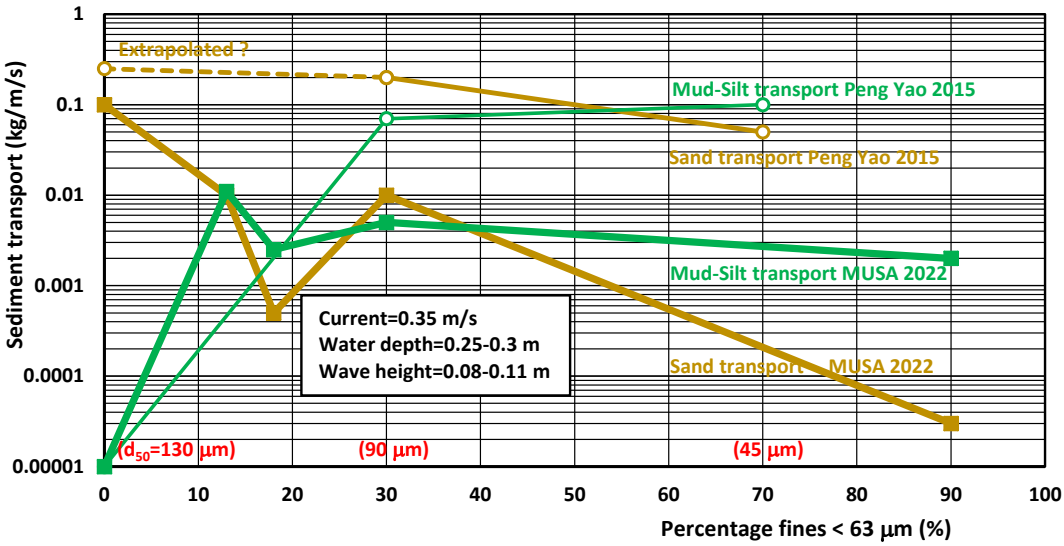

Figure 3.4.3 *Sand transport: current=0.35 m/s; wave height=0.08 m; water depth=0.25 m*

The results of two of the MUSA long-bed experiments with only waves and with combined waves and currents have been used to evaluate the sand transport model of Van Rijn (2007). The input parameters for the transport model are listed in Table 3.4.1. Calibration of the model results is focused on the reproduction of near-bed sand concentrations, as these are build up by locally eroded sand particles instead of sediment supply from upstream of the sediment sample.

The computed sand concentration profiles are shown in Figures 3.4.4 and Figure 3.4.5. The sand concentrations for a pure sand bed can be reasonably well (within factor of 2) represented by the model for both cases. Inclusion of mud (fines) in the model yields a higher critical bed-shear stress, resulting in lower computed sand concentrations. Compared to the flume measurements, these sand concentrations are somewhat too high in the near-bed region. The β-exponent of the critical bed-shear stress relationship (Equation 3.2.1) giving the best agreement is 2. Further research with additional flume experiments is required to improve the modelling of the sand and mud concentration profiles, especially with respect to the effect of the mud content on the near-bed reference concentrations and the effective wave-related mixing of fine sediments.

Table 3.4.1 Input settings for the Van Rijn (2007) sediment transport model to reproduce measured concentration profiles. The two mixing calibration factors are used to calibrate the wave- and current-related mixing.

Test	Sediment bed	Dry density (kg/m^3)	Water depth (m)	Wave height; period (m; s)	Current velocity (m/s)	Model input data			
						settling velocity (mm/s)	bed roughness (m)	mixing calibration factors	β-factor
A	pure sand 130 μm	1600	0.25	0.12 1	0	10	0.02	0.7; 1	2
K	mixture of fines (p_{fines}=30%) and sand 130 μm	1150	0.25	0.08 1.3	0.35	10	0.02	1; 1.5	2

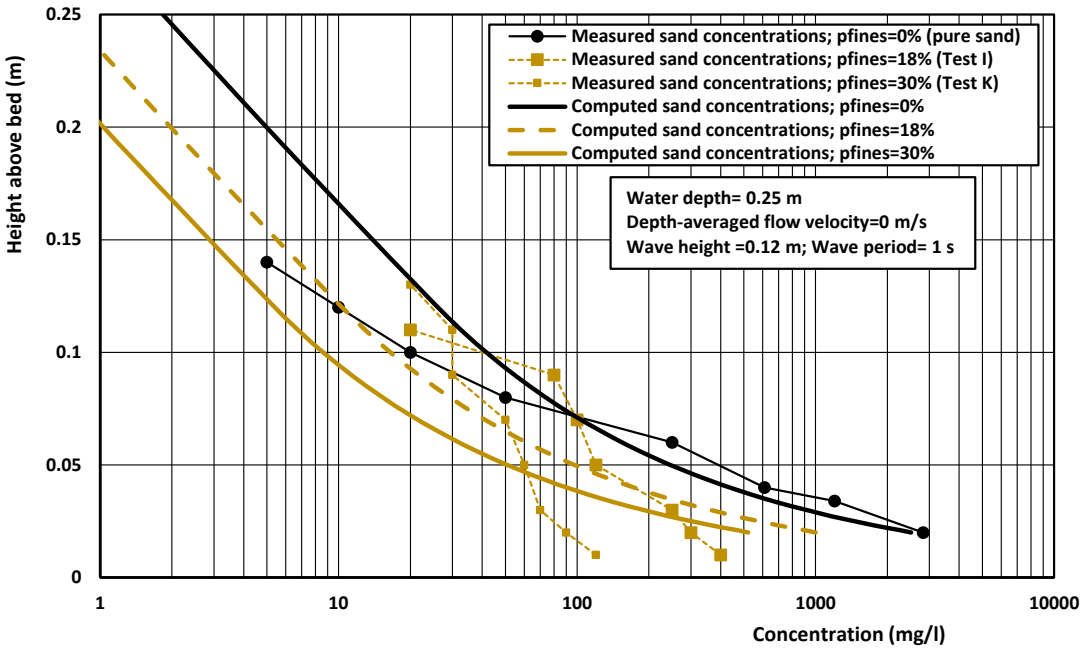

Figure 3.4.4 Measured and computed sand concentration profiles for long bed tests with only waves.

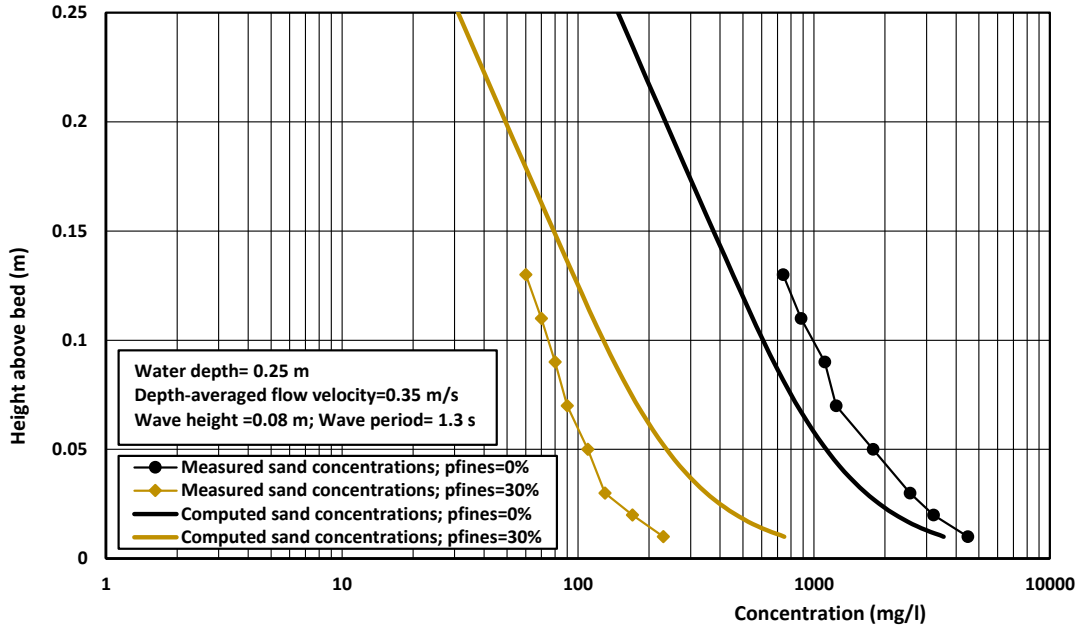

Figure 3.4.5 Measured and computed sand concentration profiles for long bed tests with waves and currents.

3.4.2 Field measurements

One of the objectives of the field work near Holwerd was to develop an instrumented bed frame for the measurement of sediment concentrations and current velocities very close to the mud bed (lowest 20 cm). The new bed frame was applied during two field campaigns in the Dutch Wadden Sea near Holwerd (MUSA report on field measurements by Boechat Albernaz et al., 2022C (MUSA)). Figure 3.4.6 shows the measurement frame and the filtration system to determine sand- and mud concentrations.

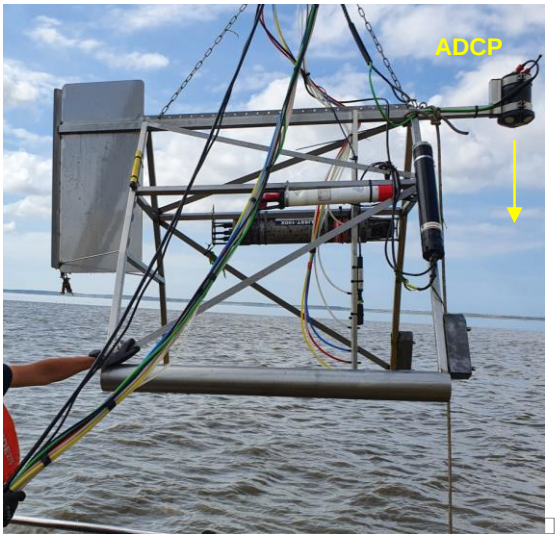

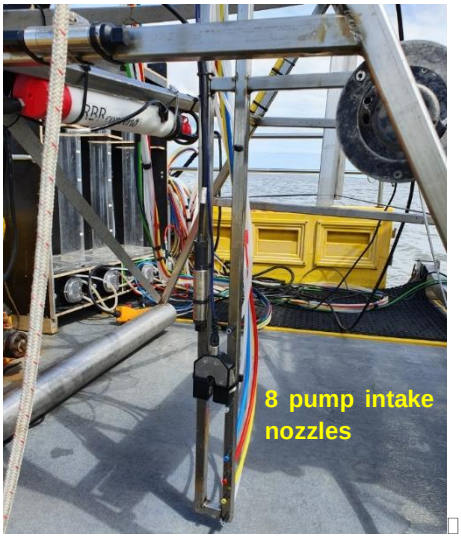

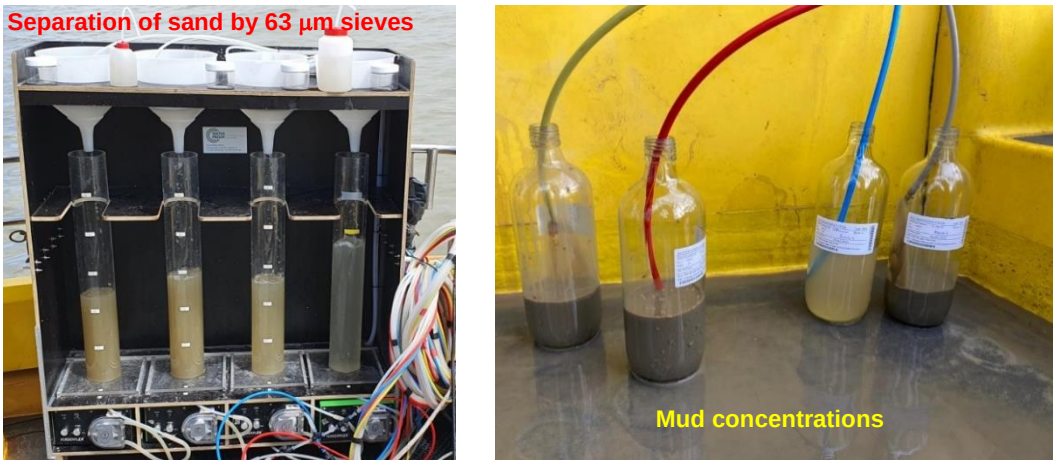

Figure 3.4.6 Measurement frame with intake nozzles and filtration system to determine sand- and mud concentrations.

The measured data have been used to determine depth-integrated mud and sand transport rates over the tidal cycle (function of tidal flow velocity).

An example of the depth-integrated mud transport over the tidal cycle is shown in Figure 3.4.7. The local peak tidal current velocities are in the order of 1 m/s (Day 3 of the measurement campaign; 14 June 2022). The part of the tidal period in which flow velocities exceed 0.5 m/s during ebb and flood is rather short (3 to 4 hours). The maximum depth-integrated mud transport is measured at maximum current velocity during ebb. Analysis of all the data obtained near Holwerd (i.e. during the multiple-day measurement campaign) shows that the mud concentrations and transport rates during the flood period are generally somewhat higher than during the ebb period, except for Day 2. Very marked hysteresis effects in the mud concentrations are absent.

The depth-averaged mud and sand concentrations and the depth-integrated sand and mud transport for distinct velocity classes between 0.5 and 1.5 m/s are visualized in Figure 3.4.8 and Figure 3.4.9. For comparison, measured sediment concentrations and transport rates (error bands of ±50%) in the coastal zone of Bengal Bay (Bangladesh; Van Rijn, 2021) are also shown.

The sand and mud transport rates show a good correlation with the depth-averaged flow velocity. The sand transport rate can be represented by

$$q_{s,sand}=0.7\ u_{mean}^{4.5};$$

whereas the mud transport rate can be represented by

$$q_{s,mud}=2\ u_{mean}^{2}.$$

These empirical transport functions for sand and mud are specifically valid for flow velocities > 0.7 m/s around peak flow conditions near Holwerd with a sandy mud bed (coarse silt bed).

The mud transport is around a factor 10 higher than the sand transport at low flow velocity of 0.5 m/s and about a factor 1.3 higher at high velocity of 1.5 m/s. This is caused by the rapid settling of sand particles around slack tide, whereas settling lag effects are important for the mud concentrations. Depth-averaged sand concentrations are in the range of 15 to 600 mg/L for velocities between 0.5 and 1.5 m/s. Depth-averaged mud concentrations are in the range of 150 to 1000 mg/L for velocities between 0.5 and 1.5 m/s. The mud and sand concentrations at Holwerd are very similar to those measured at the muddy/silty coastal zone of Bengal Bay, particularly at higher flow velocities > 1 m/s.

The depth-integrated mud transport values of the MUSA-measurement campaign in 2022 in the velocity range < 1 m/s are in the same range as those of other field campaigns in 2016 and 2019 (Deltares, 2016; 2021; WaterProof, 2019; Van Rijn, 2019). The sand transport rates of the MUSA-field campaign in 2022

are somewhat higher, which is probably caused by the larger number of sampling points close to the bed, where concentrations are relatively high.

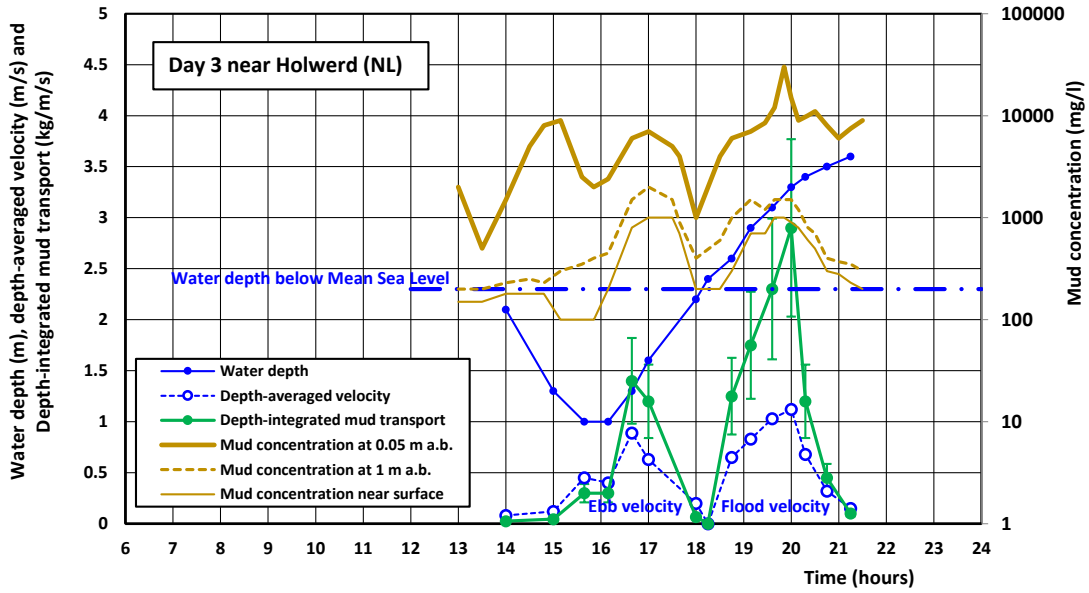

Figure 3.4.7 Measured water depth, flow velocity, mud concentration and mud transport on Day 3 of the MUSA-measurement campaign (14 June 2022).

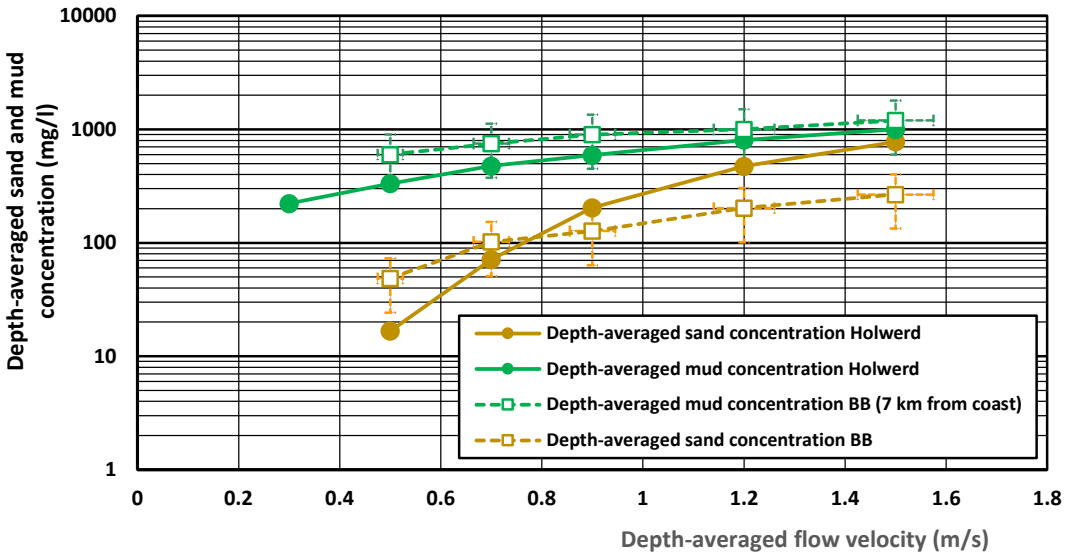

Figure 3.4.8 Depth-averaged sand and mud concentration as function of depth-averaged flow velocity for measurements at Holwerd and in the coastal zone of Bangladesh (BB).

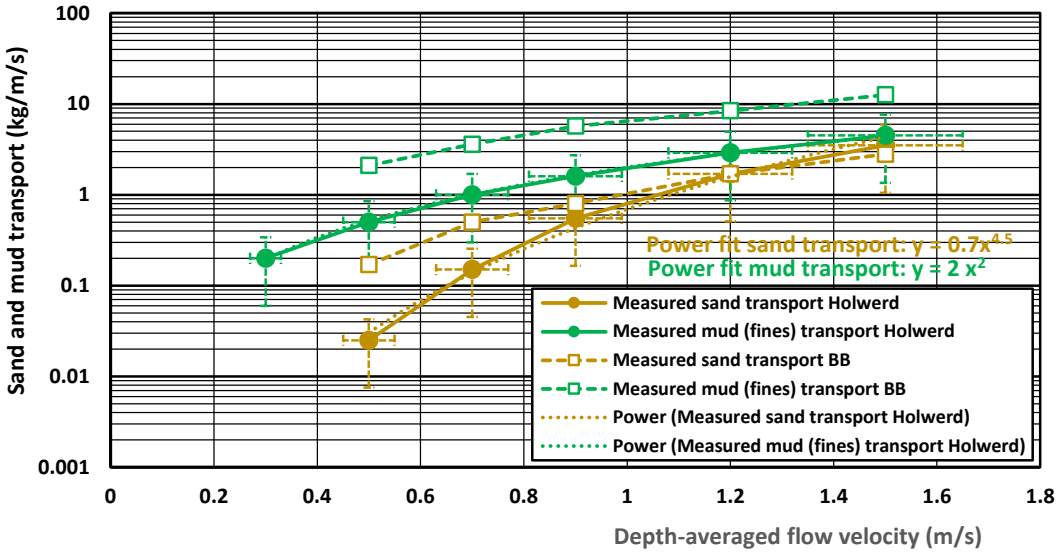

Figure 3.4.9 Depth-integrated sand and mud transport as function of depth-averaged flow velocity for measurements at Holwerd and in the coastal zone of Bangladesh.

3.4.2.1 Sand transport

The sand transport model of Van Rijn (2007) has been used to compute the sand concentration profiles. The input data for the transport model is given in Table 3.4.2. The decrease in bed roughness for higher flow velocities represents the effects of bed irregularities to be washed out by large flow velocities. Both the results for a pure sand bed and for a sand bed with $p_{fines} = 0.3$ are listed in Table 3.4.2. The difference between these results is caused by (1) a damping factor on the fluid (momentum) mixing coefficient, (2) by an increasing critical bed-shear stress of sand for increasing p_{fines} (Equation 3.2.1), and (3) by scaling the sand concentrations by the availability of sand in the bed (i.e. multiplication by a factor $1-p_{fines}$).

The computed sand transport rates are shown in Figure 2.10.10. Additional data from literature are also shown (Bauamt fur Kustenschutz, Norden, 1987; HR Wallingford, 1996,1997; Van den Berg & Van Gelder, 1993). The measured sand transport rates measured near Holwerd are somewhat lower (factor 2) than the measured values at the comparable Nessmersiel site in the German Wadden Sea, particularly in the low velocity range <0.7 m/s. It is noted that the bed of the Nessmersiel channel is somewhat more sandy than the channel bed near Holwerd. The mud concentrations at Holwerd are higher than at the Nessmersiel site. The UK-sites are more sandy tidal flats. The Huanghe river site has a very fine and easily erodible silty bed, which may explain the relatively high transport values at low velocities.

The computed values for a pure sand bed are too low compared to the data from literature, particularly for lower velocities <0.7 m/s. Compared to the measured sand transport rates at Holwerd, the computed values are somewhat too high for a pure sand bed (factor 3) and somewhat too low when the effect of the mud fraction (β=1 in Equation 3.2.1) is taken into account.

Figure 3.4.11 shows measured and computed sand concentration profiles for a pure sand bed (dashed curves) and mud-sand mixture with p_{fines}=0.3 (β=1; dotted curves). In the latter case, the critical bed-shear stress for erosion of sand are higher resulting in lower near-bed concentrations. The extra damping of turbulence due to the presence of the mud concentrations is not yet taken into account in these concentration profiles, although that would lead to less mixing of sand particles and thus to less steep sand concentration profiles in the near-bed layer.

As regards the β-factor, it is noted that a value of 1 produces the best agreement for field data, whereas a value of 2 gives better results for the flume data.

Flow velocity class (m/s)	Water depth (m)	Wave height and peak period (m; s)	Bed sand $d_{50,bed}$ (um)	Sus-pended sand $d_{50,sus}$ (um)	Settling velocity (mms/)	Bed rough-ness (m)	β-factor	Computed depth-integrated sand transport (kg/m/s)	
								pure sand bed	sand bed with p_{fines}= 0.3
0.5	4	0.2; 4	120	80	5.0	0.05	1	0.048	0.016
0.7	4	0.2; 4	120	90	6.3	0.04	1	0.25	0.10
0.9	4	0.2; 4	120	100	6.8	0.03	1	0.95	0.41
1.2	4	0.2; 4	120	110	8	0.02	1	4.5	2.0
1.5	4	0.2; 4	120	120	9.5	0.02	1	12.1	5.3

Table 3.4.2 Input data and results for the Van Rijn (2007) sand transport model. Temperature = 15 °C; Salinity = 30 promille; Sea water density = 1020 kg/m^3; Sediment density = 2650 kg/m^3.

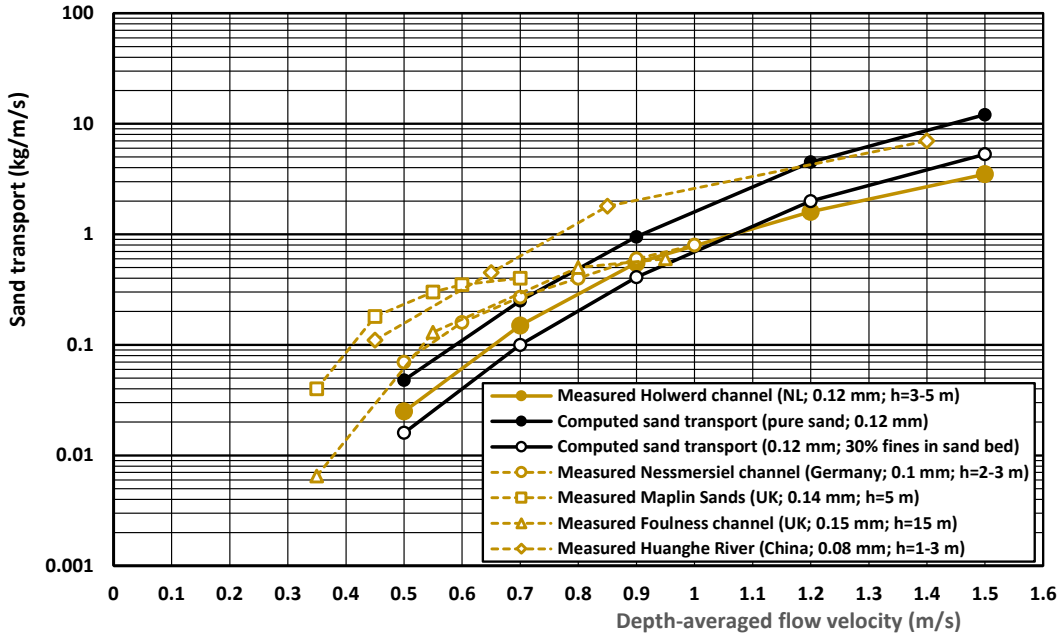

Figure 3.4.10 Measured and computed sand transport rates as function of depth-averaged flow velocity; field data from Holwerd ferry channel and from literature.

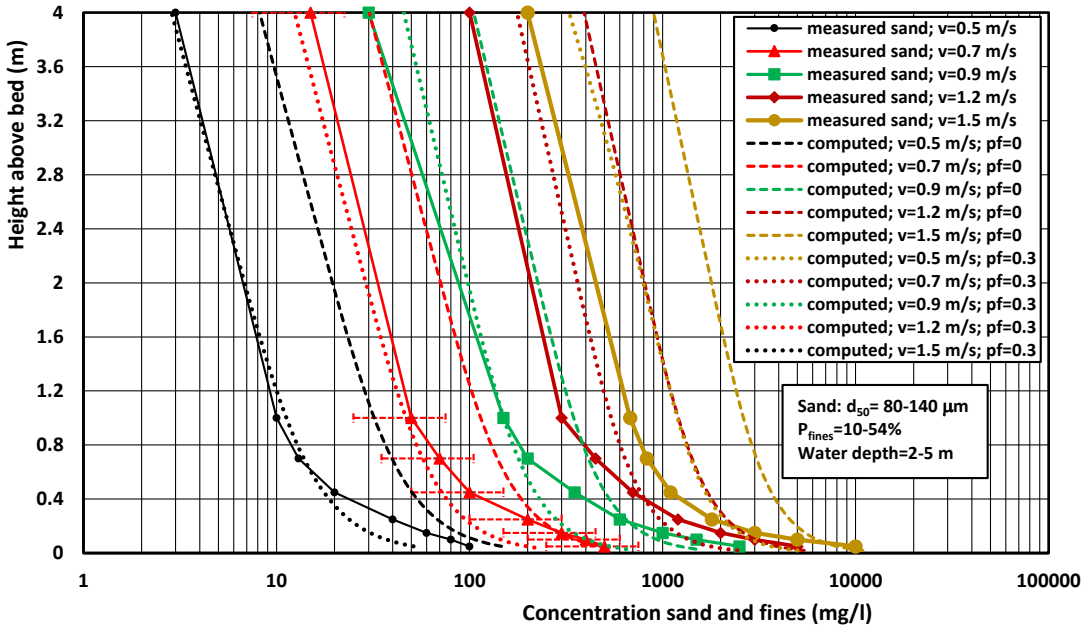

Figure 3.4.11 *Measured and computed (with and without a fraction of fines (p_{fines} = 0.3)) sand concentration profiles for 5 velocity classes from 0.5 m/s to 1.5 m/s.*

3.4.2.2 Mud transport

The simplified TMUD model for mud transport (Van Rijn, 2007; 2015) has been used to compute the mud concentration profiles at peak tidal flow velocities during the measurement campaign (see Figure 3.4.12).

The numerical TMUD-model is a simple model for mud transport in tidal flow based on the quasi-steady computation of the mud concentration profiles largely neglecting the $\partial c/\partial t$-term of the 2DV advection-diffusion equation. The full time-dependent 2DV-advection-diffusion equation is modelled by more sophisticated models (DELFT3D and SUSTIM (Van Rijn and Meijer, 2023).

The TMUD-model is expected to be reasonably valid to reproduce the sediment concentrations in the Holwerd-ferry channel with mud-dominated bed, as the sediment concentrations are to large extent governed by local erosion and deposition, although some mud may also be supplied by advection.

Figure 3.4.12 and Figure 3.4.13 show the computed mud concentration profiles at maximum flow conditions on Day 3 of the measurement near Holwerd (14 June 2023). The scaling coefficient (α_{mud}) of the near-bed concentration is calibrated set to a value that gives a bed concentration in the order of 5 kg/m^3. The bed concentration is prescribed at a level of a = 0.02 m above the bed (at top of the high-concentration layer near the bed). The settling velocity as function of the sediment concentration is about 4 mm/s in the near-bed region, decreasing to about 0.17 mm/s near the water surface. The agreement between computed and measured concentrations is quite good for peak flood flow conditions (Figure 3.4.13) and somewhat less good for peak ebb flow conditions (Figure 3.4.12). Generally, the computed mud concentrations are somewhat too high in the near bed region and somewhat too low near the water surface.

It is noted that the computed concentration profiles of the TMUD-model are constrained by many parameters for the near-bed concentration, settling velocity and vertical mixing. If the same model with the same settlings would be applied to a different location at a different time of the year, the parameters involved may be different. Thus, the model requires substantial calibration based on concentration data. Further research is required to study the generality of these parameters.

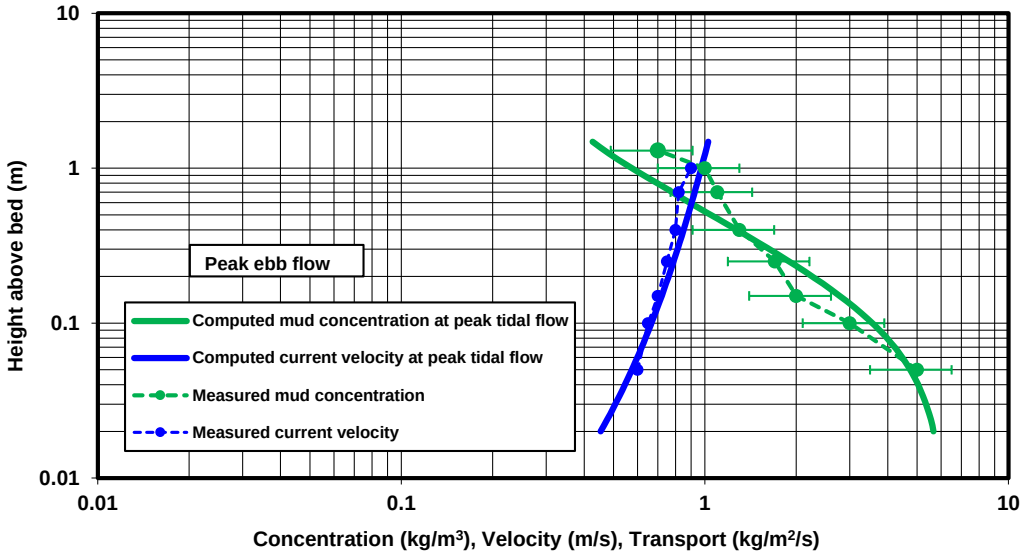

Figure 3.4.12 Measured and computed mud concentration and transport rate at peak ebb flow on Day 3 of the measurement campaign near Holwerd (14 June 2022).

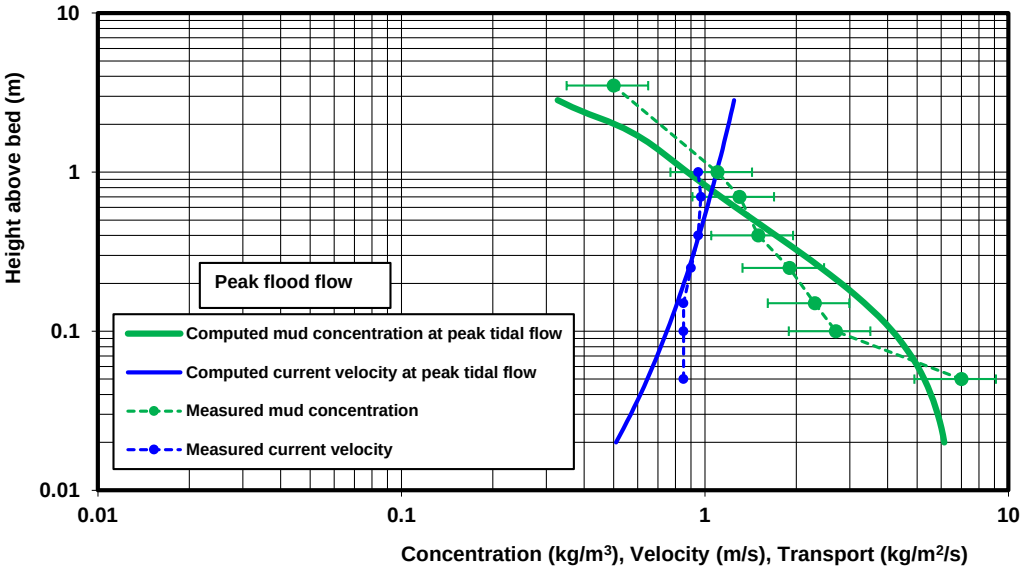

Figure 3.4.13 Measured and computed mud concentration and transport rate at peak flood flow on Day 3 of the measurement campaign near Holwerd (14 June 2022).

The effect of a different settling velocity in the range of 0.1 to 5 mm/s on the computed mud concentration is illustrated in Figure 3.4.14 for peak flood flow conditions. For a settling velocity of 5 mm/s, the mud concentrations are much too low in the upper part of the water column. The mud concentrations are almost uniform over the depth for a settling velocity of 0.1 mm/s. Based on this, it is concluded that a concentration-dependent mud settling velocity is essential for a good representation of the measured mud concentrations near Holwerd, particularly when only one fraction is used. Using multiple fractions, the sediment concentrations in the upper part of the water column can be sufficiently accurate represented by a low settling velocity in the range of 0.1 to 0.5 mm/s, while the near-bed concentrations can be modelled by a much higher settling velocity in the range of 1 to 3 mm/s. The multi-fraction approach is the best possible approach as it involves more physics and less fitting/calibration. However, a concentration dependent settling velocity remains necessary to properly represent the flocculation process.

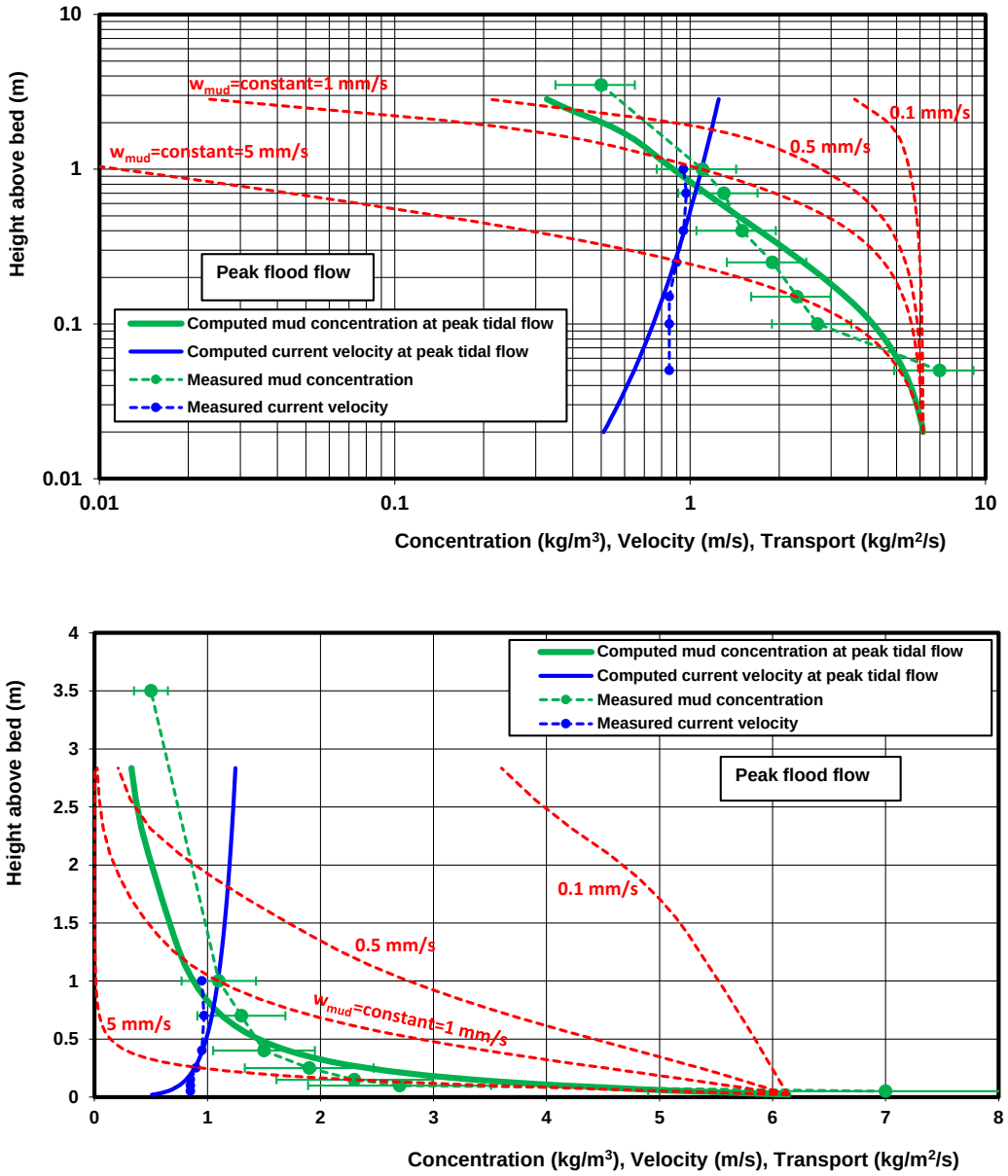

Figure 3.4.14 Computed concentration profiles for different settling velocities at peak flood flow, visualized on a logarithmic (top) and on a linear scale (bottom).

The TMUD-model has also been used to determine the depth-integrated (equilibrium) mud transport rate as function of the depth-averaged tidal current velocity, see Figure 3.4.15. The computed (equilibrium) values show good agreement with measured values for current velocity values > 0.7 m/s. The computed values are substantially too low for velocities < 0.7 m/s; for a velocity of 0.5 m/s, the concentrations are up to a factor 10 too low. It is noted that the part of the tidal period with low current velocities below critical conditions for erosion (<0.4 m/s) is dominated by settling processes, which are slow processes for very fine sediments with low settling velocities < 0.5 mm/s. For example, the settling time of sediments with settling velocity of 0.5 mm/s over a water depth of 3 m is about 6000 s (about 2 hours). Obviously, the mud settling lag processes around slack tide with low current velocities cannot be modelled by a local, quasi-equilibrium approach as implemented in the TMUD-model. At high current velocities, the erosion and upward mixing is a much faster process (minor erosion lag), such that a quasi-equilibrium approach is relatively accurate in reproducing measured sediment concentrations.

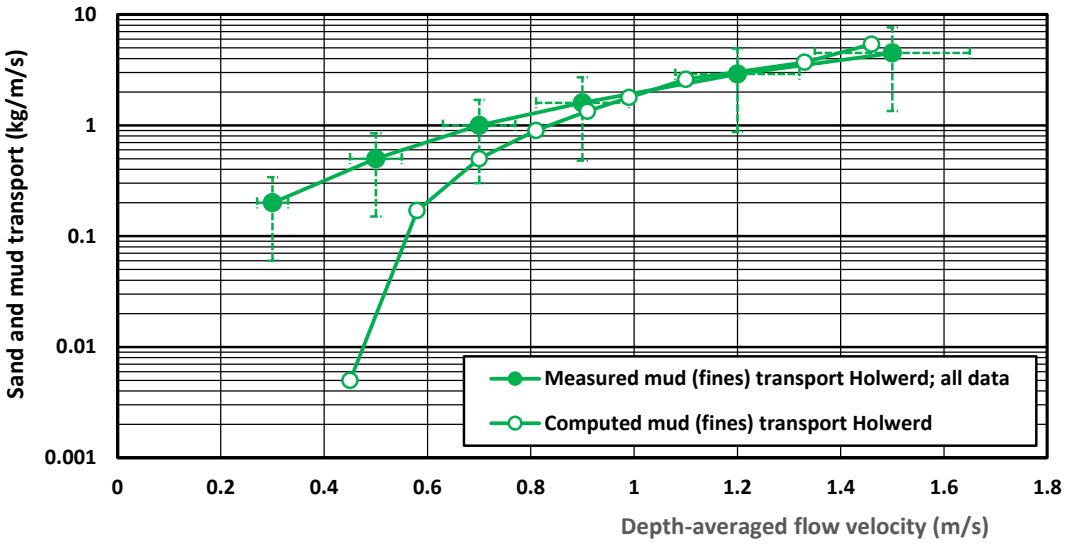

Figure 3.4.15 Measured and computed mud transport rates as function of the depth-averaged flow velocity.

The measured mud transport data of Figure 3.4.15 suggest a fairly simple relationship between mud transport and depth-averaged tidal velocity. This may be true for the Holwerd site where silty materials are dominant (16 to 63 μm) and the channel is relatively shallow (water depth of 2 to 4 m) resulting in relatively rapid exchange of sediments between the bed and the water column. In general, the relationship between mud transport and tidal flow velocity shows a hysteresis effect, which may be weak or strong depending on the type of sediments (clay or silt dominated) and the water depth (small or large). Figure 3.4.16 shows this hysteresis effect for a muddy channel with water depth of 10 m and maximum tidal velocity of 1.35 m/s based on computed results of the SUSTIM-model which solves the time-dependent mud advection-diffusion equation for fine sediments (Van Rijn and Meijer, 2023). The mud transport is substantially higher during decelerating flow with particles settling towards the bed (hysteresis effect), which is a slower process than the erosion of mud from the bed and the upward transport of mud into the water column by turbulent eddies.

The trend lines (red dotted curves in Figure 3.4.16) show that the mud transport is related to: $q_{mud} \approx u^{1.1}$ for accelerating flow and $q_{mud} \approx u^{1.3}$ for decelerating flow. The value of exponents is dependent on the tidal characteristics, the water depth and the type of sediments (clay, silt or sand-dominated). Higher values are obtained for smaller water depths and coarser sediments. In the case of a sandy bed the hysteresis effect is very minor and $q_{s,sand} \approx u^{3 \text{ to } 4}$.

A pragmatic approach is to represent the hysteresis curve by one single mean curve between mud transport and tidal flow velocity (green dashed curve in Figure 3.4.16). Using this approach, some errors of the order of ±30% are introduced which is of the same order of magnitude as the errors related to the measured mud transport (about ±50% for the Holwerd data, see Figure 3.4.15).

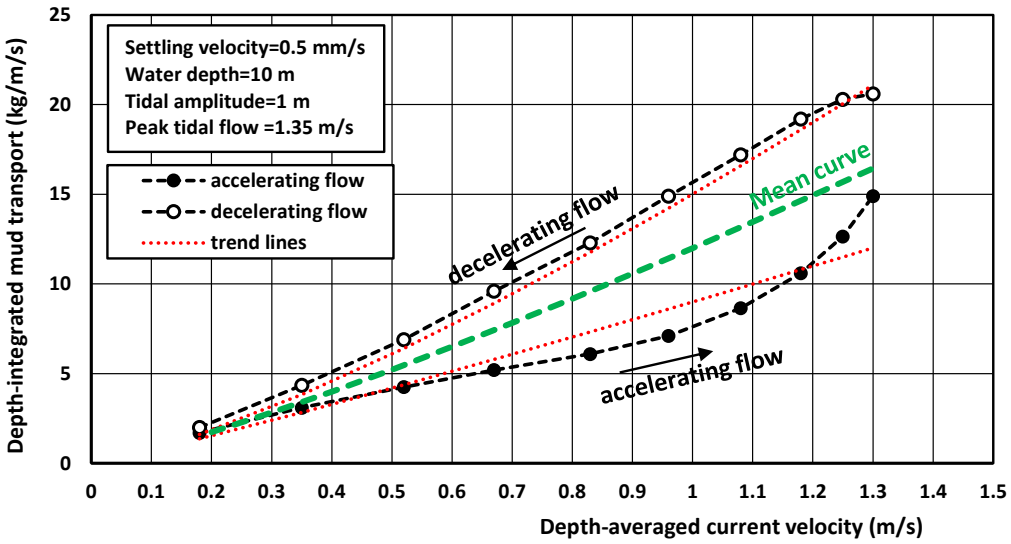

Figure 3.4.16. *Computed depth-integrated mud transport as function of depth-averaged current velocity; SUSTIM-model (Van Rijn and Meijer, 2023)*

4 Numerical modelling

4.1 Introduction

Part of the MUSA project was dedicated to improving numerical models. New formulations were implemented in both the Delft3D and MIKE3 numerical models, and in both modelling systems digital flumes were developed in analogy to the real flume experiments. The following numerical model studies have been executed as part of the MUSA project:

- Implementation of new sediment transport formulations in MIKE3 (the Wu et al. (2014) method) and testing in a numerical flume;
- Testing of sand-mud interaction formulations recently implemented in Delft3D by modelling the long bed experiments using a digital flume;
- Implementing a relationship between density and erodibility and testing this in an idealized tidal basin.

These three studies are summarized below. Besides, Delft3D modelling results for the Ems-Dollard estuary were analyzed on differences between the default (Partheniades-Krone) and Van Ledden formulation by Arcadis. In general, based on expert judgement and for this case, enabling Van Ledden results in a more realistic tide-averaged spatial suspended silt concentration pattern.

4.2 The MIKE digital flume

A digital copy of the laboratory flume used to measure erosion rates was built in the MIKE 3 Flow Model FM (Fontana, Petridis, Kaergard, 2023 (MUSA)). The hydrodynamics module (HD) simulates the hydrodynamics, and the mud transport module (MT) calculates the sediment dynamics. The horizontal mesh elements are dx of 5 cm and dy of 40 cm, and 10 sigma layers in the vertical. The flume recirculation scheme is also represented in the model by introducing a source/sink scheme. In this way, the hydrodynamics condition of the specific run is set in the source and sink specifications. A constant wave field is utilized as forcing for both the HD and MT modules. The modelled bed shear stress (τ_{RMS}) follows the Soulsby et al. (1993) RMS formulation for combined wave-current action.

In the sediment transport formulation, linear wave theory is used to compute the near-bed wave orbital velocity, which is utilized for calculating the bed shear stress under combined waves and currents. Due to the current-wave interaction in the flume, the wave height had to be modified in the model in order to obtain a good match between the measured wave orbital velocities and the wave orbital velocities used in the sediment transport model (which uses linear wave theory without interaction with the mean current). It is noted that in field conditions, the effect of the currents on the wave orbital motions is normally limited and the linear wave approximation is generally valid.

The sand fraction is modelled according to Wu et al. (2014), and the mud fraction is calculated following the existing MT module with specific improvements. The new sand transport formulation utilizes a modified critical shear stress introduced by Wu et al. (2000), which is a function of the hiding and exposure probabilities – stochastically associated with the size and gradation of the bed materials.

A key parameter for the sediment transport description is the critical bed shear stress for erosion. The estimation of the critical bed shear stress for the sand/mud mixtures is based on the reported incipient or near incipient motion conditions. More specifically, the maximum bed shear stress is calculated for the hydrodynamic conditions in the flume, which subsequently determines the range of the critical bed shear stress for each bed. The critical bed shear stresses calculated in this manner, are compared with the ones predicted using Wu et al. (2018). The two estimated bed shear stresses differ up to 33%, which is within what can be expected for this type of method. Furthermore, both the estimated and calculated bed shear stresses increase with increased mud percentage in the bed.

For the pure sand bed (Experiment A), it is observed that the simulated suspended sand concentration points along the water column differ from the observations by a maximum factor of 2 to 5 (Figure 4.2.1).

While a factor of 5 seems large, this result is typical for sediment transport models and shows that the new model implementation for the sand fraction is usable.

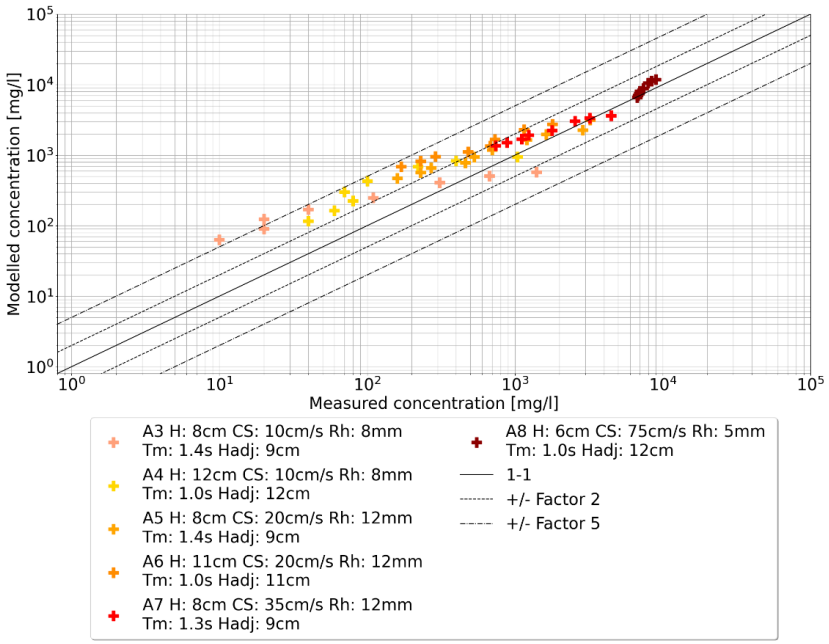

Figure 4.2.1. *Modelled morphological 1:1 representation of measured and modelled suspended sand concentration for experiment A.*

Figure 4.2.2 presents the simulated and measured suspended sand concentrations at the measurement points along the water column for experiments I, J, and K where the bed consists of a sand-mud mixture. The observed concentrations in the flume for run I5 are too low and thus this case is understood as an outlier.

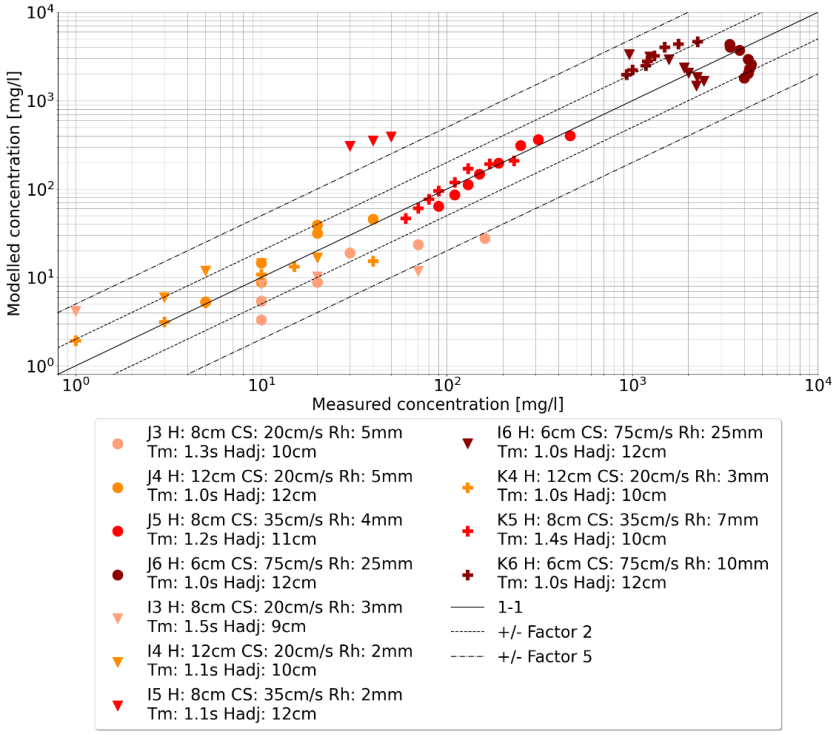

Figure 4.2.2. *1:1 representation of measured and modelled suspended sand concentration for experiments I, J, and K*

For the sand-mud mixed beds, the model predictions are within the factor of 2 to 5 for both the sand and mud fraction although the comparisons are a little worse than for the pure sand case. Overall, the model performance is similar to results from the literature with respect to the comparison with this type of measurements. Therefore, the new combined mud and sand transport model is deemed able to represent the dynamics of the sand and fines fractions in a sand-mud mixed bed for combined waves and currents.

It is noted that in the present study, the model predictions are compared to the experimental data by calibrating the critical shear stress for erosion and the erosion factor of each of the different bed compositions where the percentage of sand and mud in the bed is varied. The results show that the sediment transport model is able to reproduce fairly well the suspension of sand and mud in the water column and thereby also the sediment transport (see Fig. 4.2.3).

The next step is to be able to predict the critical shear stress for erosion and erosion coefficient based on the composition of the bed. Here, we face the challenge that the bed mixtures in the experiments are artificial and not representative of the natural beds. In the MUSA experiments phase 1A it was found that the natural beds had much higher critical bed shear stresses (at least due to pure current) than what can be achieved in the small wave flume which made it impossible to conduct experiments using combined waves and currents for the natural beds.

However, the results from the MUSA project does show that the density of the bed plays an important role in the critical shear stress for erosion and the erosion coefficient. Hence, when using the model for practical simulations, a relationship between the density of the bed (which may change through the simulation) and the critical shear stress for erosion and the erosion coefficient is applied.

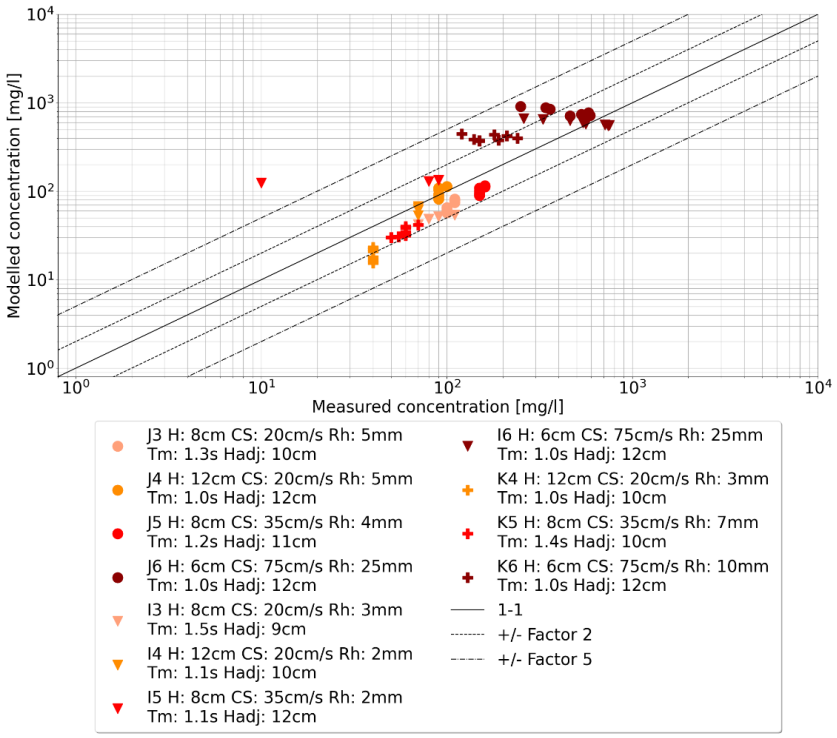

Figure 4.2.3. *1:1 representation of measured and modelled suspended mud concentration for experiments J, I, and K*

4.3 The Delft3D digital flume

The WaterProof flume of 13 m long and 0.4 m wide is also schematized into a digital flume in Delft3D, using 65 grid cells of 0.2 x 0.4 m and 20 equidistant σ-layers. The recirculation of water is generated in the digital flume by using a coupled intake and outfall. The intake is located in the most downstream grid cell and the outfall is located in the most upstream grid cell. In this way, flow velocities in the digital flume

are regulated by the imposed discharge at the intake and outfall (see Figure 4.3.1). Generating the recirculation by means of such a coupled intake and outfall is preferred over hydrodynamic up- and downstream boundary conditions because the intake and outfall allow suspended sediment concentrations to recirculate through the flume.

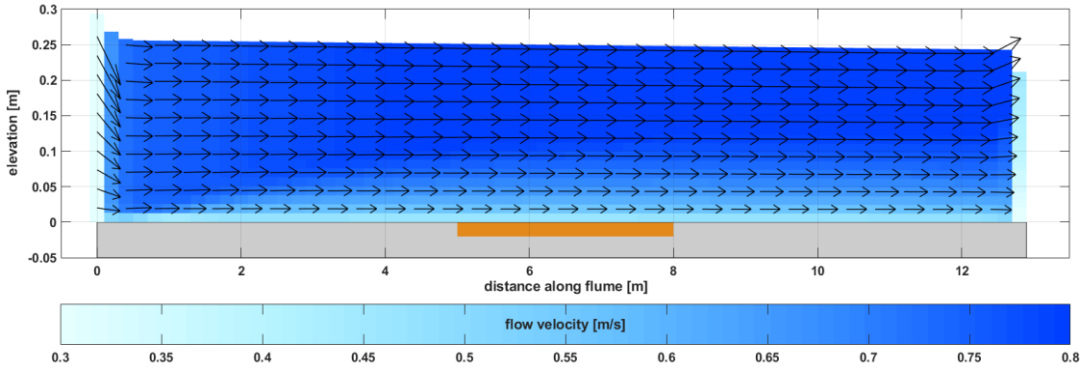

Figure 4.3.1. *Side view of flow velocities in the digital flume in Delft3D. The flow through the flume is generated by the coupling between an intake in the rightmost grid cell and an outfall in the leftmost grid cell.*

Waves are included in the digital flume by a coupling to a Delft3D-WAVE model. The boundary conditions imposed to each of the boundaries of the wave model are constant and uniform and are corresponding to the wave conditions in the laboratory flume experiments. Waves are propagating in the direction of the flume (φ = 270°).

Transport of sediment is computed with standard formulations of Partheniades and Krone for mud and van Rijn (2007) for sand. Sand-mud interaction is modelled using the method of van Ledden (2003) while the impact of mud on the erosion of sand with a Beta parameter in van Rijn (2007) - see van Weerdenburg et al. (2023 (MUSA)) for details. The numerical flume is deployed to better understand and analyze suspended sediment concentration observations in the Water Proof flume.

In terms of sand modelling, the digital flume revealed two important findings. First, the observed reduction in sand concentration with increasing mud content in the bed (left panel of Figure 4.3.2) is not numerically reproduced when modelling individual fractions only influencing each other by their relative availability in the bed. Two numerical methods are available to lower sand concentrations with increasing mud content in the bed: using Beta = 3 in the van Rijn (2007) formulation (increasing the bed shear stress of sand in case of a mud fraction) and the erosion formulations developed by van Ledden (2003). Within the applied parameter space provided by both methodologies, the modification of van Rijn has a larger influence on sand concentrations than the van Ledden approach. Which of the two is better could not be verified because of limitations related to the exact implementation of the van Rijn formulations.

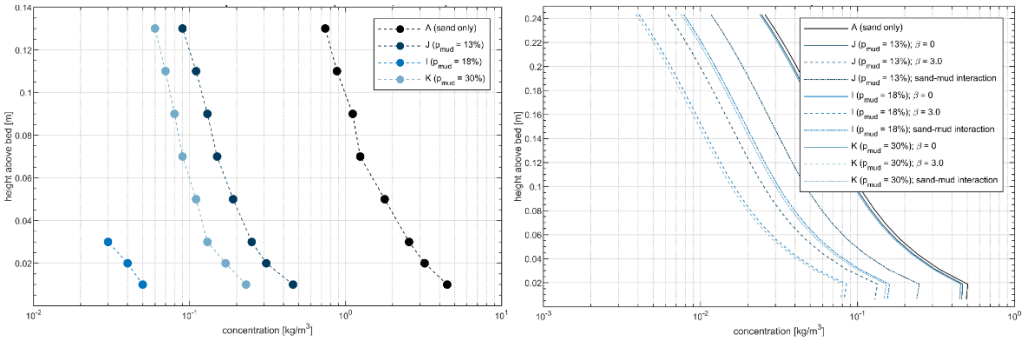

Figure 4.3.2. *Measured (left) and computed (right) sand concentrations without sand-mud interaction (solid lines), using van Rijn's Beta factor (dashed lines) and van Ledden's sand-mud interaction formulations (dash-dotted lines).*

Secondly, the absolute values of the computed sand concentration (also for a sand-only bed) where lower than observed but also predicted with point models such as DelCon and TR2004 (Figure 4.3.3). This is caused by a difference in the implementation of van Rijn in Delft3D relative to the original formulation, resulting in a substantial underestimation of sand concentrations relative to the measured sand concentrations and point models. This difference is caused by Delft3D using (1) a significant wave height Hs instead of a Root-Mean-Square wave height (Resulting in a $\sqrt{2}$ smaller orbital velocity) and (2) linear wave theory with a Rayleigh distribution spectrum (resulting in an orbital velocity $2/\sqrt{\pi}$ smaller). Correcting for these differences (by upscaling wave conditions) leads to a concentration profile more closely following the observations and point models, but also influencing the flow velocity structure. It is recommended to verify these discrepancies between the original van Rijn formulation and the Delft3D implementation in more detail as part of future work.

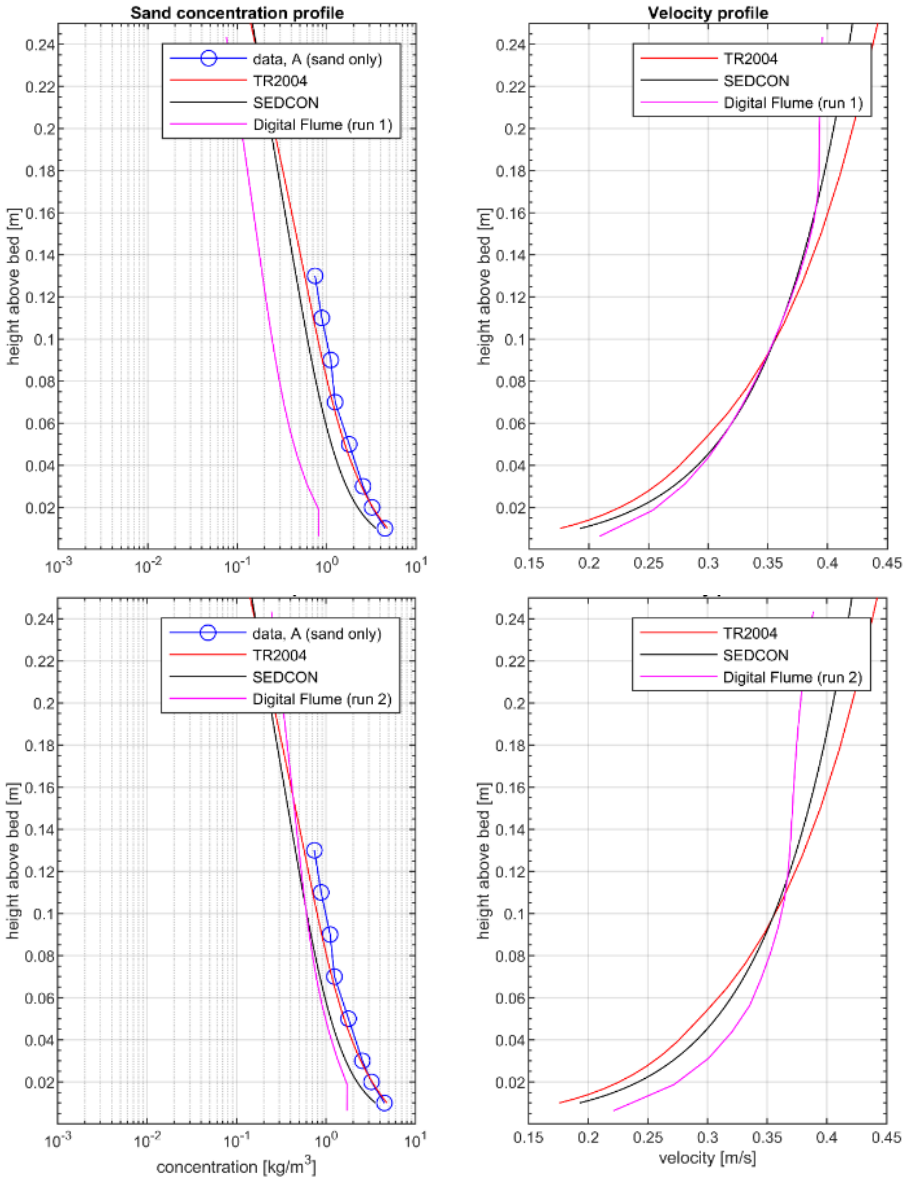

Figure 4.3.3. *Sand concentration (left panels) and flow velocity (right panels) with standard wave conditions (top panels) and after upscaling the wave height in the digital flume with √(8/π) (lower panels)*

An interesting and possibly important phenomenon that was observed in the physical flume experiments was that mud concentrations decreased with increasing mud content while the observed critical bed shear stress appeared largely unchanged. This implies that the erodibility of the mixture reduces (with

increasing mud content) through a reduction in the erosion parameter. Such a relationship is surprising, because most earlier work related erodibility of the bed to its mud content via the critical bed shear stress (and not the erosion parameter). However, such a reduction in erodibility also follows from van Ledden's sand-mud interaction theory (and may therefore be reproduced by Delft3D), and therefore tested with the digital flume.

Unfortunately, reproducing the observed suspended sediment concentration profiles proved difficult because of two reasons. First, the computed SSC is very sensitive to the period of erosion because the bed slowly eroded, and the mud content in the water column increased over time. This period of erosion was not recorded for the concentration profiles, and therefore difficult to compare to the model results (see Figure 4.3.4). Secondly, the observations are sometimes physically unreliable (a downward decrease in mud concentrations or an unrealistically low vertical variation).

The OBS measurements were used to determine erosion parameters by fitting the Partheniades-Krone equations to observed increase in mud concentrations over time (see Boechat Albernaz, 2022B (MUSA)). The numerical flume was used to deduce erosion parameters from the OBS in another way. The model was run with different sets of erosion parameters and calibrated against the OBS observations (i.e. a classical calibration procedure). Unfortunately, both methodologies provided very different results with the numerical flume having erosion parameters an order of magnitude larger than those obtained from direct data fitting. We believe that these differences mainly arise from the background concentration in the flume at the beginning of each experiment. This initial concentration was the same (and low) after placement of the bed, but after each hydrodynamic cycle (with gradually increasing wave height and / or velocities) the initial concentration became higher. The long bed erosion experiments are probably not the most suitable methodology to determine erosion parameters of the mud.

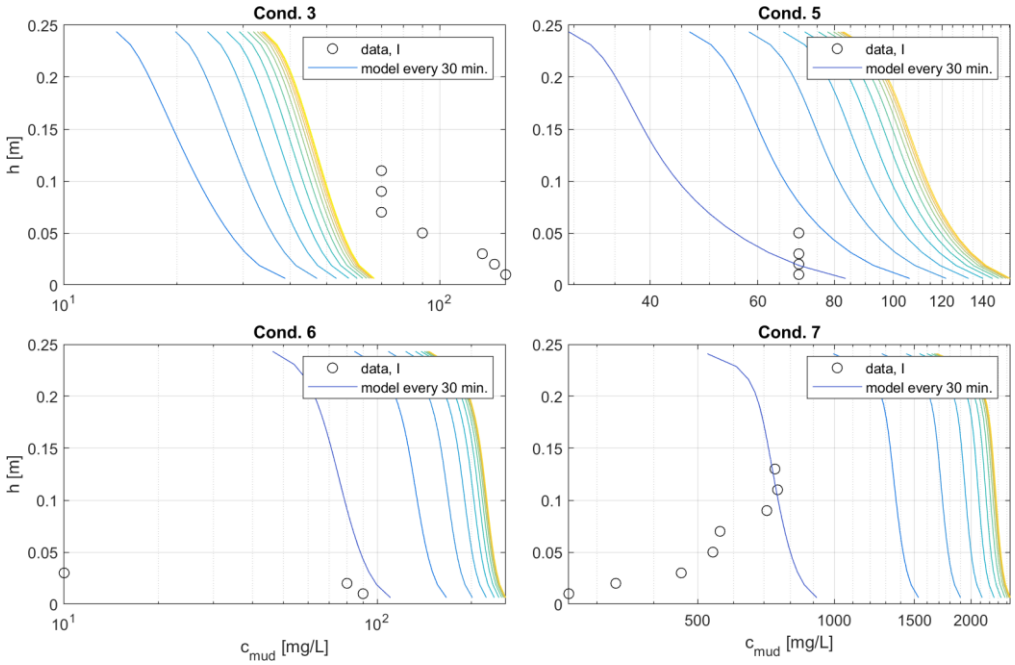

Figure 4.3.4. *Observed mud concentration (circles) and computed mud concentration profiles over time for 4 flume scenarios.*

4.4 Bed density effects on erodibility – implementation in Delft3D

Intertidal environments are often characterized by sandy channels and muddy intertidal flats. Mud is transported through the channels and deposited on the intertidal flats during relatively calm conditions. The mud subsequently develops strength and is able to resists erosion during subsequent storm events. This increase in strength is reflected in the relationship between density and critical bed shear stress in Figure 3.2.3. Low density deposits are often very muddy, and such deposits take so much time to consolidate that in practice such mud-dominated deposits remain easily erodible. Sand, on the other

hand, consolidates instantaneously but does not have a high critical shear stress against erosion. Over muddy intertidal flats, the greatest strength against erosion is typically observed for mixed mud-sand sediment beds. Sand results in relatively rapid consolidation rates while the cohesive behaviour of the mud results in great strength against erosion.

Implementing the dry density effect on erodibility in numerical models may therefore provide an important advancement in morphodynamic modelling. In general, it is very difficult (if not impossible) to model long-term morphodynamic development including mudflat formation with mudflats that are capable of surviving episodic storms. In order to evaluate the potential of a relation between density and erodibility, the relation between density and critical bed shear stress developed as part of MUSA (Eq. 3.2.2) was implemented in Delft3D see section 3.2 and in particular Figure 3.2.2). This equation requires a range of model input values (such as the minimum density and maximum density) which can be based on specific site conditions (see van Weerdenburg et al., 2023 (MUSA)) for details. It also requires a relationship between density and mud content, for which a simple formulation was proposed as:

$$\rho_{dry} = 500\ p_{mud} + 1600\ p_{sand}. \qquad (4.4.1)$$

in which p_{mud} and p_{sand} are volume fractions such that $p_{mud} + p_{sand} = 1$. The relation between density and critical bed shear stress (Equation 3.2.2) provides a range of additional calibration parameters for optimizing the morphological evolution and the mud content of the bed, which were tested using a schematized tidal developed earlier by Colina Alonso et al (2023, see Figure 4.4.1). This model is initialized with a constant but linearly sloping bed consisting of 5% mud and 95% mud. The model is forced with tidal conditions for a period of 45 years to evaluate channel patterns evolving over time – earlier work suggested the model is close to an equilibrium condition after 45 years. The model is subsequently run for 5 years with more energetic wave conditions.

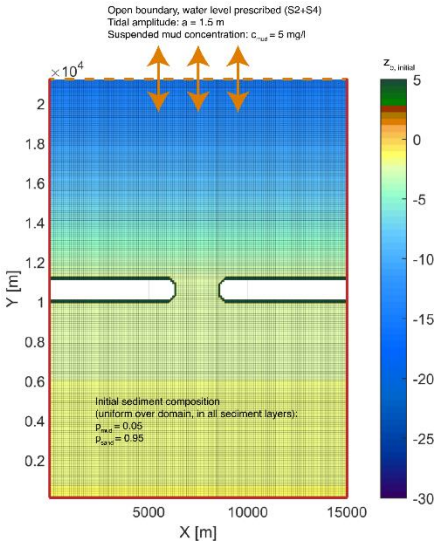

Figure 4.4.1. *Overview of the model set-up, showing the initial bathymetry, the closed boundaries (red lines), the open boundary (orange dashed line) and the computational grid (for both flow and wave computations, with a resolution of 100 x 100 m.)*

The range in potential additional input parameters (see Figure 4.4.2 and van Weerdenburg et al. 2023 (MUSA) for much more details) provide methods to better calibrate existing numerical models. But more importantly, it provides a methodology in which a realistic bathymetry may evolve over time during tide-dominated conditions which has sufficient strength to remain in place during a period of storm conditions. The simulation depicted in the left panels of Fig. 4.4.3 was computed without density effects, using a bed shear stress against erosion of 0.5 Pa, and during storm conditions most of the muddy intertidal flats erode. In reality, the critical shear stress against erosion of such mudflats are closer to 1-2 Pa or more (Colosimo et al., 2023). The simulation on the right has a bathymetry and mud distribution comparable to

the simulation on the left, but has a resistance against erosion varying with the density and associated mud content, and is typically 1 to 1.5 on the mudflats. Such values are much closer to observed critical bed shear stresses and as a result the synthetic mudflats using a density-dependent critical bed shear stress suffer from much less (unrealistic) erosion.

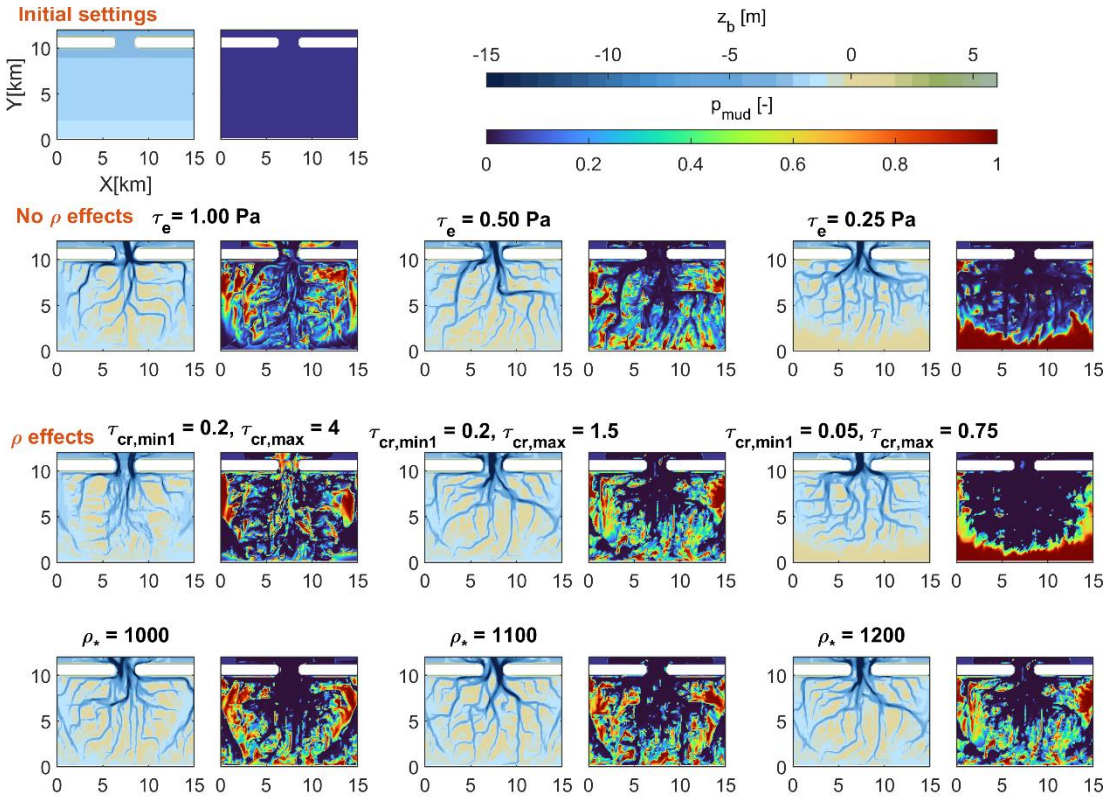

Figure 4.4.2. *Modelled morphological evolution (45 years, without storms) for a range of erosion settings without density effects (2nd row), and with density effects (rows 3 and 4). Every row explores the sensitivity to a specific parameter of the formulations. The plots show computed bed levels (left panel per model realization) and sediment composition (mud content, pmud) of the upper bed (0.1 m, right panel).*

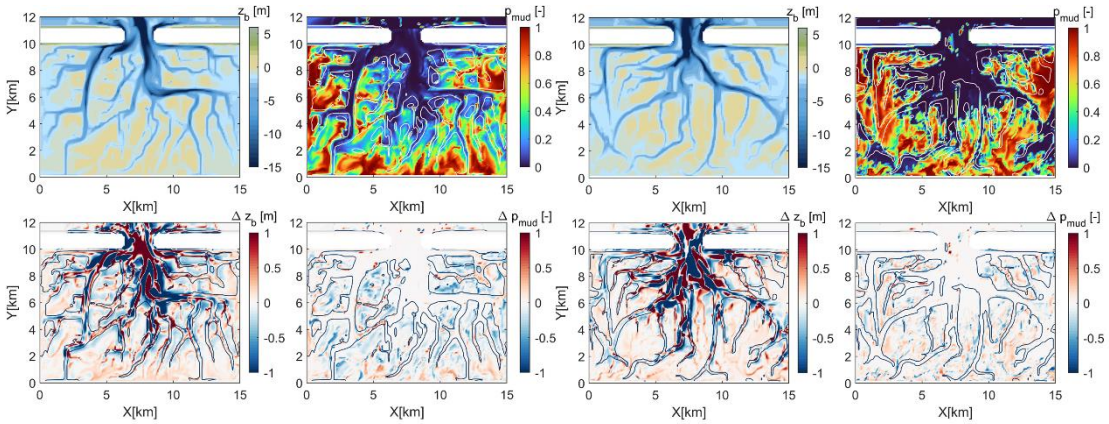

Figure 4.4.3. *Effect of modelling density effects on sediment mobility. The four panels on the left are results from a simulation without density effects; the four panels on the right are results from a simulation with density effects. For each cluster of 4 the top left (z_b) is the bathymetry computed after 45 years of tide-dominated conditions whereas the lower left provides the change in bathymetry during a storm. The top right (per cluster) is the mud content after 45 years while the lower right depicts the change in mud content after 5 years with storm conditions.*

5 Engineering tools

The improved and new formulations have been implemented in practical engineering tools, set up in either Excel, Python, or Matlab. The existing engineering tools by Leo van Rijn (https://www.leovanrijn-sediment.com/page4.html) are thereby extended. Modifications to SEDHAR have been implemented to CoDeS 2.0 (**Co**astal **De**sign and **S**upport tools).

5.1 SEDHAR

The SEDHAR-model is a semi-analytical box model which describes the time-dependent behaviour of the mud concentration in a harbour basin and associated mud deposition considering the in and outflow of mud by tidal filling/emptying processes, horizontal exchange processes and salinity-induced exchange processes through the harbour entrance. The mud concentration is assumed to be uniform over the water depth. The in and out flow of sand through the harbour entrance is included. An additional storage basin may be present at the end of the main harbour basin. The banks of the harbour basin may consist of mud flats/banks with lateral inflow of mud.

The original version of the SEDHAR-model has not been changed.

The experimental results of the MUSA-project can be used to get better estimates of the input data (dry bulk density, settling velocity).

5.1.1 Implementation of SEDHAR in CoDeS

The harbour sedimentation model in a simple engineering tool (CoDeS) is validated on the applicability and the correctness for eleven harbours at the Belgian, Dutch and German North- and Wadden Sea (Lammers, 2023). Annual maintenance dredging masses were compared to the modelled sedimentation masses to validate the similarity. The validation of the model shows that an accessible, quick and robust model is able to predict annual harbour sedimentation masses correctly, provided that the most important input parameters are accurate. Assessing the most important parameters was done through a sensitivity analysis. Through changing each input parameter both plus and minus ten percent respectively, a good image of the resultant effect of the parameter on the sedimentation rate was produced. The similarity between the output of CoDeS and observed sedimentation heavily depends on the constant- and variable suspended sedimentation concentrations outside the harbour, the harbour depth and entrance width, the constant settling velocity and the significant wave height inside the harbour. For using CoDeS, the emphasis is mainly on determining the constant SSC outside the harbour as this shows to be most important. Harbours allocated at an estuary show a significant model underestimation, which might be attributed to excluding river sediment inflow and the interaction of brackish water. For harbours with relatively high wave heights, the SSC was also significantly underestimated in CoDeS. The relative high wave heights cause more mud to remain in suspension while no sand was transported into the harbour when expecting creating a lower inflow and deposition rate.

Overall, CoDeS proves to be a convenient and quick model for the early stages of harbour design, suited for project proposals. It is best applied in areas where no sand transport is expected as sand transport does not show up even though it is included in the model design. Furthermore, CoDeS does not incorporate fluviatile sediment from upstream the harbour when allocated at an estuary.

5.2 SEDCON

The SEDCON-model is a new point model of the MUSA-project which can be used to compute the vertical distribution of mud, silt and sand concentrations and associated transport values in quasi-equilibrium conditions for combined (steady) current and wave conditions. The sediment concentration profiles are computed by numerical solution of the advection-diffusion equation including flocculation effects, hindered settling and damping of turbulence. The grid points over the depth (50 points) are distributed according to an exponential function resulting in very small grid near the bed and larger grid sizes near the water surface. The basic model formulations are similar to those of the TMUD-model.

The experimental results of the MUSA-project can be used to get better estimates of the input data (dry bulk density, settling velocity, critical bed-shear stress for erosion).

5.3 SEDPAR

The SEDPAR-tool is a new tool of the MUSA-project which can be used to determine a range of parameters for input of sediment models, as follows:

- settling velocity of individual mud, silt, sand and coral particles;
- settling velocity of mud particles including effects of flocculation and hindered settling;
- critical bed-shear stress and critical depth-averaged velocity for initiation of motion and suspension of mud-sand beds;
- dry bulk density of mud-sand beds;
- sand transport and pickup in combined current and wave conditions;
- sediment pickup at mud-sand beds (Van Ledden approach DELFT3D).

5.4 SEDPIT

The simplified SEDPIT-model of LVRS-Consultancy is a semi-analytical model which can be used to estimate the deposition of mud and sand from a flow crossing a channel or trench.

The channel cross-section is schematized into a rectangular cross-section.

The deposition is computed as a multiplication of a trapping efficiency factor and the incoming sediment load from the both sides of the channel. The trapping efficiency factor depends on the geometrical channel dimensions, the sediment characteristics and the hydrodynamic conditions. The (approach) angle between the main tidal flow direction and the axis channel may vary between 0^o and 90^o, but the model is less accurate for very small angles ($<30^o$). The deposition is 0 for an angle equal to 0. The model neglects the erosion of sediment which may occur at the downstream channel slope.

The basic parameters determining the trapping efficiency of a channel, are: approach velocity (v_o), approach angle (α_o), water depth outside channel (h_o), approach bed-shear velocity ($u_{*,o}$), particle fall velocity (w_s), wave height (H_s), channel depth below surrounding bed (d), effective channel width (B) and bed roughness (k_s).

The original version of the SEDPIT-model has been modified by including the exponent β of the critical bed-shear stress and a new equation for the dry bulk density (based on MUSA-data).

The experimental results of the MUSA-project can be used to get better estimates of the input data (dry bulk density, settling velocity).

The SEDPIT-model has been tested by Dredging Contractor DEME in Belgium, see work flow diagram for SEDPIT-calculations below. The general steps are:

- First step is to collect as much input data on the soil as possible. As a minimum some information about characteristic grain sizes is needed, and the amount of fines in the soil. The MUSA database can be consulted to find similar type of soils, from which additional parameters can be extracted.
- Next, the tools SEDPAR and TMUD can be used, containing updated knowledge from the MUSA project, to estimate missing parameters such as suspended concentrations of silt and clay, fall velocities and β parameter.
- Finally, SEDPIT can be used to estimate the sedimentation using all input.

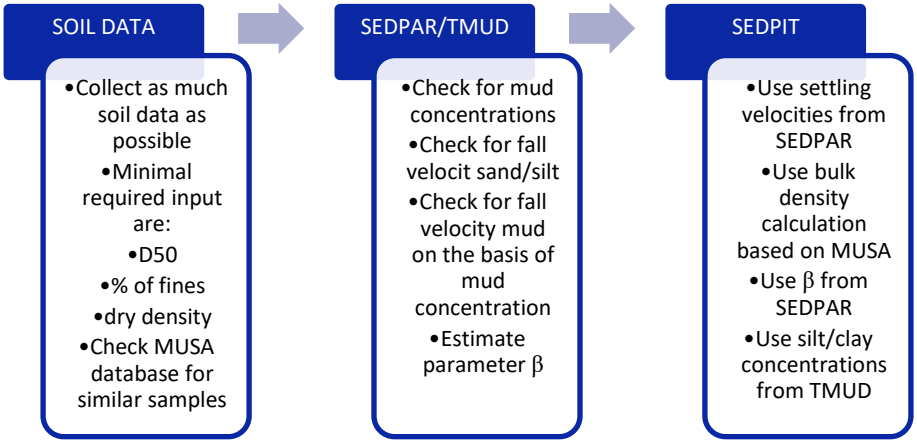

The SEDPAR-tool is consulted to derive various parameters that are needed in SEDPIT-tool, as follows:

1. Mud concentration
   In SEDPIT, the background concentration of clay and silt need to be specified. Often, there is little or no information available about this parameter. Using SEDPAR (sheet 7 'Mud concentration-transport'), estimated mud concentrations for a given depth and flow velocity can be derived, although the critical shear stress is not taken into account (so presumably this is for a full muddy bed, which might not be the case in this example). This has been used in the input of SEDPIT to specify for each flow case the clay and silt concentration. The resulting mud concentration is divided equally over the silt and clay fraction.
2. Settling velocity for sand, silt and clay. For sand/silt, sheet 1 'Fall velocity sand-coral' is used. Since the D_{50} of the total soil sample is 180 µm, it is expected that the sand is a bit coarser, so a D_{50} value of 200 µm is assumed. This gives a settling velocity of 25 mm/s. For the silt, a settling velocity of 0.75 mm/s is assumed. For the clay, sheet 2 'Settling velocity mud' is used. As mud concentration, a value of 50 mg/l is used, which means the hindered settling effect and flocculation effect are quite absent. Therefore, a settling velocity of 0.1 mm/s is used for the clay fraction.
3. Estimate parameter β of ther critcal bed-shear stres for erosion
   The β parameter is included in the equations to calculate the critical velocities of currents and waves. The default value is β = 1.5. Within SEDPAR (sheet '4 Critical stres sand+mud'), the value for beta can be estimated. For P_{fines} (< 63 µm) = 40%, P_{clay} (< 8 µm) = 22% and a dry density of 1000 kg/m^3, β becomes 2.9.

Next, the updated values based on SEDPAR-tool, they can be used within SEDPIT-tool. Besides these updated values, it is chosen for the calculation of the bulk density to use the MUSA equation instead of using a constant value. This is done by setting cell E29 to 0. The β parameter is set to 2.9.

The results of the original SEDPIT calculation are compared to the new calculation:

1. In general, the sedimentation has decreased significantly, mainly because the import of sand into the trench is strongly reduced.
2. The reduced input of sand is mainly related to the change in the parameter β. By increasing this parameter from the original default value of 1.5 to 2.9, the critical shear stress for erosion / pick-up rate of sand has reduced, leading to lower sand transports.
3. While in the original calculation the sand fraction dominated the infill, now sedimentation is mainly due to the silt and clay fractions. This is due the reduced sand transport (as discussed above), but also since the background concentrations of clay and silt have been increased from 20 mg/l in the original calculation to about 45 mg/l (averaged over the conditions) in the updated calculation.

5.5 TMUD

The TMUD-model is a point model which can be used to compute the variation of the depth-integrated mud and sand transport in tidal conditions over a mud-sand bed. The suspended sand transport is included assuming that the sediment bed consisting of mud and sand behaves as a cohesive mixture. The model includes combined tidal and river flow including residual salinity-induced flow. This latter type of flow is generated by gravitational circulation in a tidal channel with fresh water inflow. The residual flow is landward near the bottom and seaward near the water surface.

The velocities and mud concentrations are computed over the water depth and over time by numerical solution of the advection-diffusion equation for mud, silt and sand and sand in a quasi-steady flow. The grid points over the depth (50 points) are distributed according to an exponential function resulting in very small grid near the bed and larger grid sizes near the water surface. The effect of flocculation and hindered settling of mud particles is taken into account automatically. The effect of damping of turbulence in the high concentration layer near the bed is also taken into account.

The original version of the TMUD-model has not been changed.

The experimental results of the MUSA-project can be used to get better estimates of the input data (dry bulk density, settling velocity, critical bed-shear stress for erosion).

6 Conclusions and recommendations

6.1 Conclusions

Measurements of the settling velocity and the grain size distribution in sand-mud environments are sensitive to the measurement methodology.

The median settling velocity of mud samples in suspension measured with a flocculation camera (LABSFLOC2) was much larger than with a settling tube device (PIRANHA). The main causes for the difference in results are: floc destruction in the settling tube, underestimation of small particles by the flocculation camera, or a combination of both.

The particle size distribution (PSD) of mud-sand samples was measured with sieving for the sand fraction, while the finer fraction (< 63 μm) was measured with Laser Diffraction (LD) (using optical scattering), Sedigraph-method and hydrometer-method (both sedimentation methods, relating the settling speed of particles to a PSD using a Stokes settling velocity). The grain size measured with LD is significantly coarser than the grain size resulting from the Hydrometer and the Sedigraph.

The actual size of individual fine particles is best represented by the Laser-Diffraction method. The Sedigraph and the Hydrometer are sedimentation methods and produce an effective settling diameter and are therefore preferred in case the results are used to determine settling velocities, for example in siltation studies. The Hydrometer method is more laborious, but the variability in the results is low due to the relatively large sample that is measured. The LD-method offers an attractive solution for a rapid indication of particle sizes, but shows much more scattering for similar samples, suggesting a random sensitivity requiring repetition of measurements (many small samples required for representative results).

The dry bulk density of mud-sand samples strongly depends on the percentage of clay, silt sand sand and the consolidation stage.

The consolidation process of mud-sand mixtures strongly depends on three parameters, which are the percentage of clay/lutum< 2 to 8 μm, the percentage of sand particles > 63 μm and the layer thickness. Other parameters like the type of mud (i.e. mineral composition) and the percentage of organic materials in the range of 0 to 10% are of minor importance.

Natural mud-sand deposits with thickness of about 1 m with a low sand content (< 20%) can reach a dry density of about 350 kg/m^3 after 1 day. Natural mud-sand deposits with high sand content (40%-50%) can reach a dry density of about 450 kg/m^3 after 1 day. Dry density values in this range are the onset of the primary consolidation phase with the gradual build-up of grain stresses in a matrix-type network structure. Natural mud-sand deposits with low sand content (≅ 20%) can consolidate to 400 to 450 kg/m^3 after 20 to 50 days. Natural mud-sand deposits with a high sand content of 40% to 50% can consolidate to dry density values of 600 to 700 kg/m^3 after 10 to 30 days. The time scale is relatively small up to 60 days for a small thickness of 1 m and increasing to 180 days for a mud thickness of about 3 m and low sand content. The consolidation to relatively high dry density (order of 1000 kg/m^3) values is a long term process (secondary consolidation stage)

The dry bulk density at the end the primary consolidation stage can be described by a fairly simple relationship depending on the percentages of clay, slit and sand. The consolidation stage can be taken into account by an empirical factor.

The critical bed-shear stress and the erosion rate strongly depend on the preparation and composition of the mud-sand bed in the case of flume experiments.

The short flume experiments were carried out with remoulded natural sediments, with diluted (and consolidated over-night) natural samples, and with undisturbed field samples (including biota with stabilizing and destabilizing effects). The critical shear stress for all experiments was established through visual observations, distinguishing between particle erosion (first erosion mode at low bed shear stress)

and floc erosion (surface erosion of larger particles at higher bed shear stress, often accompanied by formation of scour marks and ripples). For a smaller set of observations the critical bed shear stress (and the erosion parameter) was additionally determined by fitting erosion formulations to continuous Suspended Sediment Concentration (SSC) observations.

Highest critical bed shear stress occurs at intermediate density and sand-mud ratio

The observed values of the critical bed shear stress were related to both the density and the mud (or sand) content of the sediment bed. The highest critical bed shear stress was typically observed for samples with intermediate densities (400-800 kg/m^3) and intermediate sand/mud ratios (50%/50%). High density mixtures were mostly sand-dominated whereas low density mixtures were typically mud-dominated; both end members were more easily erodible compared to the intermediate density/mud content samples. The bed shear stress was more coherently related to the density of the sediment bed than to the mud (or sand) content of the bed. Therefore, a formulation was derived to empirically relate the bed shear stress to density.

The erosion parameter of a sediment mixture decreases with increasing mud content

The exploring long flume experiments revealed that: i) the critical bed-shear stress of a long bed is much lower than that of a short mud-sand bed and ii) the erodibility of both sand and of mud decreased with increasing mud content. Earlier experiments predating MUSA related such erosion rate dependence on the critical bed shear stress for erosion. However, in contrast to these earlier experiments, the MUSA observations suggest that the erosion rate dependence results from a modification of the erosion parameter (lower at high mud contents).

Existing tools are able to reproduce observed sediment transport at high concentration conditions near Holwerd

Field experiments on mud and sand transport were executed near Holwerd, in the Dutch Wadden Sea. This site is characterised by very high SSC (up to several g/l) consisting of both sand and mud. Existing engineering tools that calculate the transport of sand and of mud were able to predict the observed sediment concentrations with remarkable accuracy using local hydrodynamics. These tools therefore appear to be very useful for predicting the sediment dynamics also for such turbid environments. Reproducing the observed mud concentration required the use of a flocculation model – predicted SSC values using constant settling velocities strongly deviated from observations.

Digital flumes were developed in MIKE3 and Delft3D

A new sediment transport formulation was implemented in MIKE3 and tested in a numerical flume resembling the long flume. These experiments revealed that the new formulations resolve observation within a factor of 2-5. The same flume was also implemented in a Delft3D application and applied to test existing sand-mud interaction formulations recently implemented in Delft3D. These numerical experiments revealed some inconsistencies in the implementation of the Van Rijn formulations in Delft3D, and that the erosion rates determined with the OBS were probably flawed by the background concentration.

The MUSA sediment bed density formulation is implemented in Delft3D

The relationship between critical bed-shear stress, dry bed density and erodibility derived from the MUSA observations was implemented in Delft3D and tested in an idealized tidal basin. These new formulations provide a means to model the development of muddy intertidal areas during tide-dominated conditions which are preserved during subsequent wave-dominated conditions (which is difficult to realize with a model assuming constant critical erosion shear stresses).

6.2 Recommendations

Erosion rates

The long flume experiments suggest that erosion rates decrease with increasing mud availability, due to a change in the erodibility parameter and not the critical bed shear stress for erosion (as commonly assumed). However, this relationship was established with a small number of observations. It is recommended that this relationship be investigated more systematically with (1) a larger set of long bed flume experiments, and (2) continuous suspended sediment concentrations that are minimally influenced by the background sediment concentration. It is also recommended to investigate the potential to develop or use flumes with a larger range in bed shear stress – the remoulded non-diluted samples and several undisturbed field samples were too strong to erode with the currently used flumes. It would also be beneficial to cooperate with other groups at universities working on this topic.

Measuring settling velocities

The range of in-situ and laboratory instrumentation used during the MUSA experiments resulted in a wide range of settling velocities. It is recommended that a series of laboratory and field measurements with different types of instrumentation be carried out to investigate in more detail how and why instrumentation influences the measured settlement velocity values.

Resuspension at different timescales

The erodibility of sand-mud mixtures appears to be correlated to the dry bulk density. Dry bulk density is therefore an important parameter, but this parameter is difficult to measure in the field and difficult to predict due to consolidation effects. It is recommended that practical methods for measuring bulk densities are investigated and that the effect of consolidation on resuspension rates over tidal timescales is systematically investigated using flume experiments.

Improved field measurements of sand-mud transport

Distinguishing between sand and mud transport under field conditions is laborious (requiring sampling and labour-intensive measurements) but important for understanding sediment transport mechanisms. It is recommended that methods and instruments for measuring near-bed sediment concentrations and transport rates in field situations be improved, using direct sampling combined with acoustic and optical equipment to measure sand-mud concentrations and bed load transport.

Global database

The MUSA results are largely based on the characteristics of sediment samples from the Netherlands. For the more general applicability of the formulations and tools, it is recommended to extend the existing database. This would require input from (internationally operating) consortium partners, feeding into a comprehensive dataset of detailed sediment characteristics and sediment transport.

Modelling tools for sand and mud

It is recommended that the acquired datasets and improved formulations are used to further improve and validate engineering tools and process-based models. Preferably through a combination of field experiments and numerical modelling in the Dutch Wadden Sea and/or the Western Scheldt.

References

Andersen, T.J., Lanaru, M., Van Bernem, C., Pejrup, M. and Riethmueller, R., 2010. Erodibility of a mixed mudflat dominated by microphytobenthos and Cerastoderma edule, East Frisian Wadden Sea, Germany. Estuarine, Coastal and Shelf Science, Vol. 87, 197-206.

Bauamt fur Kustenschutz, Norden, 1987. Tiefenstabilisierung von Aussentiefs mit Naturuntersuchungen am Nessmersieler Aussentief.

Boechat Albernaz, M., Van Rijn, L.C., Schoonhoven, D.C. & Perk, L.M., 2022A. Results of laboratory experiments Phase 1A & 1B. MUSA report

Boechat Albernaz, M., Van Rijn, L.C., Schoonhoven, D.C. & Perk, L.M., 2022B. Results of laboratory experiments Phase 1C & 1D. MUSA report

Boechat Albernaz, M., Van Rijn, L.C., Schoonhoven, D.C. & Perk, L.M., 2022C. Results of MUSA field measurement campaigns at Holwerd, the Netherlands. MUSA report

Colina Alonso, A., van Maren, D. S., van Weerdenburg, R. J. A., Huismans, Y., & Wang, Z. B. (2023). Morphodynamic modeling of tidal basins: The role of sand-mud interaction. Journal of Geophysical Research: Earth Surface, 128, e2023JF007391. https://doi.org/10.1029/2023JF007391.

Colosimo, I., van Maren, D. S., de Vet, P. L. M., Winterwerp, J. C., & van Prooijen, B. C. (2023). Winds of opportunity: The effects of wind on intertidal flat accretion. Geomorphology, 108840. https://doi.org/10.1016/j.geomorph.2023.108840

De Smit, J., Bruckner, M., Mesdag, K.I., Kleinhans, M.G. 2021. Key Bioturbator Species Within Benthic Communities Determine Sediment Resuspension Thresholds. Frontiers in marine Science, Vol.8

Deltares, 2016. KPP Navigation channel Holwerd; analysis of dredging data, bottom soundings and bottom composition. Report No. 1230378 (in Dutch), Delft, The Netherlands.

DHI A/S. 2022. MIKE 3 Flow Model FM. Hydrdynamic and Transport module. Scientific Documentation. Horsholm: DHI A/S.

Grasmeijer, B., Van Weerdenburg, R. and Van Kessel, T., 2021. Invloed baggerstrategie op slibconcentraties en baggervolumes vaarweg Holwerd-Ameland. Rapport 11206799-006-ZKS-0001, Deltares, Delft, The Netherlands

HR Wallingford, 1996. Sediment transport measurements at Maplin Sands, outer Thames estuary. Report TR 15, HR Wallingford

HR Wallingford, R.J. Whitehouse et al., 1997. Sediment transport measurements at Foulness, in the outer Thames estuary. Report TR 33, HR Wallingford

Jacobs, W., Le Hir, P., Van Kesteren, W. and Cann, P., 2011**.** Erosion thresholds of sand-mud mixtures. Continental Shelf research, Vol. 31 (10), S14-S25.

Lammers, 2023. Improving, validating and analysing SEDHAR tool in CoDeS

Le Hir, P., Cann, P., Waeles, B., Jestin, H., and Bassoullet, P., 2008. Erodibility of natural sediments: experiments on sand/mud mixtures from laboratory and field erosion tests. Sediment and Ecohydraulics, Intercoh 2005, Saga, Japan. Proceedings in Marine Science, Vol. 9. Edited by Kusuda, T., Yamanishi, H., Spearman, J. and Gailani, J.Z.

Maycon Machado Fontana, Athanasios Petridis, Kasper Kaergard, 2023. Multi-fraction Sediment Transport Modelling in MIKE 3 FM. MUSA report

MIKE by DHI A/S. 2021. “MIKE 21 & MIKE 3 Flow Model FM - Mud Transport Module Scientific Documentation.”

Mitchener, H. and Torfs, H., 1996. Erosion of mud/sand mixtures. Coastal Engineering, Vol. 29, 1-25.

Peng Yao et al. 2015. Experiment inspired numerical modeling of sediment concentration over sand–silt mixtures by Coastal Engineering, Vol. 105, 75-89

Soulsby, R.L., Clarcke, S., 2005, Bed Shear-stresses under combined waves and currents on smooth and rough beds, report TR 137

Soulsby, R. L., 1997. Dynamics of Marine Sands. London: Thomas Telford.

Soulsby, R. L., L. Hamm, G. Klopman, D. Myrhaug, R. R. Simonns, and G.P. Thomas. 1993. “Wave current interaction within and outside the bottom boundary layer.” Coastal Engineering, 21 41-69.\

Te Slaa, S., He, Q., Van Maren, D.S. and Wintwerwerp, J.C., 2013. Sedimentation processes in silt-rich sediment systems. Ocean Dynamics, Vol. 63 (4), 399-421

Van den Berg, J.H. and Van Gelder, A., 1993. Prediction of suspended bed material transport in flows over silt and very fine sand. Water Resources Research, Vol. 29, No. 5 p. 1393-1404

Van Ledden, M., 2003. Sand-mud segregation in estuaries and tidal basins. Ph.D. Thesis, Delft University of Technology, The Netherlands, Report No. 03–2, ISSN 0169-6548, 217pp.

Van Ledden, M., Van Kesteren, W.G.M. and Winterwerp, J.C., 2004. A conceptual framework for the erosion behaviour of sand-mud mixtures. Continental Shelf Research 24, 1-11.

Van Rijn, L.C., 2007. Unified view of sediment transport by currents and waves, part I,I,III and IV. Journal of Hydraulic Engineering, ASCE, Vol. 133, No 6, 7

Van Rijn, L.C., 2018. Consolidation of mud-sand mixtures. LVR-Sediment Consultancy, Blokzijl, The Netherlands (www.leovanrijn-sediment.com)

Van Rijn, Leo C. and Rene Barth, 2018. SETTLING AND CONSOLIDATION OF SOFT MUD-SAND LAYERS. J. Waterway, Port, Coastal, Ocean Eng., 2019, Vol 145, No. 1Van Rijn. L.C., 2019. Settling velocity of mud. LVRS-Consultancy, The Netherlands www.leovanrijn-sediment.com

van Rijn, L. C. (2020). Erodibility of mud–sand bed mixtures. Journal of Hydraulic Engineering, 146(1), 04019050.

Van Rijn, L.C., 2021. MODELLING OF SEDIMENT DEPOSITION TRIAL PITS AND SHIPPING CHANNEL, PAYRA, BANGLADESH (classified). LVRS-Consultancy, The Netherlands (www.leovanrijn-sediment.com)

Van Rijn, L.C. & Koudstaal, K.R., 2021. Measuring and interpretation of settling velocity and particle size. MUSA report

Van Rijn, L.C., Boechat Albernaz, M. & Manning, A.J., 2023. Field measurements of settling velocities and floc sizes in the ferry channel near Holwerd. MUSA report

Van Weerdenburg, R.J.A., Colina Alonso, A. & Van Maren, D.S., 2023. Modelling sand-mud dynamics in a digital flume in Delft3d. MUSA report

Veld et al., 2016. Monster- en meetprotocol ten behoeve van geologisch onderzoek zoekgebieden Noordzee zandwinning. Deltares report 1230624-000-BGS-0012

WaterProof bv, 2019. Metingen Holwerd-Ameland; meetresultaten en laboratoriumanalyse metingen januari-maart 2019. Rapport WP2018_1155-R3r2, Lelystad, The Netherlands (in Dutch)

Winterwerp, J.C., Cornelisse, J.M. and Kuijper, C., 1992. Erosion of natural sediments from The Netherlands; analysis of laboratory experiments. Report 38, Deltares, Delft, The Netherlands.

Winterwerp, J.C. and Van Kesteren, W.G.M., 2004. Introduction to the physics of cohesive sediment in the marine environment. Elsevier, Developments in sedimentology, ISBN 0-4444-51553-4.

Winterwerp, J. C.,W. G. M. Van Kesteren, B. Van Prooijen, and W. Jacobs. 2012. “A conceptual framework for shear flow-induced erosion of soft cohesive sediment beds.” J. Geophys. Res. 117: C10020. https://doi.org/10.1029/2012JC008072.

Wu, Weiming, and Qianru Lin. 2014. “Nonuniform sediment transport under non-breaking waves and currents.” Coastal Engineering 90 1-11.

Wu, Weiming, Chamil Perera, Jarrel Smith, and Alejandro Sanchez. 2018. “Critical shear stress for erosion of sand and mud.” Journal of Hydraulic Research, 56:1 96-110.

Wu, Weiming, Sam S. Y. Wang, and YAFEI JIA. 2000. “Nonuniform sediment transport in alluvial rivers.” Journal of Hydraulic Research, 38:6 427-434.

Yao, P., Su, M., Wang, Z., van Rijn, L. C., Stive, M. J. F., Xu, C., & Chen, Y. (2022). Erosion Behavior of Sand-Silt Mixtures: Revisiting the Erosion Threshold. Water Resources Research, 58(9), [e2021WR031788]. https://doi.org/10.1029/2021WR031788

A Appendices

A.1 Overview sample characteristics

Location	Sample	d_{50} d_{90}	Wet density	Dry density	> 63 µm (Sand)	< 63 µm (Silt+ clay)	< 8µm	< 2µm	Organic matter	Dominant minerals in fraction < 10 µm	Plasticity Index PI= WL-Wp
		µm	kg/m³	kg/m³	%	%	%	%	%		%
Bengal Bay (BB)	BB2	20 80	1940	1500	8	88	42	21	<3	S I K C 0% **82%** 0% 19%	
	BB3	14,8 52,6	1262	1760	6	94	29,8	16,4	3	S I K C 0% **81%** 0% 19%	17.2
	BB-TP1	18,2 77,7	1750	1205	17,9	82	27,1	16,1	-		
	BB-TP2	13,4 65,9	1750	1205	10,5	89,5	30,6	17,5	-		
	BB-TP3	81,1 125,5	1750	1205	14	86	24,8	13,1	-		
Western Scheldt (WS)	GR1	15 55	1408	680	5	95	37	17	6,7		
	ZW2	22 65	1516	835	10	90	37	23	4,8		
	WAW1	40 110	1581	910*	37	63	24	11	4,7		
	BH1	70 230	1712	1145	55	45	14	8	3,2		
	HU1	150 190	1797	1300	88	12	8	5	1,9		
	BAPU	20,3 126,2	1405	650	28,8	71,2	36,6	24,6	8,8	S I K C 8% **55%** 20% 17%	44.4
	APP	144,4 212	1785	1238	77	23	10	5	4,9	S I K C 8% **55%** 21% 16%	13.4
	BA4	126,7 170,8	1594	1367	99,8	0,2	0	0	2,3		
	SO3	77,5 418,5	1507	837	56,1	43,9	20,8	12,3	6	S I K C 10% **55%** 21% 14%	21.5

	PA1	5,5 54,7	1332	554	6,3	93,7	56, 4	37, 5	13	S 4%	**I** **56%**	K 18%	C 22%	60.1
Plymouth	PLUK1	37,5 69,8	1407	644	12,7	87,3	23	14, 2	10,2	S 0%	I 45%	**K** **55%**	C 0%	28.1
	PLUK4	23,4 88,6	1373	611	22,3	77,7	26, 5	16, 6	10,5	S 0%	**I** **49%**	**K** **51%**	C 0%	25.7
Wadden Sea Noord-polder-zijl (NPZ)	H2	8 75	1275	435	12	88	51	38	7,7					
	B5	19,5 85,1	1391	644	28,1	71,9	35	22, 3	10	S 8%	**I** **55%**	K 19%	C 18%	52.8

S=Smectite (Montmorillonite); I=Illite; K=Kaolinite; C=Chlorite